Distribution Agreement

In presenting this thesis or dissertation as a partial fulfillment of the requirements for an advanced degree from Emory University, I hereby grant to Emory University and its agents the non-exclusive license to archive, make accessible, and display my thesis or dissertation in whole or in part in all forms of media, now or hereafter known, including display on the world wide web. I understand that I may select some access restrictions as part of the online submission of this thesis or dissertation. I retain all ownership rights to the copyright of the thesis or dissertation. I also retain the right to use in future works (such as articles or books) all or part of this thesis or dissertation.

Signature:

_____ _____

Pai Liu Date

High-fat Diet-induced Diabetes Couples to Alzheimer's Disease through Inflammation-activated C/EBPβ/AEP Pathway

By

Pai Liu

Doctor of Philosophy
Graduate Division of Biological and Biomedical Science
Neuroscience

Keqiang Ye, Ph.D.
Advisor

Arthur W. English, Ph.D.
Advisor

Guy Benian, MD
Committee Member

Lih-Shen Chin, Ph.D.
Committee Member

Randy Hall, Ph.D.
Committee Member

Accepted:

Kimberly Jacob Arriola, Ph.D., MPH
Dean of the James T. Laney School of Graduate Studies

Date

High-fat Diet-induced Diabetes Couples to Alzheimer's Disease through Inflammation-activated C/EBPβ/AEP Pathway

By

Pai Liu

B.S., Emory University, 2018

Advisors: Keqiang Ye, Ph.D., Arthur W. English, Ph.D.

An abstract of
A dissertation submitted to the Faculty of the James T. Laney School of Graduate Studies of Emory University in partial fulfillment of the requirements for the degree of Doctor of Philosophy

Abstract

High-fat Diet-induced Diabetes Couples to Alzheimer's Disease through Inflammation-activated C/EBPβ/AEP Pathway

By

Pai Liu

Diabetes is a risk factor for Alzheimer's disease (AD), which is also known as type 3 diabetes and is characterized by insulin resistance and insulin signaling impairment in the brains of AD patients. However, the molecular mechanism coupling diabetes to AD is still unknown. In this dissertation study, I report that inflammation, which is linked to obesity and diabetes induced by high-fat diet (HFD), activates neuronal C/EBPβ/AEP signaling that leads to AD pathologies and cognitive dysfunctions. In neuronal Thy1-C/EBPβ transgenic (Tg) mice, HFD induces diabetes and insulin resistance, along with mouse Aβ accumulation and hyperphosphorylated Tau aggregation in the brain, resulting in cognitive impairments. These effects are significantly diminished when AEP is deleted from C/EBPβ Tg mice. Chronic treatment with inflammatory lipopolysaccharide (LPS) facilitates AD pathologies and cognitive disorders in C/EBPβ Tg but not in wild-type mice, and these deleterious effects were substantially alleviated in C/EBPβ Tg/AEP -/- mice. Remarkably, the anti-inflammatory drug aspirin strongly attenuates HFD-induced diabetes and AD pathologies in neuronal C/EBPβ Tg mice. Therefore, the findings presented in this study demonstrate that inflammation-activated neuronal C/EBPβ/AEP signaling couples diabetes to AD.

High-fat Diet-induced Diabetes Couples to Alzheimer's Disease through Inflammation-activated C/EBPβ/AEP Pathway

By

Pai Liu

B.S., Emory University, 2018

Advisors: Keqiang Ye, Ph.D., Arthur W. English, Ph.D.

A dissertation submitted to the Faculty of the James T. Laney School of Graduate Studies of Emory University in partial fulfillment of the requirements for the degree of Doctor of Philosophy in Neuroscience, 2022

Acknowledgment

I am very grateful to many people who have made substantial contributions to the work presented in this dissertation.

First and foremost, I would like to express my deepest gratitude to my mentors, Dr. Keqiang Ye, and Dr. Arthur English, for their guidance and support. I have been provided with every opportunity to learn and grow and learned to appreciate the importance of collaboration. I have benefited greatly from their wealth of knowledge and experience. Throughout my training, I have learned critical thinking, understood the importance of collaboration, and appreciated the beauty of nature and science.

I am indebted also to my thesis committee members, Dr. Randy Hall, Dr. Guy Benian, and Dr. Lih-Shen Chin. Their detailed feedback and thoughtful advice have been very important to me. All these members have kept track of my progress and have spent a significant amount of time on meetings and communications. I am grateful for their support, criticism, and encouragement.

I would also like to show my appreciation to Xia Liu, Zhi-hao Wang, Seong Su Kang, and Yiyuan Xia. Ms. Liu has taught me many critical techniques that underlie much of this dissertation work. Dr. Wang had supervised my projects since I was a sophomore student at Emory University, always cheering me up at the most difficult times. Dr. Kang never hesitated to share his knowledge and resources with me. Dr. Xia was always ready to help with any questions that I had.

Many thanks to all the faculty and students in the Neuroscience graduate program at Emory University for their kind support during my Ph.D. study. It has been a pleasure to work with so many extraordinary individuals. I would like to especially thank Dr. David Weinshenker, Dr. Shannon Gourley, Dr. Robert Liu, Dr. John Hepler, Dr. Ellen Hess, and Chanell Loiseau. I would also like to thank Emory Rodent Behavioral Core (RBC) and Emory HPLC Bioanalytical Core (EHBC) for your help.

Lastly, my family deserves endless gratitude. To my parents, Xianzhang Liu and Yan Wang, thank you for your unconditional love and support that have kept me motivated and confident. Without your understanding and encouragement in the past few years, this thesis would not have been possible.

Table of Contents

List of Figures

Abbreviation

ACC	Acetyl-CoA carboxylase
AD	Alzheimer's disease
AEP	Asparagine endopeptidase
AKT	Protein kinase B
AMP	Adenosine monophosphate
AMPK	AMP-activated protein kinase
ANOVA	Analysis of variance
APOE	Apolipoprotein E
APP	Amyloid precursor protein
ATM	Adipose tissue macrophages
ATP	Adenosine triphosphate
AUC	Area under the curve
BACE1	β-Site amyloid precursor protein cleaving enzyme 1
BAT	Brown adipose tissue
BBB	Blood brain barrier
BDNF	Brain-derived neurotrophic factor
BEH	Bridged hybrid
CA	Cornu Ammonis
C/EBPβ	CCAAT Enhancer Binding Protein β
CNS	Central Nervous System
COX	Cyclooxygenases
CRP	C-reactive protein
CSF	Cerebrospinal fluid
DAPI	4′,6-diamidino-2-phenylindole
DEA	Diethylamine
DIV	Days in vitro
DNA	Deoxyribonucleic acid
DT	Dichlorodiphenyltrichloroethane
EDTA	Ethylenediaminetetraacetic acid
EGTA	Egtazic acid
ELISA	Enzyme-linked immunosorbent assay
EM	Electronic microscope
fEPSP	Field excitatory postsynaptic potential
ER	Endoplasmic reticulum
FDA	Food and Drug Administration
FDG	18F-fluorodeoxyglucose
FFA	Free Fatty Acids
GFAP	Glial Fibrillary Acidic Protein

GFP	Green fluorescent protein
GLUT4	Glucose transporter type 4
GSK	Glycogen synthase kinase
GST	Glutathione S-transferase
GTT	Glucose tolerance test
HA	Homology arms
HEK293	Human embryonic kidney 293 cells
HFD	High fat diet
HLH	Hemophagocytic lymphohistiocytosis
HPLC	High-performance lipid chromatography
HRP	Horseradish peroxidase
hRTE	Human renal tubular epithelial
I2PP2A	Protein phosphatase-2A inhibitor-2
IB	Immunoblot
IF	Immunofluorescence
IGF	Insulin-like growth factor
IHC	Immunohistochemistry
IKK	IκB kinase
IL1	Interleukin 1
IL6	Interleukin 6
IR	Insulin receptor
IRS	Insulin receptor substrate
ISF	Interstitial fluid
ITT	Insulin tolerance test
JAK2	Janus kinase 2
JNK	c-Jun N-terminal kinase
KD	Kinase-dead
KO	Knockout
LAP	Liver-enriched activator protein
LIP	Liver-enriched inhibitor protein
LOX	Lipoxygenase
LPS	Lipopolysaccharide
LTP	Long-term potentiation
MAPT	Microtubule Associated Protein Tau
MCI	Mild cognitive impairment
MM	Multiple myeloma
MMSE	Mini-mental state examination
MRI	Magnetic resonance imaging
MT	Microtubules
MWM	Morris water maze

NAFLD	Non-alcohol fatty liver disease
NF-κB	Nuclear factor kappa B
NFT	Neurofibrillary tangles
NGF	Nerve growth factor
NIH	National Institutes of Health
NMDA	N-methyl D-aspartate
NSAID	Nonsteroidal anti-inflammatory drug
NT3	Neurotrophin-3
OGD	Oxygen-glucose deprivation
PAGE	Polyacrylamide gel electrophoresis
PBS	Phosphate buffered saline
PCR	Polymerase chain reaction
PD-1	Programmed cell death protein 1
PET	Positron Emission tomography
PFA	Paraformaldehyde
PG	Prostaglandin
PHF	Paired helical filaments
PI3	Phosphatidyl-inositol-3
PIKE	PI3-Kinase Enhancer
PKB	Protein kinase B
PKC	Protein kinase C
PP2A	Protein phosphatase 2A
PPAR	Peroxisome proliferator-activated receptor
PSD95	Postsynaptic density protein 95
PSEN1	Presenilin-1
PSEN2	Presenilin-2
RER	Respiratory exchange ratio
RIPA	Radioimmunoprecipitation assay
RT-PCR	Reverse transcription-polymerase chain reaction
RNA	Ribonucleic acid
SDS	Sodium dodecyl-sulfate
SEM	Standard error of the mean
SET	Suvar3-9 enhancer-of-zeste trithorax
SOCS	cytokine signaling
SPRK2	Serine/threonine-protein kinase 2
STAT3	Signal Transducer and Activator of Transcription 3
T1DM	Type 1 diabetes mellitus
T2DM	Type 2 diabetes mellitus
TBS	Theta-burst stimulation
TDP	Thiamine pyrophosphate

TG	Triglyceride
TGN	Trans-Golgi Network
TLR	Toll-like receptor
TNFα	Tumour Necrosis Factor alpha
TrkB	Tropomyosin receptor kinase B
UCP1	Uncoupling protein 1
WAT	White adipocyte tissue

CHAPTER 1: Background and Literature Review

1.1 Abstract

Diabetes is a risk factor for Alzheimer's disease (AD), which is also called type 3 diabetes with insulin reduction and insulin resistance in AD brains. However, the molecular mechanism coupling diabetes to AD onset remains incompletely understood. This dissertation study shows that inflammation, associated with obesity and diabetes induced by high-fat diet (HFD), activates neuronal C/EBPβ/AEP signaling that drives AD pathologies and cognitive disorders. HFD stimulates diabetes and insulin resistance in neuronal Thy1-C/EBPβ transgenic (Tg) mice, accompanied by prominent mouse Aβ accumulation and hyperphosphorylated Tau aggregation in the brain, triggering cognitive deficits. These effects are profoundly diminished when AEP is deleted from C/EBPβ Tg mice. Chronic treatment with inflammatory lipopolysaccharide (LPS) facilitates AD pathologies and cognitive disorders in C/EBPβ Tg but not in wild-type mice, and these deleterious effects were substantially alleviated in C/EBPβ Tg/AEP -/- mice. Remarkably, the anti-inflammatory drug aspirin strongly attenuates HFD-induced diabetes and AD pathologies in neuronal C/EBPβ Tg mice. Therefore, our findings demonstrate that inflammation-activated neuronal C/EBPβ/AEP signaling couples diabetes to AD.

1.2 Alzheimer's disease

1.2.1 Global Impact and History of Alzheimer's disease

Alzheimer's disease (AD), named after the German psychiatrist Alois Alzheimer, is a progressive neurodegenerative disease with dementia as the most prominent clinical symptom (1, 2). AD accounts for 60–70% of dementia cases (3). As a rapidly growing health issue, AD has affected more than 50 million people worldwide in 2020, and this number is estimated to double every 5 years and reach 152 million by 2050 (4). With an estimate of US $1 trillion costs, the economic and social burden of AD on families is a serious global health challenge (4). However, no therapeutics have been shown to effectively reverse or alter the disease pathogenesis in patients.

AD is characterized by senile plaques composed of amyloid-beta peptide (Aβ) and neurofibrillary tangles (NFTs) in the medial temporal lobe and neocortex (1, 5). Observation of amyloid plaques and neuron loss was made by Alois Alzheimer when he was examining the brain of his first patient, Auguste Deter, who suffered from memory loss. The disease was first characterized and named Alzheimer's disease by Emil Kraepelin in the 8th edition of the *Textbook of Psychiatry,* published in 1910. The following sections within chapter 1.3 are to give a brief description of primary markers, causes, and current treatments of AD (6).

1.2.2 Clinical Manifestation and Diagnosis of Alzheimer's disease

The most well-known clinical manifestation of AD in the early stages is difficulty in remembering recent events. Other symptoms include disorientation, lack of motivation, mood swings, language problems, and other cognitive dysfunctions (5, 7). In 1984, a workgroup (NINCDS-ADRDA) formed by The National Institute of Neurological and Communicative Disorders and Stroke (NINCDS) and the Alzheimer's Disease and Related Disorders Association (ADRDA) published AD diagnostic criteria, which were later updated by The National Institute on Aging-Alzheimer's Association (5). According to this guide, four major assessments are required to determine a patient's condition and disease stage.

First, the Mini-Mental State Examination (MMSE) is a widely used cognitive function test that categorizes patients into the mild, moderate, or severe stages of dementia. It is an 11-question test that evaluates patients' orientation, attention, memory, abstract thinking, and language usage (8). Additionally, interviews with family and friends are necessary for the doctors to gain a better understanding of patients' behavior and family history.

The second assessment is magnetic resonance imaging (MRI) which is a medical imaging technique using strong magnetic fields and radio waves to form images of the anatomy. MRI is a non-invasive way for doctors to spot abnormalities in the brain. It is now a standard practice to assess the loss of brain volume correlated with AD as it detects hippocampus atrophy by measuring the size and number of neurons (9, 10). Moreover, MRI helps eliminate other reasons for memory loss such as brain tumors, stroke, and even normal pressure hydrocephalus (11).

The third assessment is the measurement of $A\beta_{42/40}$ ratio in cerebrospinal fluid (CSF). The emergence of clinical symptoms is correlated with biochemical changes in the brain (12). CSF biomarkers $A\beta_{42/40}$ ratio, total Tau, and phosphorylated Tau at threonine 181 (P-tau 181) are

used in the AD diagnosis. Multiple studies have demonstrated that the CSF level of Aβ42 significantly decreases in AD brains, thereby resulting in a reduction in the $A\beta_{42/40}$ ratio. Statistical analyses showed that the $A\beta_{42/40}$ ratio is a better diagnostic measurement than the CSF Aβ42 level alone, even prior to the occurrence of clinical manifestations (13). A number of large cohort studies also concluded that CSF Tau increases in AD and brain injury and phosphorylated tau increases in AD (14-16). It was also confirmed that Aβ amyloidosis occurs before the increase in Tau and p-Tau (13). Clinical practices and data analyses have shown that these CSF biomarkers for AD can predict the conversion from mild cognitive impairment (MCI) to AD with 80% accuracy (14).

Finally, Positron emission tomography (PET) is widely used for diagnosing AD as it is capable of detecting decreased cerebral glucose metabolism (10). The most commonly used PET scan is the ^{18}F-fluorodeoxyglucose (FDG) PET scan. ^{18}F-FDG is a radioactive atom that can be phosphorylated by hexokinase and retained in tissues with high metabolic activities (10, 17).

Up till now, scientists are still developing new diagnostic tools to detect AD in the earlier stages, so patients can receive early intervention and treatment before the disease has progressed to a more severe stage. One example is the discovery of the elevation of tau biomarkers phosphorylated at T181, T217, or T231 not only in CSF but also in the plasma (18-20). These novel biomarkers generate fresh insights into identifying vulnerable populations in the preclinical phase. Additionally, Vitamin B12 deficiency in the serum is closely related to neurological disorders and especially AD. B12 deficiency leads to a lack of healthy red blood cells carrying oxygen to the brain, causing brain damage due to oxidative stress and apoptosis (21). There is a growing body of literature that recognizes the role of metabolism in facilitating

AD pathogenesis. Thus, it is my hope that this study can provide valuable information for future studies developing diagnoses and help AD patients to improve the overall quality of their lives.

1.3 Alzheimer's disease Pathology and Research

1.3.1 Neuropathological Markers of Alzheimer's disease

Key neuropathological features of AD include extracellular amyloid-β (Aβ) accumulation deposited into senile plaques, neurofibrillary tangles (NFT) made of intra-neuronal hyperphosphorylated and truncated Tau, neuroinflammation, and extensive neuronal loss (22, 23). This section will briefly discuss previous studies and evidence regarding these four major AD pathological markers.

Senile plaques, also called neuritic plaques, are extracellular nonvascular deposits of Aβ proteins with various morphological forms, such as neuritic, dense-cored, and classics. Aβ monomers aggregate into mature amyloid fibrils that further assemble into amyloid plaques (6, 24, 25). The regional progression of amyloid deposition first appears in the orbitofrontal cortex, the anterior cingulate gyrus, and the bottom of the parietal lobe, then finally takes over the neocortex and subcortical regions (26). Previous research has shown that increased Aβ accumulation in the prefrontal cortex might be due to APOE4 (27). The plaques are deposits of Aβ40 and Aβ42 peptides which are proteins that are 40 or 42 amino acid residues long, respectively, due to imprecise cleavage of γ-secretase at the C-terminus of Aβ. The predominant peptide is Aβ40, less toxic than the minor Aβ42 peptides. The key component of amyloid plaques in AD brains are mostly Aβ42, though the overall concentration of Aβ40 is about several-fold higher than that of Aβ42. Aβ is derived from amyloid precursor protein (APP), which is a transmembrane protein that plays a key role in transporting cholesterol and preventing neuronal hyperactivity (28). APP can be sequentially cleaved by three enzymes: α-, β-, and γ-secretases; Aβ is a proteolytic product of APP by β- and γ-secretases. APP cleavage by β-secretases (β-amyloid cleaving

enzyme (BACE)) on the N terminal takes place outside of the membrane, while γ-secretases (mostly presenilin-1 (PSEN1) and presenilin-2 (PSEN2) in AD) cut APP inside of the membrane (25, 29, 30). The cleavage results in soluble Aβ40 and Aβ42 fragments being released into the extracellular space (25). α-secretases cut APP in the middle of the Aβ sequence in nonneuronal cells, which explains why Aβ is mostly in the nervous system (31). Three gene mutations that cause early-onset familial AD-associated are in the APP, PSEN1, and PSEN2 genes (32). Several non-enzymatic mechanisms of Aβ clearance have also been reported in previous studies, including cellular clearance involving phagocytosis of Aβ by microglia, system clearance of Aβ in the liver that requires delivery of Aβ across the blood-brain barrier (BBB) to the blood circulation, and the interstitial fluid (ISF) drainage pathway (33, 34). Previous studies have also identified different Aβ-degrading enzymes (ADE) including insulin-degrading enzyme and neprilysin (33).

Neurofibrillary tangles (NFTs) are aggregates of hyperphosphorylated isoforms of tau protein, which is a group of six highly soluble protein isoforms generated from the gene *MAPT* (microtubule-associated protein tau) through alternative splicing. Tau is a microtubule-binding protein that plays a major role in maintaining microtubule stability in axons for intracellular transport, neuronal polarity, and structural integrity (35). However, tau is hyperphosphorylated and detached from microtubules in AD and related tauopathies. Instead of associating with microtubules, these insoluble hyperphosphorylated tau proteins group into paired helical filaments (PHF) that later aggregate into NFTs. As a result, diseased neurons lose synaptic stability and stable microtubule growth, which leads to cell dysfunction and death (35). NFTs have a stronger correlation with learning and memory impairment than Aβ, but it appears that Aβ triggers tau-dependent microtubule disassembly and promotes tauopathy. Since no familial AD

case is caused by mutations of the tau gene, some believe that NFTs are merely a consequence of AD instead of its cause. However, Tau P301S (PS19) transgenic mice, with the expression of the mutant human MAPT that is five-fold higher than the endogenous mouse MAPT protein expression, display cognitive impairments, synaptic loss, and NFTs by the age of six months. By the time of eight months, the mice show neuronal loss primarily in the hippocampal regions and other brain regions (36).

Synapse loss is the strongest correlate for the severity of AD and cognitive dysfunction. As an early feature of AD, synapse damage and loss are downstream effects of amyloid deposition, NFTs, and inflammation involved in the AD pathology (37, 38). The reduction in spine density and dendritic arborization correlates with cognitive decline, demonstrated by studies using transgenic mice with gene mutations of the human familial AD (24, 39, 40). Previous investigations have provided clear evidence that local synapse loss and synaptic plasticity deficits cause decreased connectivity in neuronal networks, associated with memory decline and senile plaques (7, 41). In mouse models with APP and presenilin mutations, loss of synapses leads to reductions of volume in the affected regions such as the temporal lobe, parietal lobe, parts of the cingulate gyrus, and neocortex (38). Synapse damage and loss eventually lead to reductions in dendritic spines and presynaptic terminals (38).

Chronic inflammation has recently emerged as a major hallmark in AD pathogenesis. Starting in the 1990s, scientists and physicians have observed that anti-inflammatory treatments used for other diseases show a protective effect against AD (22, 42). More than 15 epidemiological studies have reported the inverse association between long-term nonsteroidal anti-inflammatory drug (NSAID) use and AD development, indicating that conventional NSAIDs may slow down AD progression. Sustained inflammatory responses were detected in AD brains with NFTs and

senile plaques deposits (22, 43-45). Similar inflammatory responses were also confirmed in different studies using postmortem brain tissues from AD patients and animal models (46-48). Unlike acute inflammation, which is in response to injuries and infections, chronic inflammation (e.g. neuroinflammation) lasts for a prolonged period and links with several diseases, such as heart diseases, diabetes, and cancer (22, 49). Chronic neuroinflammation is a result of microglia cell activation and increased levels of cytokines. In healthy brains, microglia play an important role in clearing cell debris and waste through phagocytosis (50). However, long-term activation of microglia promotes the production of various neurotoxic substances such as free radicals, and proinflammatory cytokines, such as IL-6, IL-1β, and TNF-α (50–52). Elevated TNF-α is reported to kill cortical neurons, and TNF-α synthesis inhibitor treatment significantly alleviates impairments in memory and learning (53, 54). Studies have suggested that IL-1β and IL6 may slow down Aβ clearance by reducing the transport of Aβ across BBB (34). Bacterial lipopolysaccharides (LPS), a component in the outer membrane of Gram-negative bacteria, are widely used in animal models to initiate the inflammation process and induce pro-inflammatory cytokine expressions. Peripheral LPS causes elevated hippocampal Aβ deposits in a wild-type mouse strain (55). Thus, the evidence together suggests that chronic neuroinflammation is a central mechanism and primary hallmark of AD.

1.3.2 Risk Factors of Alzheimer's disease

In the light of recent evidence, over 20 risk factors associated with AD have been identified. Less than 5% of the AD patients are early-onset familial AD (EOFAD) cases that involved mutant alleles of APP or presenilin genes. Most AD patients are late-onset sporadic AD (LOSAD) associated with different genetic, lifestyle, and environmental risk factors (4, 6).

The greatest known risk factor for AD is age. About 10% of people over 65 years old have AD and the prevalence increases dramatically with age (3). The primary genetic risk factor in sporadic late-onset AD is a polymorphism in the apolipoprotein E (*APOE*) gene (23, 56). Three alleles of *APOE* (*ApoE2, ApoE3,* and *ApoE4*) are reported. In healthy individuals, *APOE* proteins are involved in cholesterol and lipid metabolism, but individuals with the *ApoE4* allele in heterozygosity have a 3-fold higher risk of developing AD and 12-fold higher if it is homozygous (4, 57). Longitudinal and epidemiological studies suggest that patients with cerebrovascular diseases and hypertension are also at increased risk for AD (56, 58, 59). In addition, women have a higher risk of developing AD. Other lifestyle risk factors include inadequate sleep, lack of exercise, and smoking. Many investigations also suggest a strong correlation between type 2 diabetes mellitus and AD development (56, 60). Evidence and findings related to diabetes as a risk factor for AD will be discussed in later chapters.

1.3.3 Current treatments of Alzheimer's disease

Although no treatment has been proven to effectively cure or reverse AD, scientists have made tremendous progress in developing new medications. U.S. Food and Drug Administration (FDA) has approved several prescription medicines treating AD, but most drugs work best for early to moderate AD patients.

In 2021, accelerated approval was provided by FDA for aducanumab, which is the newest medicine that is a monoclonal antibody which binds to and reduces aggregated beta-amyloid. Inhibitors of cholinesterase, including donepezil, rivastigmine, and galantamine, were also shown to decrease AD symptoms by preventing the breakdown of acetylcholine and increasing its levels in the brain. Another AD medication is memantine, which is an N-methyl D-aspartate (NMDA) receptor antagonist. Excessive glutamate can cause excitotoxicity and cell death in the brain but memantine can block NMDA receptors, which are a glutamate receptors subfamily. Since NMDA antagonists and cholinesterase inhibitors have different mechanisms of action, these two types of drugs can also be prescribed in combination for a better effect.

These medications temporarily alleviate some of the symptoms mainly because AD is driven by many factors and proposed mechanisms. Some drugs are developed to either block Aβ or attenuate neuroinflammation while the others target synapse loss or inhibit cholinesterase. It is possible that AD is not one disease but a collection of multiple diseases, and thus, these drugs fail to cure and reverse AD (61).

1.4 Alzheimer's disease as Type 3 diabetes

1.4.1 Type 2 diabetes (T2DM)

Throughout this dissertation, the term "diabetes" or "T2DM" will be used to refer to Type 2 diabetes (T2DM). Globally, about 463 million individuals have diabetes, which is 6.28% of the world's population. The burden of diabetes on patients' functional capacities and economic costs will continuously go up to 2030 (62). Not only does this condition affect how the body converts food into energy, but it is also associated with significant morbidity and mortality. T2DM is manifested with hyperglycemia, insulin resistance, and peripheral inflammation (63, 64). The most distinctive feature of diabetes mellitus syndromes is the impairment in insulin actions and signaling, which results in chronic hyperglycemia (64). Type 1 diabetes mellitus (T1DM) is the result of destruction of pancreatic islet beta cells and thus insulin deficiency, while T2DM is due to insulin resistance occurring in the peripheral tissues, causing the body's ineffective use of insulin. Unlike T1DM which involves an inherited susceptibility in mostly children, T2DM is associated with aging, family history, obesity, and lack of exercise (65). Insulin resistance shown in T2DM is due to reduced insulin receptor expression, insulin receptor tyrosine kinase activity, insulin receptor substrate (IRS) type 1 expression, and phosphatidyl-inositol-3 (PI3) kinase activation in skeletal muscles and adipocytes (66). It has been well established that serum level of 100 to 125 mg/dL (fasting glucose level) indicates that the individual may have prediabetes, and 126 mg/dL or higher indicates the condition of diabetes. In mice, diabetes can be diagnosed by two consecutive readings of non-fasting blood glucose that are higher than 250 mg/dL (67).

1.4.2 Tissues affected by diabetes

This section will discuss tissues involved in diabetes, including adipose tissue, liver, and skeletal muscles.

Adipose tissue, also known as fat tissue, is the most dysfunctional organ in diabetes. Adipose tissues are composed of a variety of cells, including adipocytes (fat cells), preadipocytes, neurons, and fibroblasts (68). This highly dynamic organ is composed of white and brown adipose tissues that serve different functions for the body (69, 70). Brown adipose tissue (BAT) is metabolically active and converts chemical energy directly into heat, whereas excess chemical energy is stored in white adipose tissue (WAT) as triacylglycerol for later use (71). BAT can be activated by diet, exercise, and increased energy expenditure, thereby a promising therapeutic target in combating diabetes. Excessive WAT, on the other hand, is associated with elevated blood sugar, insulin resistance, and obesity (72).

The liver, the largest internal organ of the human body, plays a vital role in glucose and lipid metabolism. The key responsibilities of the liver are the storage and re-distribution of lipid, carbohydrate, and protein (73). During an anabolic state, glucose can be absorbed by hepatocytes. Through glycolysis, glucose is converted into acetyl-CoA and then adenosine triphosphate (ATP). Excess glucose is stored as glycogen in the liver and skeletal muscles. In a fasting state, the liver initiates the process of gluconeogenesis and converts non-carbohydrate substrates into glucose. Thus, the liver is essential in maintaining blood glucose levels. At least half of the diabetes patients display excess build-up of fat in their livers, causing the organ to be less responsive to insulin and ending up with a higher level of glucose left in the blood (74).

Skeletal muscles are part of the muscular system that is attached by the tendons to the bones. Glucose, the key fuel for muscle movements, enters muscle cells through insulin-induced Glucose transporter type 4 (GLUT4), resulting in an increase in ATP required for muscle

contraction (75). However, in diabetes, muscle strength is reduced, and thus the ability of the muscles to take up glucose is impaired. Recent research also reported that building muscle mass may lower diabetes risk in prediabetic patients.

In summary, adipose tissue, muscles, and livers are heavily implicated in diabetes and are commonly used in a variety of cross-sectional studies investigating diabetes. Therefore, samples from these tissues will be used in this study to assess the metabolic state of the mice.

1.4.3 Insulin resistance

Insulin is an anabolic peptide hormone that is stimulated to be secreted by pancreatic beta cells when blood glucose levels rise. When glucose level is above 100 mg/dL in a healthy individual, insulin release is triggered for glucose clearance in the blood by signaling the insulin-responsive tissues, including liver, muscle, and adipose tissue, to uptake glucose.

It is now well established that diabetes is associated with insulin resistance, also known as insulin insensitivity. In a diabetic state, insulin cannot effectively signal adipose tissue, liver, or skeletal muscles to uptake glucose. Furthermore, impaired insulin actions increase gluconeogenesis to release glucose into the circulation. This repression of glucose uptake and release of glucose together increase blood glucose levels in T2DM patients.

Ample evidence demonstrated that elevated plasma free fatty acids (FFA) and proinflammatory cytokines induce skeletal muscle and liver insulin resistance, accompanied by an increase in circulating lipid metabolites, which activate a serine/threonine kinase cascade to inhibit IRS, thereby impairing the insulin signaling pathway (66, 76, 77). Normally, when insulin binds to the α subunit of the insulin receptor (IR), the tyrosine kinase in the β subunit is phosphorylated and activated. This activates the autophosphorylation of the β subunit, leading to the amplification of the kinase activity by phosphorylation of Tyr-1158, Tyr-1162, and Tyr 1163 (78). Insulin receptor tyrosine kinase phosphorylates IRS, which transmits signals downstream by activating the PI3-kinase/Akt pathways (79). Akt, also called protein kinase B (PKB), leads to insulin effects on the liver, including glycogen synthesis, through activating glucose transporter type 4 (GLUT4) to move to the cell surface and start transporting glucose into the cell. However, an increase in FFA or cytokines activates a serine kinase cascade. Serine phosphorylation of IRS protein results in a decreased ability of IRS in recruiting PI3 kinase. As a result, downstream

effectors such as Akt are impaired. Studies in multiple insulin-resistant rodent models reveal hyper-serine phosphorylation of IRS-1 on Ser 302, Ser 307, Ser 612, and Ser 632 (78). Thus, increased levels of FFA and proinflammatory cytokines induce serine phosphorylation of IR or IRS, thereby resulting in downstream insulin resistance. Details of how inflammation plays an important role in insulin resistance will be discussed in section 1.4.5.

1.4.4. Evidence of AD as Type 3 diabetes

A considerable amount of literature has been published on T2DM increasing the risk of AD (80). There is a growing body of literature that recognizes insulin resistance in the brain, and the accelerated accumulation of misfolded Aβ as well as hyperphosphorylated Tau (p-Tau) proteins in the pancreases of T2DM animal models (81, 82). On the other hand, memory loss and impaired executive function are also observed in T2DM individuals, especially in older adults (60). Even in the absence of T2DM, insulin resistance is implicated in accelerated age-related cognitive decline (83, 84). T2DM patients display an increased risk of developing MCI, dementia, or AD, and AD patients show progressive brain insulin resistance and insulin deficiency. Hence, it is now well established from a variety of studies, that AD is also called "Type 3 diabetes" (79, 85).

Clinical trials have demonstrated that intranasal insulin improves both memory performance and metabolic integrity of the brain in AD and MCI patients (86). When insulin is delivered through nasal administration, it can enter the brain through olfactory nerve (86). Therefore, alterations in the brain's insulin metabolism have been suggested as a pathophysiological factor underlying the AD mechanism (84, 87, 88). Accumulating evidence supports the idea that reduced glucose utilization and deficient energy metabolism occur early in the course of AD progression, suggesting a role for impaired insulin signaling in the pathogenesis of AD. Growth factor levels are markedly decreased in central nervous system (CNS) neurons, leading to abnormal insulin signaling in the AD brains (79, 89). Reduced expression of insulin and IGF-I and their receptors suggest that AD may represent a neuro-endocrine disorder that resembles (but remains distinct from) diabetes (85).

On a molecular level, data from several studies suggest that the insulin signaling pathway is involved in tau phosphorylation. Many biological responses, including survival, energy

metabolism, and inhibition of apoptosis are signaled through IRS molecules. Tau can be regulated by insulin/ insulin-like growth factor-1 (IGF-1) stimulation as tau phosphorylation and ubiquitination increase with activation of glycogen synthase kinase-3 (GSK-3) (85, 90, 91). GSK-3, as a downstream target of PKB, can phosphorylate tau, reduce its affinity, and promotes tangle-like filament morphology (92). Under normal conditions, the activity of GSK-3 can be downregulated by insulin or IGF-1 through the PI3 Kinase pathway. However, with the insulin/IGF-1 signaling mechanism impaired or reduced, GSK-3 is no longer downregulated by PKB and is able to phosphorylate tau (90) (Figure 1.1).

So far, very little attention has been paid to understanding why certain T2DM patients are more susceptible to developing AD. Hence, the molecular mechanism accounting for the link between diabetes and AD is not well established.

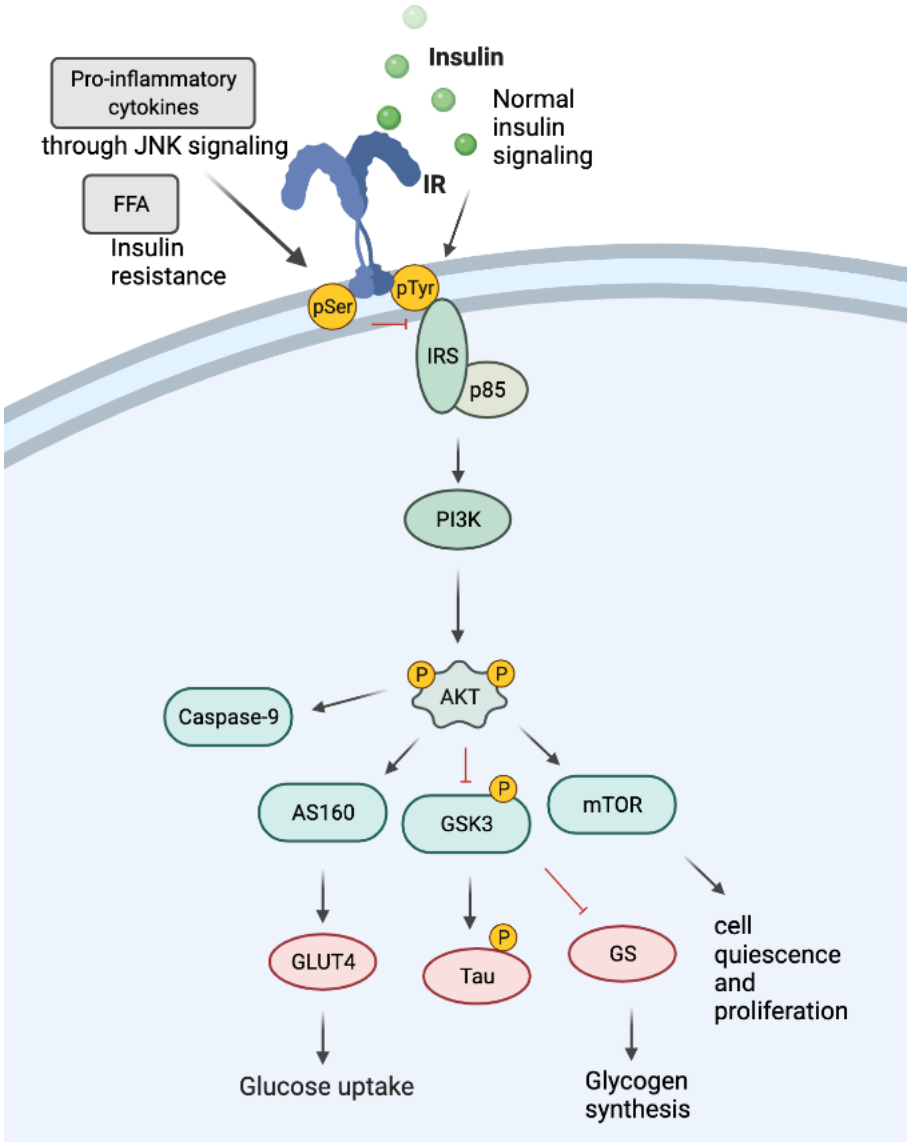

Figure 1.1 Schematic illustration of insulin signaling pathway and its role in AD

Insulin binding to insulin receptor tyrosine kinase phosphorylates IRS, signaling downstream cascades by activating the PI3-kinase/Akt pathways to activate GLUT4 transporting glucose into the cell. Under normal conditions, this pathway also downregulates GSK-3 which phosphorylates Tau and glycogen synthase. Under conditions of insulin resistance, insulin signaling is impaired due to the activation of the serine kinase cascade.

1.4.5 The role of inflammation in diabetes, insulin resistance, and Alzheimer's disease

Recent evidence suggests that obesity and diabetes are associated with chronic inflammation. Higher levels of circulating c-reactive protein (CRP) and inflammatory cytokines are found in T2DM patients (93). In healthy individuals, insulin binding leads to glucose uptake in muscles and adipose tissues through the insulin signaling pathway. However, in T2DM patients, this process is disrupted, thereby resulting in insulin resistance (94). Moreover, T2DM individuals have expanded adipose tissues with reduced blood flow and thus a lack of oxygen in the fat depots. This hypoperfusion leads to adipose tissue death, triggering adipocytes debris to recruit adipose tissue macrophages (ATMs) to release pro-inflammatory cytokines (95). The production of cytokines further downregulates insulin signaling through activating serine/threonine kinases (for example, IκB kinase and c-Jun N-terminal kinase (JNK)) which in turn phosphorylate IRS at its serine sites. In addition, adipose cell expression of TNF-α plays an essential role in insulin resistance in T2DM and obesity (63). These cytokines can also cross the BBB to induce an inflammatory response in the brain (63, 70). Excess chemical triglycerides can also be accumulated in the liver as triglycerides, causing non-alcohol fatty liver disease (NAFLD) (74). Circulating proinflammatory cytokines inhibit insulin signaling in hepatocytes through activating suppressors of cytokine signaling (SOCS) proteins and kinases including JNK, IKKb, and PKC to phosphorylate the serine sites of IRS-1, resulting in hepatic insulin resistance (76).

As the most well-known risk factor for diabetes, high-fat diet (HFD)/obesity induces inflammation (77, 96). HFD increases the level of FFA, which results in a change in the microbiota population in the gut. This change causes an increase in gut permeability, allowing more lipopolysaccharide (LPS) into the circulation. LPS binds to and upregulates toll-like receptors (TLR), resulting in elevated production of cytokines. FFA can also cross the BBB to

activate the hypothalamic IKKb/ Nuclear factor kappa B (NF-κB) signaling pathway, upregulating pro-inflammatory gene expression and cytokine production in the CNS, thereby mediating neurodegeneration (54, 97, 98).

Several investigations have reported a strong correlation between peripheral inflammation and cognitive dysfunction in AD patients (22, 46, 99). Inflammation disrupts insulin signaling mechanisms by increasing the serine phosphorylation of IRS. Diabetes and AD share a similar chronic inflammatory pathway, as enhanced levels of inflammatory markers such as IL-6, IL1-β, and TNF-α are detected in both CNS and plasma of diabetes and AD individuals (100). Chronic peripheral inflammation caused by diabetes may damage and penetrate the BBB to initiate brain-specific inflammation (101). Proinflammatory cytokines in the brain accelerate the rate of apoptosis and synaptic dysfunction, contributing to neuronal death (42). In addition, elevated IL-6 and TNF-α have inhibitory effects on Aβ clearance (99). Activated microglia are found to localize in the Aβ plaques in the AD neocortex. Accumulation of Aβ leads to microglia action, increasing the production of TNF-α and other pro-inflammatory cytokines. In AD patients' CSF, TNF-α concentration can rise 25-folder higher than those of age-matched healthy individuals (102). Increased pro-inflammatory cytokines in the brain subsequently phosphorylate IRS-1 serine to downregulate brain insulin signaling. Moreover, insulin resistance and alterations in insulin levels in T2DM also impact the functionality of neurons and glial cells (103, 104). Multiple epidemiological studies have also found that long-term use of non-steroidal anti-inflammatory drugs (NSAID) can delay the development of AD (105). Hence, chronic inflammation is a primary marker and mechanism of diabetes and AD pathogenesis, connecting these two conditions.

1.5 The role of C/EBPβ in Alzheimer's disease and metabolic diseases

1.5.1 C/EBPβ: General Introduction

C/EBPβ belongs to the CCAAT/enhancer-binding protein (C/EBP) family of basic leucine-zipper (bZIP) transcription factors (106). It regulates gene expression through binding a deoxyribonucleic acid (DNA) binding site (consensus sequence CCAAT), which presents in many gene promoters and enhancer regions. C/EBPβ contains a basic leucine zipper (bZIP) domain at the carboxyl-terminus (C-terminus) which is essential in dimerization and DNA binding. Members of the C/EBP family form homodimers or heterodimers with other C/EBPs and with other transcription factors, which may or may not contain the leucine zipper domain. The dimerization is required for C/EBPβ binding with DNA (106, 107).

To date, C/EBPβ gene has been cloned and characterized in different species, including mice, rats, and humans. C/EBPβ is expressed throughout the body, especially at high levels in the intestine, liver, and lungs. Four isoforms of C/EBPβ are full-length C/EBPβ (38kDa), liver-enriched activator protein (LAP, transcriptional activator, 35 kDa), liver-enriched inhibitor protein (LIP, transcriptional inhibitor, 20 kDa), and a small 16 kDa isoform (106). The substantial sequence identity in the C-terminal 55-65 amino acid residues, where the bZIP domain is located, is shared by all four isoforms. The expression of C/EBPβ can be regulated on various levels during different physiological and pathophysiological conditions by a broad range of factors, such as hormones, cytokines, nutrients, and toxins. Studies over the past two decades have provided important information on C/EBPβ's role in inflammation, metabolism, and cellular proliferation and differentiation (49, 106, 108-110).

1.5.2 The role of C/EBPβ in Alzheimer's disease

C/EBPβ is an inflammatory cytokine-mediated transcription factor that can also be regulated by inflammatory cytokines (110, 111). Previous studies have reported that C/EBPβ is heavily involved in inflammation in neurodegenerative diseases and brain injury (109, 110, 112, 113). It is also implicated in learning and memory (114). Multiple investigations have also identified the upregulation of C/EBPβ in AD and found that Aβ can mediate C/EBPβ action in glial cells (115-117). C/EBPβ deficiency has a protective effect against excitotoxic injuries and brain damage (113, 118, 119). Moreover, C/EBPβ plays a role in aging and liver regeneration (120). Deprivation of brain-derived neurotrophic factor (BDNF)/TrkB upregulates pro-inflammatory cytokines and the Janus kinase 2/signal transducer and activator of transcription 3 (JAK2/STAT3) pathway. As a result, the level of C/EBPβ is upregulated and subsequently elevates AEP expression, triggering APP and tau fragmentation and other AD manifestations (121). Recently, our lab has reported that C/EBPβ promotes AD pathogenesis in various AD mouse models through increasing both delta-secretase (AEP) and inflammatory cytokines expression. C/EBPβ plays a pivotal role in regulating AEP expression in the CNS neurons in an age-dependent manner. 3xTg (APPswe, $PS1_{M146V}$, Tau $_{P301L}$) mice with C/EBPβ overexpression display earlier onset of AD-like pathologies while 5XFAD ($APP_{KM670/671NL\ (Swedish)}$, APP_{I716V}, APP_{V717I}, $PSEN1_{M146L\ (A>C)}$, $PSEN1_{L286V}$) mice with depletion of C/EBPβ exhibit restoration of memory decline and other AD hallmarks. Deletion of C/EBPβ alleviates AD pathologies by abating AEP expression (122). C/EBPβ is also a key transcription factor for regulating APP, BACE1, and MAPT gene expression (123). On top of that, C/EBPβ regulates *ApoE* and preferentially mediates *ApoE* 4 expression in AD. AD mouse models with C/EBPβ knockout show reduce *ApoE* expression and senile plaques. Stronger activation of C/EBPβ was observed

in human AD neurons and brains when the allele is *ApoE* 4/4 versus *ApoE* 3/3 (123).

1.5.3 The role of C/EBPβ in inflammation and metabolism

C/EBPβ is transcriptionally activated by inflammatory cytokines such as IL-6, IL-1β, and TNF-α and bacterial LPS (49). When the transactivation domain of C/EBPβ is phosphorylated by inflammatory stimuli, C/EBPβ gene transcription increases (124). On the other hand, C/EBPβ feeds back and elevates the expression of certain proinflammatory genes (111).

Existing research also recognizes the critical role played by C/EBPβ in metabolism. Mice with a deletion of the C/EBPβ gene show fasting hypoglycemia, impaired hepatic glucose production, and decreased blood lipids (125, 126). C/EBPβ mediates adipose tissue differentiation, glucose and insulin metabolism, triacylglycerol metabolism, hepatic steatosis, endoplasmic reticulum (ER) stress, inflammation, etc. (107). C/EBPβ also induces PPAR-γ transcription during the early stage of adipogenesis. Mice with C/EBPβ deficiency show impairments in white adipocyte development because the lipids cannot be stored inside the adipocytes, even with the presence of PPAR-γ (127). Studies of Wnt-β signaling also demonstrate the importance of C/EBPβ in adipogenesis. C/EBPβ inhibits Wnt-β and Wnt-β can inhibit activation of PPAR-γ, and thus C/EBPβ deletion may lead to impairments in adipogenesis (128). In addition, C/EBPβ is increased in β cell lines exposed to high glucose concentrations as well as in pancreatic islets of diabetic animals, and it inhibits insulin mRNA transcription in β cell lines (129). C/EBPβ deletion results in the downregulation of hepatic lipogenic genes and increased expression of β-oxidation genes in brown adipose tissue (BAT). Since C/EBPβ is implicated in mediating insulin and IR expression, C/EBPβ knockout mice are resistant to HFD-induced obesity (130).

1.5.4 C/EBPβ regulates AEP expression

Our lab has reported that C/EBPβ regulates AEP mRNA transcription and protein expression in an age-dependent manner, acting as a transcription factor for AEP increasing both delta-secretase (AEP) and inflammatory cytokines expression in promoting pathogenesis in AD mouse models. C/EBPβ binds to the Site 2 motif in the promoter of *LGMN*, which encodes AEP, thereby mediating its mRNA transcription Knockdown of C/EBPβ reduces AEP levels in primary neurons. Silencing C/EBPβ diminished oxygen-glucose deprivation (OGD)-induced protein and mRNA levels and Aβ induced an increase in AEP. We have also observed a concomitant increase in the expression of both C/EBPβ and AEP in an age-dependent manner in mice and human brain samples.

C/EBPβ overexpression escalates AEP expression and triggers APP and Tau fragmentation, accelerating neuronal cell loss and cognitive dysfunction in young 3xTg mice. Inhibiting AEP by co-expression of the dominant-negative C189S mutant significantly attenuates these C/EBPβ induced effects. Reduction of C/EBPβ decreases AEP expression and subsequent AD-like pathologies such as Aβ production, learning defects, and cognitive dysfunction in old 5XFAD mice. Hence, the evidence together suggests that C/EBPβ/AEP signaling pathway plays an essential role in AD pathogenesis (122).

1.6 The role of Asparagine endopeptidase (AEP) in Alzheimer's disease

1.6.1 AEP: General Introduction

Asparagine endopeptidase (AEP, also called legumain, gene name: *LGMN*) is an endo-lysosomal cysteine protease that cleaves peptide bonds C-terminally to asparagine residues. It was first identified in legume seeds but is now detected in a broad range of plants and animals. AEP can be detected in the brain, spleen, liver, and heart (131). It is especially abundant in the kidney as it is required for normal protein degradation (132). The protein is predominantly localized to the lysosomes and the endosomes. AEP is synthesized as a zymogen, but it can be activated from a zymogen (56 kDa) to its active form (46 kDa) under acidosis by removing pro-peptides (133). This post-translational process is autoproteolysis for catalytic activation. The mature form of AEP with high enzymatic activity is roughly 37 kDa. It has been shown that AEP plays an important role in immunity and cancer progression. AEP enhances the effect of checkpoint inhibitors drugs, such as Programmed cell death protein 1 (PD-1) antibodies, in treating advanced melanoma (134). Additionally, AEP is implicated in promoting cancer cell invasiveness (135).

AEP's biological role in the brain was first reported by our lab in 2008. We found that AEP is activated under acidic conditions induced by epilepsy and ischemia in the brain. Activated AEP can cleave SET, which is a DNAse inhibitor. This leads to DNA damage and neuronal cell death. SET also inhibits protein phosphatase 2A (PP2A), which plays an important role in tau regulation, and thus, AEP cleavage of SET also results in Tau hyperphosphorylation in AD. PIKE-L (PI3-kinase enhancer long isoform) inhibits the cleavage and degradation of SET by AEP, thereby resulting in resistance to neuronal cell death. In addition, AEP mediates stroke-induced SET cleavage and neuronal death in the brain (136).

1.6.2 AEP-cut APP and tau promote Alzheimer's disease pathogenesis

Our lab has previously reported that AEP, acts as δ-secretase, cleaves both tau and APP. AEP cuts tau at N255 and N368, and abolishes its binding to microtubules, resulting in NFT formation and cognitive dysfunctions. AEP cleaved tau 1–368 fragment is neurotoxic and prone to aggregate into filamentous structures which form paired helical filaments (PHFs). AEP cleavage of tau impairs the functions of tau in binding to and stabilization of microtubules. Primary neurons transfected with a variety of tau fragments exhibit not only increased apoptosis and neurotoxicity but also increased hyperphosphorylation and aggregation of tau. Deleting AEP in Tau P301S (PS19) transgenic mice alleviates AD pathologies, reversing the synaptic plasticity defect and cognitive dysfunction (137-139). Blockade of AEP with a small molecular inhibitor diminishes senile plaques and NFT pathologies in both the 5XFAD and tau P301S mouse models, rescuing cognitive disorders (137). On the other hand, AEP cuts APP at both the N373 and N585 residues and enhances Aβ production by decreasing the steric hindrance for BACE1. Primary neurons with AEP-cleaved APP fragments show elevated Aβ production and neuronal cell death. 5XFAD or APP/PS1 mice with AEP deletion show reductions in senile plaques, improved long-term potentiation, and better performance in memory tests (138, 139). Several studies also reported that AEP expression levels are elevated in the brains of aged mice and AD patients. AEP activity is higher in brains of AD patients compared with healthy controls (138). Additionally, AEP regulates nervous system regeneration and locomotor recovery after spinal cord injury in zebrafish (140). Our lab also reported the therapeutic effect of a brain permeable AEP inhibitor, compound 11. Long-term treatment of compound 11 in P301S and 5XFAD transgenic mice alleviate tau and APP fragmentation and improve learning and memory (141). Hence, AEP plays a pivotal role in mediating AD pathology and is an innovative therapeutic

target for neurodegenerative diseases.

1.6.3 The Role of AEP in Metabolic Diseases

The *LGMN* gene was identified as a key mediator in pancreas regeneration. Pancreatic β cell deterioration is associated with diabetes, and thus, the regeneration of β cells has been an essential approach in diabetic treatments. Researchers have screened for genes that exhibit high mRNA levels after pancreatectomy, using subtractive hybridization and DNA sequencing, and found that *LGMN* changes the expression of islet cell marker genes. Therefore, *LGMN* may be a target in diabetes gene therapy (142). A research study also reported that in acidic conditions, such as diabetes, AEP cleaves and inhibits SET/I2PP2A, which contributes to tau hyperphosphorylation in AD. This work suggests the role of AEP in diabetes and hyperglycemia (143). Additionally, AEP plays an important role in the cell growth of multiple myeloma (MM) under chronic hypoxia. Increased glucose metabolism is a direct mechanism underlying hypoxia in MM cells and AEP is increased in primary MM cells compared to control cells. Depletion of AEP in MM cells leads to a proliferation defect and reduced cellular viability under chronic hypoxia. Thus, AEP might be a promising therapeutic target in MM (144). Recently, experiments performed on human renal tubular epithelial cells (hRTE) revealed that the lysosome was identified as the most affected organelle in response to elevated glucose concentration. As a lysosomal gene, *LGMN* shows a marked reduction in its expression when exposed to high glucose levels, as suggested by global gene expression analysis (145). However, the mechanism underlying this reduction is still unknown. Although multiple studies indicate that AEP is involved in cancer, hyperglycemia, and pancreas regeneration, there remains a paucity of evidence on the function of AEP in glucose and lipid metabolism. The findings of this study should make a contribution to research on AEP by demonstrating its role in diabetes and

insulin resistance.

1.7 Dissertation Overview

Mounting evidence has established that inflammation plays a critical role in linking diabetes and AD pathology (89, 146, 147). Activated by inflammatory cytokines, C/EBPβ regulates AEP mRNA transcription and protein expression in an age-dependent manner, promoting AD pathogenesis (111, 122). Thus, we hypothesize that neuronal C/EBPβ may modulate insulin signaling in the brain and peripheral tissues, coupling diabetes to AD. In the current study, we investigated if inflammation activated-neuronal C/EBPβ/AEP signaling links HFD-induced diabetes to AD pathology in Thy1-C/EBPβ transgenic mice. We also interrogated whether AEP depletion might alleviate diabetes and AD onset. In order to further understand the role of inflammation, we treated mice with the NSAID, aspirin, to reduce their inflammation levels and examine their AD pathologies. This study aims to contribute to this growing area of research by exploring the link between diabetes and AD. Both qualitative and quantitative methods were used in this study.

CHAPTER 2: Materials and Methods

2.1 Animals

Wild-type C57BL/6J and C/EBPβ -/- were purchased from the Jackson Laboratory (MMRRC stock # 000664 and #006873, respectively). Since some of the homozygous mutations are lethal on pure-strain backgrounds, C/EBPβ mice were maintained as heterozygotes on two separate strain backgrounds (C57BL/6 and 129Sv).

For the generation of the Thy1-human C/EBPβ transgenic mouse, mouse genomic fragments containing homology arms (HAs) were amplified from bacterial artificial chromosome (BAC) clones by using high fidelity Taq and were sequentially assembled into a targeting vector together with recombination sites and selection markers. After confirming correctly targeted ES clones via Southern Blotting, we selected some clones for blastocyst microinjection, followed by founder production. Founders were confirmed as germline-transmitted via crossbreeding with wild-type. In the end, male and female F1 heterozygous mutant mice were confirmed as the final deliverables for this project. The genotypes of transgenic mice were validated by PCR (Figure 3.1).

AEP-knockout (AEP-/-) mice on a mixed C57BL/6 and 129/Ola background were generated as reported (Shirahama-Noda, 2003, 278, 33194). The following animal groups were analyzed: WT, Thy1-C/EBPβ, C/EBPβ$^{+/-}$, C/EBPβ/AEP$^{-/-}$. Both female and male mice were used.

2.2 LPS treatment

LPS (from Escherichia coli 055:B5; Sigma, St. Louis, MO) was dissolved in PBS at a concentration of 0.1 mg/ml and administered intraperitoneally to 2.5-month-old mice (n = 8-10 per group; half males and half females) twice per week for 6 weeks at a dose of 0.5 mg/kg body weight. Control groups (n = 8-10 per group; half males and half females) received injections in the same manner with PBS only. The body weight of each mouse was recorded weekly. After 1.5- months of behavioral tests, mice were sacrificed for pathological assessments. An additional injection of LPS (i.p. 0.5 mg/kg) was administered to activate C/EBPβ 24 h before sacrifice. Animal care and handling were performed according to the NIH animal care guidelines and approved by the Emory Institutional Animal Care and Use Committee.

2.3 HFD treatment

Twelve-week-old female mice were fed with chow or HFD (D12079B, Research Diets) for 12 weeks. The body weight of each mouse was recorded biweekly. After 1.5- months of behavioral tests, mice were sacrificed for pathological assessments. The protocol was reviewed and approved by the Emory Institutional Animal Care and Use Committee.

Aspirin treatment: Aspirin treatment was given for the last 4 weeks of HFD through pH 6.4 drinking water (120 mg/kg body weight/day). The protocol was reviewed and approved by the Emory Institutional Animal Care and Use Committee. (Figure 2.1)

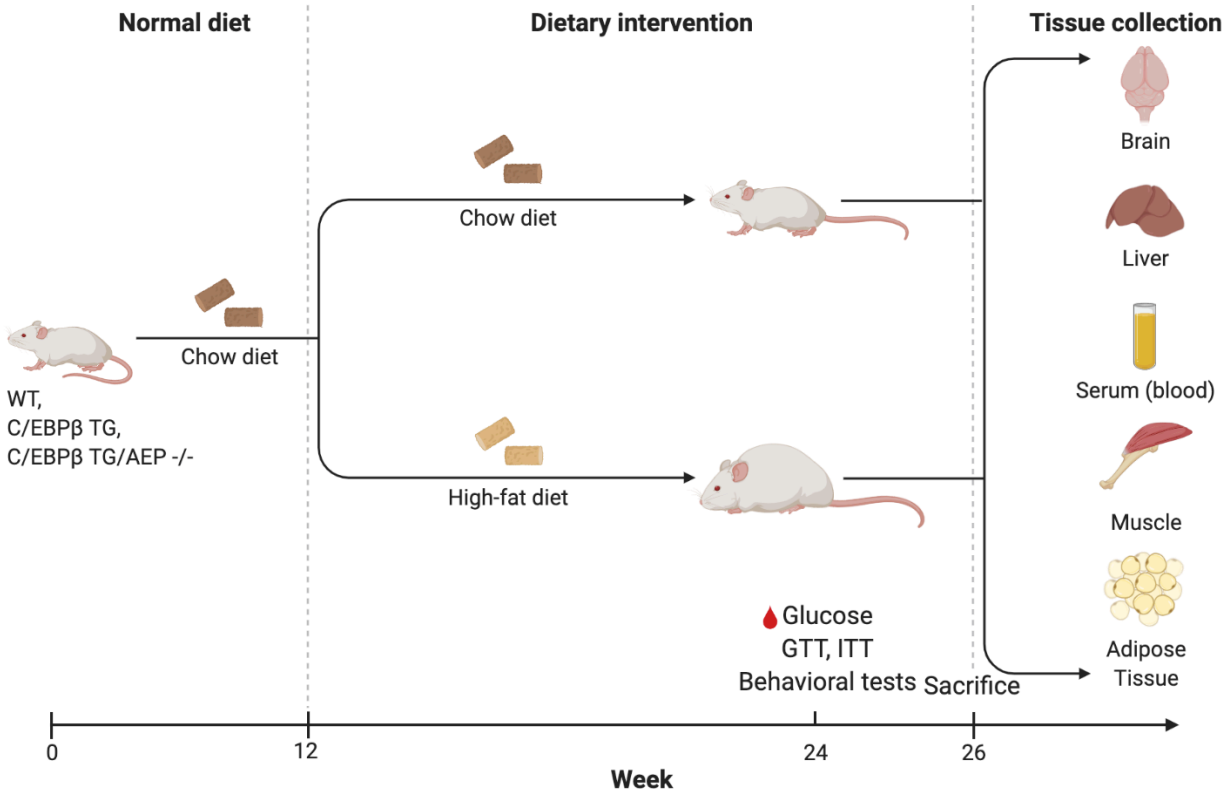

Figure 2.1 Schematic illustration of the HFD and sample collection timeline

Chow or HFD (D12079B, Research Diets) were fed to 12-week-old female mice for 12 weeks. Each mouse's body weight was measured twice a week. Mice were euthanized for pathological evaluations after 1.5 months of behavioral testing, GTT (glucose tolerance test), and ITT (insulin tolerance test).

2.4 AEP activity assay

Tissue homogenates or cell lysates (50 µg) were incubated in 100 µL reaction buffer (20 mM citric acid, 60 mM Na_2HPO_4, 1 mM EDTA, 0.1% CHAPS and 1 mM DTT, pH 5.5) containing 10 µM AEP substrate Z-Ala-Ala-Asn-AMC (Bachem). AMC released by substrate cleavage was quantified by measuring at 460 nm in a fluorescence plate reader at 37°C in kinetic mode.

2.5 Immunoblotting analysis

Mouse brain tissue samples were lysed in lysis buffer (50 mM Tris, pH 7.4, 40 mM NaCl, 1 mM EDTA, 0.5% Triton X-100, 1.5 mM Na3VO4, 50 mM NaF, 10 mM sodium pyrophosphate, 10 mM sodium-glycerophosphate, supplemented with protease inhibitors cocktail) on ice for 30 minutes. For the experiment *in vitro*, cells were lysed in RIPA buffer (20 mM Tris-HCl pH 7.5, 150 mM NaCl, 1 mM Na_2EDTA, 1 mM EGTA, 1% Triton X-100, 2.5 mM sodium pyrophosphate, 1 mM beta-glycerophosphate, 1 mM Na_3VO_4, 1 µg/mL leupeptin, 1 mM phenylmethylsulfonyl fluoride) on ice for 30 minutes. The lysates were centrifuged for 10 minutes at 15,000 rpm. Protein concentration from the supernatant was determined using a Coomassie Brilliant Blue protein assay kit (Bio-Rad). The same amount of the supernatant was boiled in the SDS loading buffer. After SDS-PAGE, the samples were transferred to a nitrocellulose membrane. The membranes were blocked in 5% non-fat milk for 1 hour at room temperature and then incubated with primary antibody at 4°C overnight. Primary antibodies to the following targets were used. Then the blots were incubated with IRDye 800CW-conjugated affinity-purified anti-mouse or anti-rabbit IgG secondary antibody (Rockland). Immunoreactive bands were visualized using Odyssey Infrared Imaging System (Licor Biosciences, Lincoln, NE, USA).

2.6 Metabolic Measurements

All animal experiments were performed according to the care of experimental animal guidelines from Emory University. Twelve-week-old female mice were fed with chow or HFD (Research Diets) for 12 weeks. Blood glucose level was measured using the Advanced Bluetooth Glucose Meter (CVS Health) sampled from the tail vein during both fed and 16-hour fasted states. Serum and brain insulin was measured by ELISA (Crystal Chem). Serum Leptin was measured by ELISA (Invitrogen). Triglyceride, cholesterol, and free fatty acids levels in serum and brain lysates were measured by Diagnostic Lab, Division of Animal Resources (Emory University). Serum and brain tumor necrosis factor-α (TNF-α), IL-1β, and IL6 were measured by ELISA (Thermo Fisher).

2.7 Glucose and insulin tolerance tests

A glucose tolerance test (GTT) was performed on 16-hours fasted mice after peritoneal injection of D-glucose (2 g/kg body weight). Each mouse was weighed before the injection to determine the dose. Blood samples from the tail vein were determined at different time points at 0-minute, 15-minute, 30-minute, 60-minute, and 90-minute post-injection. For the Insulin tolerance test (ITT), the mice fasted for 6 hours. Each mouse was weighed and received an intraperitoneal injection of insulin (0.75U/kg body weight). Blood glucose levels from the tail vein were determined at 0-minute, 15-minute, 30-minute, 60-minute, and 90-minute post-injection.

2.8 Immunostaining and Thioflavin S staining

IHC staining was performed with the immunohistochemistry staining kit (Invitrogen). Briefly, 4% paraformaldehyde (PFA)-fixed mice brain frozen slides were treated with 3% hydrogen peroxide at room temperature for 10 minutes. Manufacturer-supplied blocking buffer

(Invitrogen) was used for each reaction. Then the sections were incubated with primary antibodies overnight at 4 °C. Biotin-conjugated secondary antibodies (Jackson ImmunoResearch), and streptavidin-conjugated HRP (Invitrogen) were applied to enhance the signals. For double immunofluorescence staining, brain sections were incubated with an Alexa Fluor 488 or 568 conjugated isotype-specific secondary antibody (Jackson ImmunoResearch, West Grove, PA) for 1 hour at room temperature. For Thioflavin S (ThS) + Aβ/AT8 double staining, slides were rinsed in PBS after finishing the Aβ/AT8 first antibodies and the second antibody staining. Freshly dissolved 3.125 mg Thioflavin S in 100 ml 50% Ethanol. Incubated the Aβ/AT8 stained slides in this solution at room temperature for 7 minutes in the dark. Then wash the slides in PBS three times. The fluorescence staining was visualized with an Olympus confocal microscope. Immunostaining images and their colocalization were quantified using Volocity 6.3 from Perkin Elmer and Fiji/ImageJ Coloc 2, respectively.

2.9 Oil red O staining

To identify adipocytes, liver samples were fixed overnight in 4% paraformaldehyde dissolved in PBS. Frozen sections from these livers were stained with Oil Red O working solutions for 8-15 minutes (Oil red O (Sigma-Aldrich)). Sections were rinsed in H_2O, immersed in diluted saturated Li_2CO_3, and eventually rinsed under tap water before mounting. The quantification of lipid droplets and accumulations are calculated through images imported into ImageJ (148) .

2.10 H&E staining

Fresh liver and white adipose tissues were fixed in 4% paraformaldehyde dissolved in PBS. The samples were sent to the Pathology Core Research Laboratory/Department of Pathology (University of Alabama at Birmingham) for sectioning, deparaffinization, and hematoxylin and

eosin (H&E) staining. Serial sections 5μm thick were cut from the formalin-fixed, paraffin-embedded tissue blocks and floated onto charged glass slides (Super-Frost Plus, Fisher Scientific, Pittsburgh, PA) and dried for at least 30min at 60° C. All sections for H&E stains were deparaffinized and hydrated using xylene (3 changes) and graded concentrations of ethanol (2 changes of 100% ETOH then 2 changes of 95% ETOH) to the tap water. The slides were stained in the Hematoxylin (STAIN HARRIS, Cardinal health, CAT#S7439-33) for 2 min, then differentiated in 1% Acid alcohol quickly (1 dip) and bluing in ammonia water (7 dips). After Hematoxylin stain, the slides were counterstained in Eosin (Stain Eosin-Y, Cardinal health, CAT#S7439-24) for 30 sec followed by graded concentrations of ethanol then xylene for clearing prior to the coverglass step using Paramount.

2.11 Golgi staining

Mouse brains were fixed in 10% formalin for 24 hours and then immersed in 3% potassium dichromate for 3 days in the dark. The solution was changed each day. Then the brains were transferred into a 2% silver nitrate solution and incubated for 24 hours in the dark. Vibratome sections were cut at 60 μm, air-dried for 10 minutes, dehydrated through 95% and 100% ethanol, cleared in xylene, and cover-slipped. For Sholl analysis, a template consisting of circles with consecutively increasing diameter was placed on the inverted pictures of the neurons, and the number of intersections was determined at every level.

2.12 Morris Water Maze

Mice were trained in a round, water-filled tub (52-inch diameter) in an environment rich with extra-maze cues. An invisible escape platform was in a fixed spatial location 1 cm below the water surface independent of the subject's start position on a particular trial. In this manner, the

subjects needed to utilize extra-maze cues to determine the platform's location. At the beginning of each trial, the mouse was placed in the water maze with their paws touching the wall from one of four different starting positions (N, S, E, W). Each subject was given four trials/day for five consecutive days with a 15-minutes inter-trial interval. The maximum trial length was 60 s, and if subjects did not reach the platform in the allotted time, they were manually guided to it. Upon reaching the invisible escape platform, subjects were left on it for an additional five seconds to allow for the survey of the spatial cues in the environment to guide future navigation to the platform. After each trial, subjects were dried and kept in a dry plastic holding cage filled with paper towels to allow the subjects to dry off. The temperature of the water was monitored every hour so that mice were tested in water that was between 22 and 25°C. Following the 5 days of task acquisition, a probe trial was presented during which time the platform was removed and the percentage of time spent in the quadrant which previously contained the escape platform during task acquisition was measured over 60 seconds. All trials were analyzed for latency and swim speed utilizing MazeScan (Clever Sys, Inc.).

2.13 Fear conditioning tests

The ability to form and retain an association between an aversive experience and environmental cues was tested with a standard fear conditioning paradigm that occurs over a period of three days. Mice were placed in the fear conditioning apparatus (7" W, 7" D 3 12" H, Coulbourn) composed of Plexiglass with a metal shock grid floor and allowed to explore the enclosure for 3 min. Following this habituation period, 3 conditioned stimuli (CS)-unconditioned stimulus (US) pairings were presented with a 1 min intertrial interval. The CS was composed of a 20 s, 85-dB tone, and the US was composed of 2 s of a 0.5-mA footshock, which was co-terminate with each

CS presentation. One minute following the last CS-US presentation, mice were returned to their home cage. On day 2, the mice were presented with a context test, during which subjects were placed in the same chamber used during conditioning on day 1, and the amount of freezing was recorded via a camera and the software provided by Coulbourn. No shocks were given during the context test. On day 3, a tone test was presented, during which time subjects were exposed to the CS in a novel compartment. Initially, animals were allowed to explore the novel context for 2 min. Then the 85-dB tone was presented for 6 min, and the amount of freezing behavior was recorded.

2.14 High-performance lipid chromatography (HPLC) analysis

Whole blood samples were deproteinized with 0.4 N PCA. The samples were vortex mixed vigorously several times and sat on ice for 15 min. The samples were centrifuged at 13000 rpm X 30 min twice at 4 ºC to remove the precipitation. The supernatant was 10 times diluted with 0.1 N PCA for the HPLC assay. Thiamine and thiamine pyrophosphate (TDP) were purchased from Sigma. The stock solutions were prepared in 0.1 N PCA. Thiamine and thiamine pyrophosphate were measured by Waters high-performance liquid chromatography system with 717 plus autosampler set at 4 ºC, model 1525 binary pump, and model 2996 photodiode array detector (Waters). Analytes were separated using reverse-phase chromatography on a Waters X bridge BEH column (4.6 × 150 mm, 3.5 µM, Waters) with a guard cartridge (3.9 × 5 mm, 5 µM, Waters) at room temperature. Mobile phase A was 8 mM 1-octane sulfonic acid sodium, pH 2.7 adjusted with phosphoric acid; mobile phase B was 1-octanesulfonic acid sodium (8 mM, pH 2.5): acetonitrile (50:50, vol/vol). Gradient steps were programmed as follows: 0% B for 10 min, ramped to 3% B in 1min, held at 3% B for 10 min; 3% - 50 % B in 5 min, held at 50% B for 10

min, 50% - 100% B in 0.5 min, held at 100% B for 5 min; returned to initial conditions during 0.5 min; and equilibrated for 17 min. Analytes were eluted at a flow rate of 1.0 ml/min. The injection volume was 200 µl. The compounds were detected at a wavelength of 247 nm. The analytes were identified by comparing their retention times and spectral profiles to known standards.

2.15 Quantification and Statistical Analysis

All data are expressed as mean ± s.e.m. from three or more independent experiments and analyzed using GraphPad Prism statistical software (GraphPad Software). All of the statistical details of experiments can be found in the figure legends for each experiment, including the statistical tests used, number of mice in animal experiments (represented as n, unless otherwise stated), number of wells in cell culture experiments (represented as n, unless otherwise stated), the definition of center (mean). The sample size was determined by Power and Precision (Biostat). The level of significance between the two groups was assessed with an unpaired t-test with Welch's correction. For more than two groups, one-way ANOVA and Bonferroni's multiple comparison test were applied. The two-way ANOVA and Bonferroni's post hoc test compared the differences between groups that have been split into two independent factors. A value of $p < 0.05$ was considered to be statistically significant.

2.16 Key Reagent and Resource

REAGENT or RESOURCE	SOURCE	IDENTIFIER
Antibodies		
phosho-C/EBPbeta	CST	3081s
phosho-C/EBPβ	CST	3084s

C/EBPβ Antibody (H-7)	Santa Cruz	sc-7962
Anti-AEP 6E3	Colin Watts Lab	N/A
Anti-AEP	R&D Systems	AF2199
Anti-APP	Sigma-Aldrich	SAB4200536
Anti-APP N585	Ye Lab	N/A
Anti-Tau FL (Tau5)	Abcam	ab80579
Anti-Tau N368	Ye Lab	N/A
Anti-Tau22	Abcam	ABN454
Anti-α-Tubulin	Sigma-Aldrich	T6074
Anti-beta-actin	Abcam	ab8227
Anti-Phospho-Tau Ser202, Thr205 (AT8)	Thermo Fisher	MN1020
Purified anti-β-Amyloid, 4G8	BioLegend	800712
Anti-Glial Fibrillary Acidic Protein (GFAP) antibody	Sigma-Aldrich	G3893
Anti-Iba1	VWR	019-19741
Anti-BACE1	CST	5606s
Anti-Synaptotagamine	Sigma	S2177
Anti-Spinophilin	CST	9061s
Anti-PSD95	CST	3450
Anti-Synapsin	CST	6710S
Anti-Glu2	Abcam	206293
Anti-Insulin Receptor β	CST	3025
Anti-Phospho-IGF-I Receptor β (Tyr1131)/Insulin Receptor β (Tyr1146)	CST	3021
Anti-IRS1 (C-20)	Santa Cruz	559
Anti-phospho-IRS1 (Ser307 mouse/ Ser312 human)	Sigma-Aldrich	**05-1087**
Anti-phospho-GSK-3α/β (Ser21/9)	CST	**9331**
Anti-GSK-3β	CST	**12456s**
Anti-AKT	CST	4691s
Anti-Phospho-(Ser/Thr) Akt Substrate	CST	**9611**

Anti-Phospho-AMPKα (Thr172)	CST	2535
Anti-AMPKα	CST	2532s
Anti-Phospho-Acetyl-CoA Carboxylase (Ser79)	CST	3661
Anti-Acetyl-CoA Carboxylase (C83B10)	CST	3676
Anti-Phospho-Tau Ser202, Thr205 (AT8)	Thermo Fisher	MN1020
Chemicals, Peptides, and Recombinant Proteins		
DAPI	Sigma-Aldrich	D9542
Aspirin	Sigma-Aldrich	A2093
Human insulin	Eli Lilly	00002831501
D-glucose	RPI	G32040
Oil Red O	Sigma-Aldrich	O0625
Critical Commercial Assays		
Amyloid beta 40 ELISA Kit, Mouse	Thermo Fisher	KMB3481
Amyloid beta 42 ELISA Kit, Mouse	Thermo Fisher	KMB3441
IL-1 alpha Mouse ELISA Kit	Thermo Fisher	88-5019-22
IL-6 Mouse ELISA Kit	Thermo Fisher	BMS603HS
TNF alpha Mouse ELISA Kit	Thermo Fisher	BMS607-3
TNF alpha Rat ELISA Kit	Thermo Fisher	KRC3011
Lysosome Enrichment Kit for Tissues and Cultured Cells	Thermo Fisher	89839
Advanced Glucose Meter Test Strips	CVS Health™	968577
Advanced Bluetooth Glucose Meter	CVS Health™	968574
Ultra-Sensitive Mouse Insulin ELISA Kit	Crystal Chem	90080
Leptin Mouse ELISA Kit	Invitrogen	KMC2281

CHAPTER 3: The role of C/EBPβ/delta-secretase signaling in HFD-induced diabetes and insulin resistance

3.1 Introduction

Over the past decades, the increasing availability of high-fat foods leads to common diets containing high levels of fat in modern society. However, not all individuals ingesting HFD develop diabetes and AD later in life, and thus, it is critical to understand the underlying etiopathology linking diabetes and AD. Chronic overnutrition, especially increased consumption of HFD, is a risk factor for both AD and diabetes. HFD is widely used as a treatment inducing diabetes and inflammation in different studies (69, 77). HFD induces systemic low-grade inflammation, increasing endotoxin LPS levels in the brain and peripheral tissues (94). HFD-induced inflammation is observed in the CNS and peripheral tissues, such as liver, muscle, and adipose tissue (149, 150). Since C/EBPβ levels can be escalated by inflammation, we expect that mouse models with C/EBPβ overexpression in the brain will develop diabetes with the increasing availability of high-fat food, while diabetes symptoms and hallmarks might be alleviated by AEP inhibition.

3.2 Results

3.2.1 High-Fat Diet (HFD) induces diabetes in Thy1-C/EBPβ transgenic mice

To investigate whether neuronal C/EBPβ escalation contributes to diabetes and AD pathology, we developed a neuronal-specific, Thy1 promoter-mediated human C/EBPβ transgenic mouse (Thy1-C/EBPβ Tg).

The single or double C/EBPβ Tg mice were viable and fertile, and the mice transgenes were validated by genomic DNA genotyping (Figure 3.1). The mouse Thy1 expression cassette drives transgene expression mainly to the CNS. “WT” is used to designate the non-transgenic littermates of Thy1-C/EBPβ transgenic mice, “C/EBPβ Tg” to designate hemizygous transgenic mice carrying a single copy of the human CEBPβ gene, and “C/EBPβ Tg/Tg” for homozygous transgenic mice carrying two copies of the gene. The protein levels of CEBPβ are quantified in Figure 3.2.

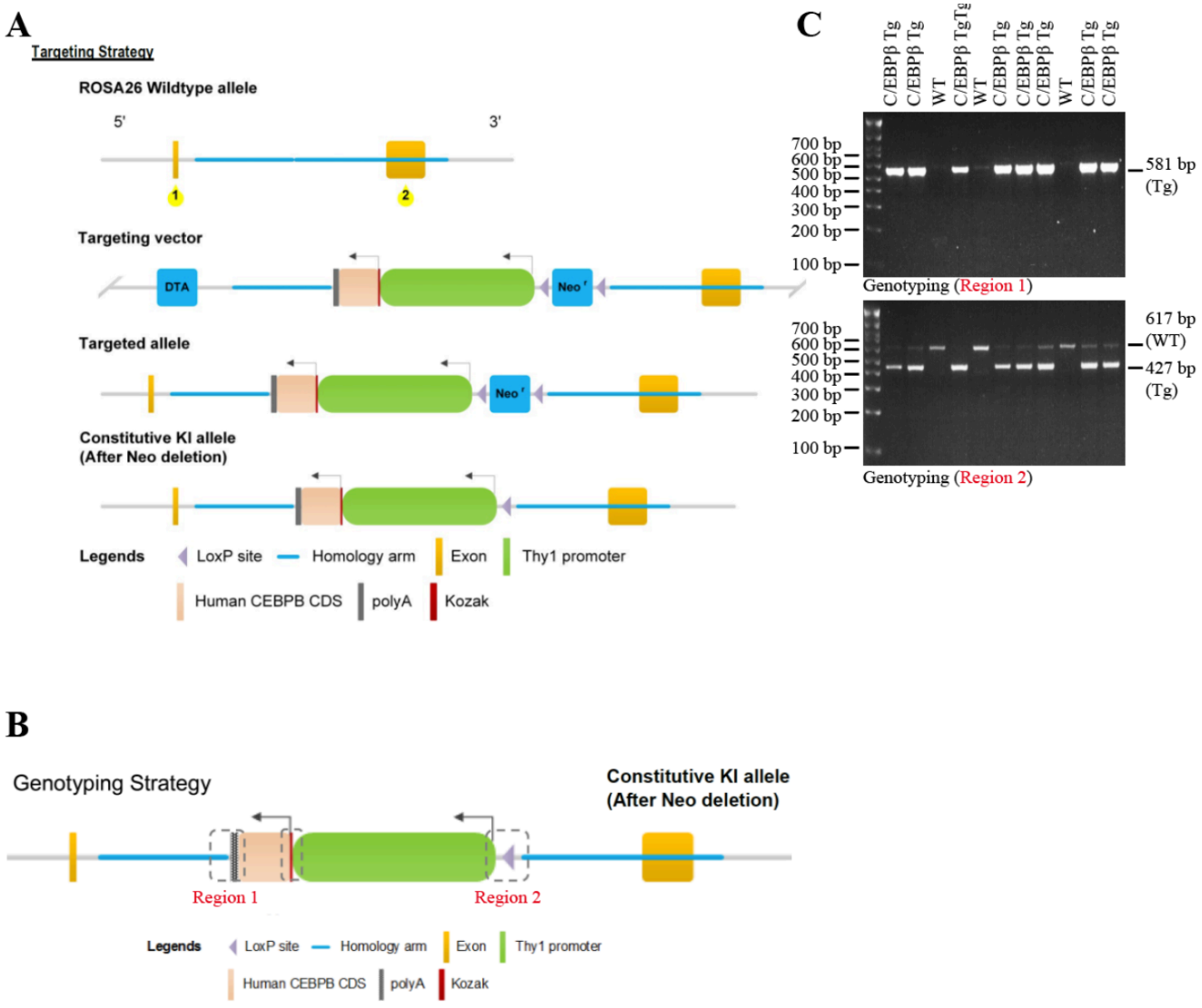

Figure 3.1: Generation of transgenic Thy1-C/EBPβ Transgenic mice

A&B. The schematic of the plasmid reveals the strategy used to develop the mice. The resultant mice were named C/EBPβ Tg. **C**. Genotyping of Non-Tg, C/EBPβ Tg, C/EBPc Tg/Tg mice. Wild-type mice only carry the WT band. Homozygotes only carry Tg band. Heterozygotes carry both bands (WT and Tg).

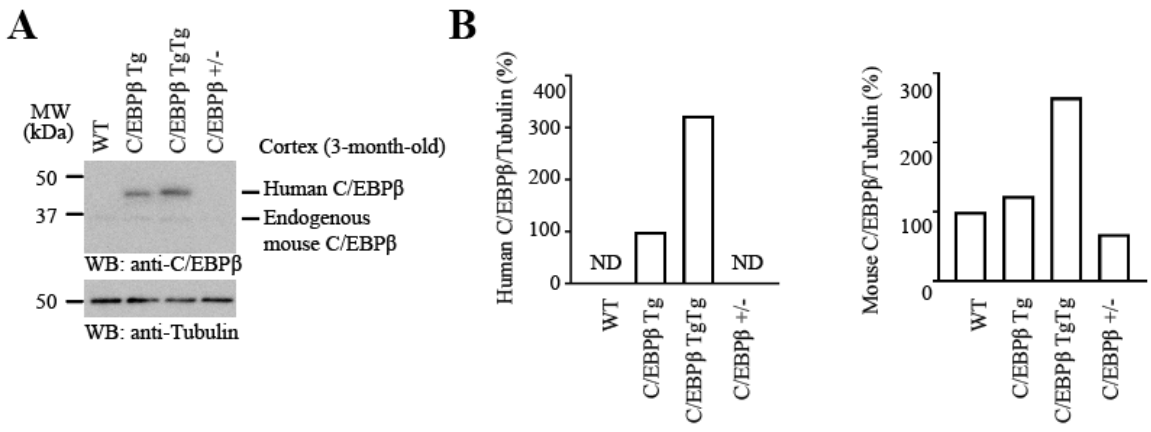

Figure 3.2 Quantification of C/EBPβ protein levels in Thy1-C/EBPβ Transgenic mice

A. Quantification of protein levels of human C/EBPβ and mouse C/EBPβ in the brain of the mice at 2 months of age (Mean ± SEM, n = 2, t-test, * $p < 0.05$, * * $p < 0.01$) and **B.** quantification of the ratios of human and mouse C/EBPβ/tubulin.

`

To induce Type 2 diabetes in these mice, we employed the high-fat diet (HFD) for 12 weeks of consecutive treatment. Immunofluorescent (IF) co-staining revealed that C/EBPβ levels were elevated and phosphorylated signals (p-C/EBPβ), a biomarker for its activation, was also enhanced in WT mice by HFD as compared to the chow diet. Both were further augmented in Thy1-C/EBPβ Tg mice (Figure 3.3).

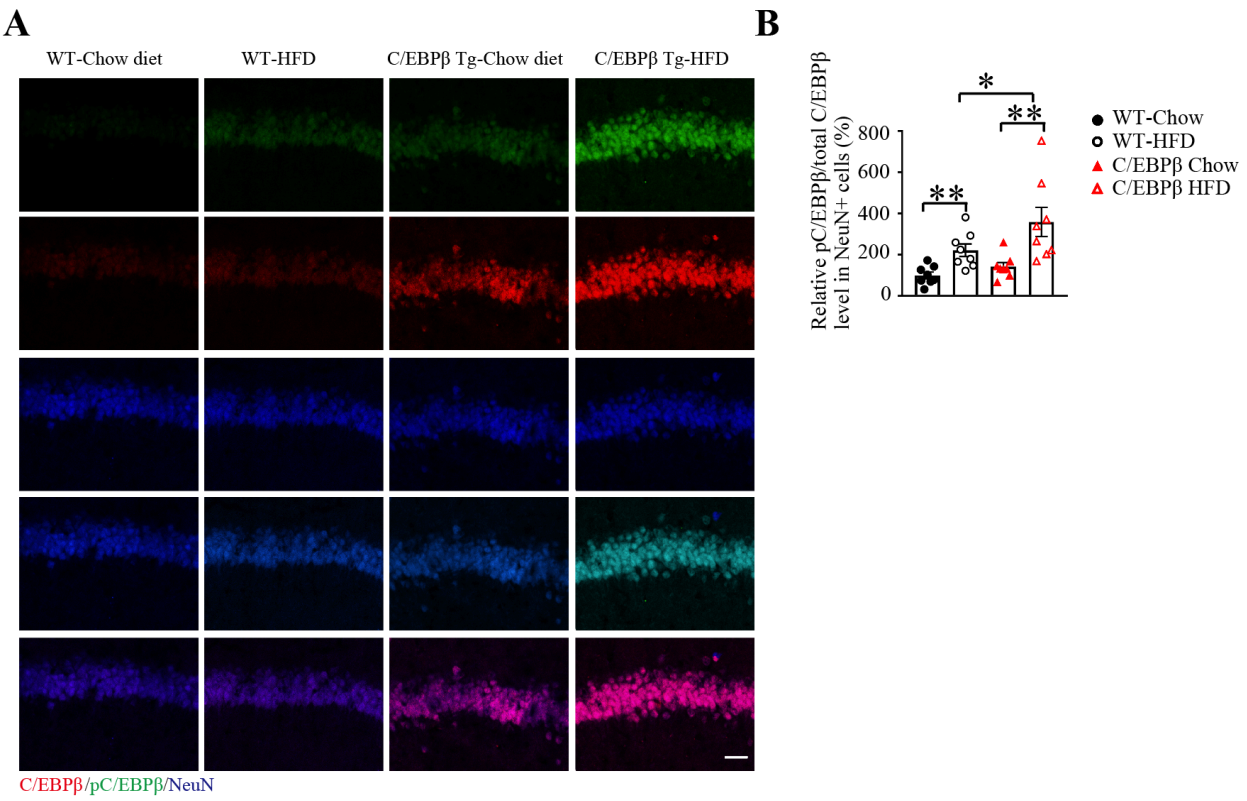

Figure 3.3 HFD activates C/EBPβ in the hippocampal neurons

A&B. Immunofluorescent staining shows that HFD elicited p-C/EBPβ co-stained with NeuN and C/EBPβ in the hippocampus of C/EBPβ transgenic mice. The relative fluorescent intensities were quantified (Mean ± SEM, n = 8, one-way ANOVA and Bonferroni's multiple comparison test, * $p < 0.05$, ** $p < 0.01$; Scale bar: 50 μm).

Since Tg/Tg mice were difficult to breed and obtain sufficient numbers, we focused on single Tg mice for the whole study. Immunoblotting (IB) showed that C/EBPβ Tg mice but not WT littermates displayed insulin signaling reduction in the brain in an age-dependent manner even under a chow diet. Notably, p-IR/p-IRS/p-Akt and p-GSK3β were significantly reduced in the brains of 16 months old C/EBPβ Tg mice; by contrast, the insulin signaling in 3- and 9-month-old C/EBPβ Tg mice remained unchanged and were comparable to their WT controls (Figure 3.4A), indicating that neuronal C/EBPβ escalation triggers insulin resistance in the brain during aging. Interestingly, both fasted and fed blood insulin levels were significantly elevated in C/EBPβ Tg mice as compared to their WT littermates at 3 and 16 months of age, respectively (Figure 3.4B&C), indicating that C/EBPβ Tg mice are insulin resistant at both ages as compared to WT littermates. Notably, the brain insulin levels in the 16-month-old groups of WT and C/EBPβ Tg mice were significantly lower than those in the 3-month-old groups (Figure 3.4D), suggesting that insulin is decreased in the brain during aging in both strains of mice.

Since C/EBPβ plays a crucial role in both diabetes and AD, and its pivotal downstream target AEP cleaves both APP and Tau in driving AD pathogenesis, we crossed AEP -/- mice with Thy1-C/EBPβ Tg mice to obtain Thy1-C/EBPβ/AEP -/- mice. Intriguingly, body weights of both C/EBPβ Tg mice and C/EBPβ/AEP -/- mice were slightly lighter than WT littermates. When fed a chow diet, body weights of C/EBPβ Tg and C/EBPβ/AEP -/- mice were significantly lower at 8 weeks old compared with wild-type mice (16.33 ~ 0.29 vs. 17.29 ~ 0.27 g, $P < 0.05$, $n = 8$, Student t-test). The difference was more prominent in mice fed with HFD. After HFD treatment for 12 weeks, the obesity was much more obvious in WT mice than in C/EBPβ Tg or

C/EBPβ/AEP -/- mice. Although C/EBPβ Tg mice also exhibited progressive body weight gain upon HFD treatment versus chow diet, they displayed substantially lighter body weight than WT littermates under both HFD and chow diet, respectively. It is worth noting that the food intake was similar between WT mice and Thy1-C/EBPβ Tg mice at both 3 and 16 months old of ages (Figure 3.4E).

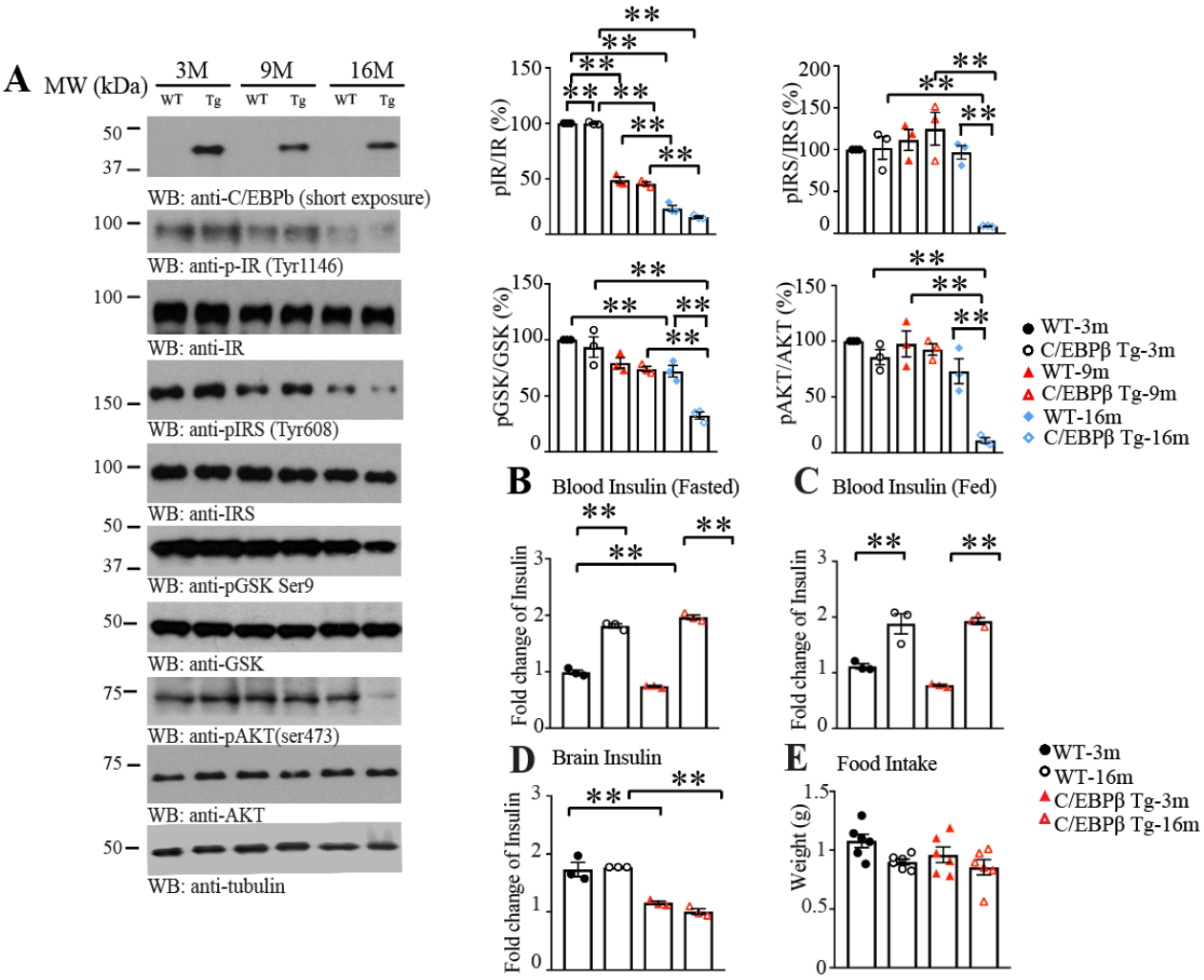

Figure 3.4 C/EBPβ levels in aging hippocampal neurons and metabolic measures in aged animals

A. Immunoblotting analysis of insulin signaling pathway in the hippocampus of wild-type and C/EBPβ transgenic mice at the age of 3-month, 9-month, and 16-month. Extracts of brain tissues were prepared and immunoblotted with C/EBPβ, IR, phosphor-IR (Tyr^{1146}), IRS, phosphor-IRS (Tyr^{608}), AKT, phosphor-AKT (Ser^{473}), GSK, GSK (Ser^{9}) antibodies. The relative abundance of various indicated proteins was quantified (Mean ± SEM, n = 2, one-way ANOVA and Bonferroni's multiple comparison test, * $p < 0.05$, ** $p < 0.01$). **B&C.** Blood insulin levels in

HFD or chow diet-fed wild-type and C/EBPβ transgenic mice at age of 3-month and 16-month. (n =3; * $P < 0.05$, ** $P < 0.01$; one-way ANOVA and Bonferroni's multiple comparison test). **D.** Brain insulin levels in HFD or chow diet-fed wild-type and C/EBPβ transgenic mice, at age of 3-month and 16-month. (n =3; * $P < 0.05$, ** $P < 0.01$; one-way ANOVA and Bonferroni's multiple comparison test). **E.** Food intake in wild-type and C/EBPβ transgenic mice at age of 3-month and 16-month. (n =7; * $P < 0.05$, ** $P < 0.01$; one-way ANOVA and Bonferroni's multiple comparison test).

By contrast, no significant difference in body weight was found in C/EBPβ/AEP -/- mice regardless of HFD or chow diet treatment (Figure 3.5A). Based on results of the insulin tolerance test (ITT), both WT and Thy1-C/EBPβ Tg mice developed insulin intolerance after HFD treatment, as compared to the chow diet. In contrast, C/EBPβ/AEP -/- mice still exhibited high insulin sensitivity under both conditions (Figure 3.5 B). The results of the glucose tolerance test (GTT) indicated that C/EBPβ Tg mice developed much stronger glucose intolerance under both HFD and chow diets than WT littermates. Again, C/EBPβ/AEP -/- mice displayed the lowest glucose intolerance. HFD treatment elicited significantly higher glucose intolerance than the chow diet among these groups (Figure 3.5 C). These effects were confirmed by the area under curve analysis (Figure 3.5 D&E). In parallel, hyperinsulinemia was observed in fed and fasted WT mice after HFD feeding, suggesting insulin resistance. Strikingly, C/EBPβ/AEP -/- mice, but not C/EBPβ Tg, mice displayed higher insulin levels after HFD treatment than their chow diet cohort in both fed and fasted conditions (Figure 3.6 A&B). HFD feeding increased the circulating leptin concentrations in all tested mice with the highest leptin level found in the WT animals, followed by C/EBPβ/AEP -/- and C/EBPβ Tg mice (Figure 3.6 C). Again, insulin levels in the brains of HFD-fed mice were more abundant than in their corresponding chow diet control, but WT mice displayed significantly higher insulin concentrations than C/EBPβ Tg and C/EBPβ/AEP -/- mice after HFD feeding (Figure 3.6 D). Thiamine deficiency contributes to hyperglycemia and diabetes complications(151). In alignment with these findings, C/EBPβ Tg mice demonstrated lower thiamine than WT controls under both chow diet and HFD, whereas thiamine diphosphate (TDP) remained comparable between the two strains under both conditions

(Figure 3.7). Together, these data support the concept that Thy1-C/EBPβ mice are more vulnerable to HFD-induced diabetes and insulin resistance.

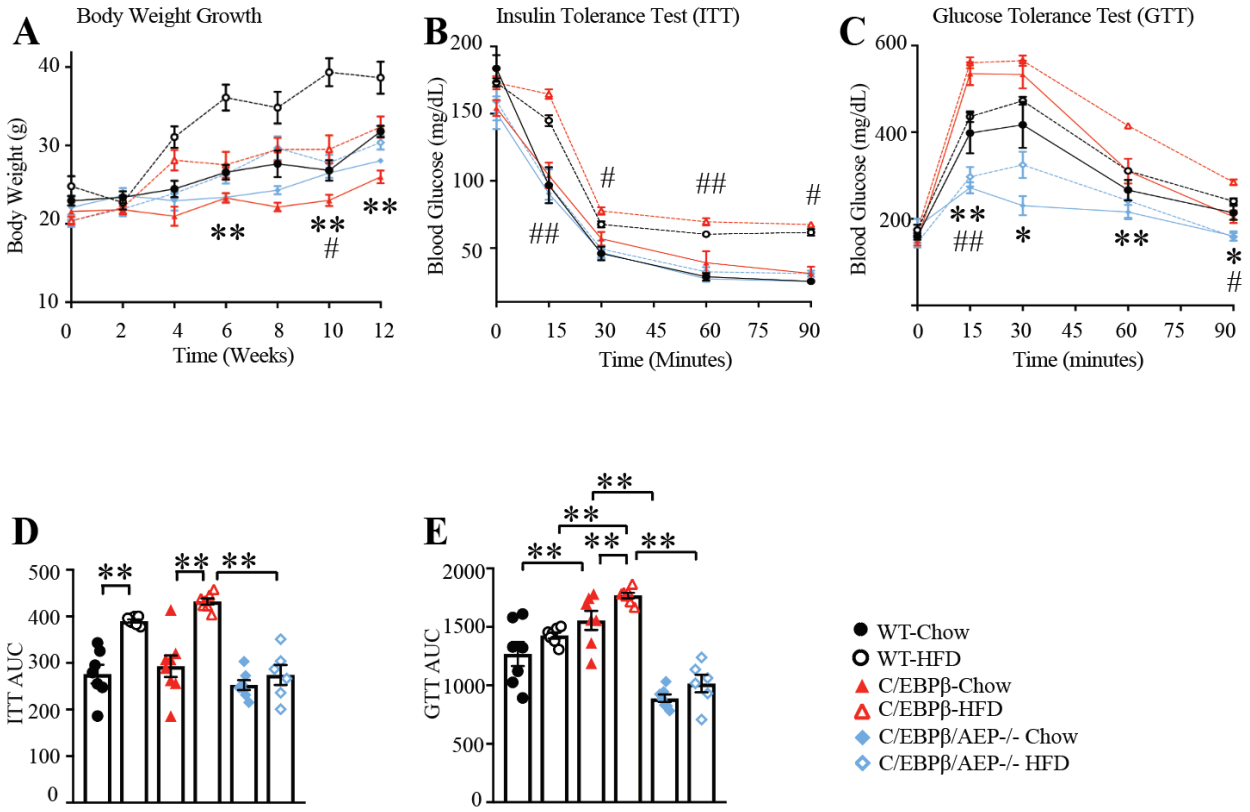

Figure 3.5 High-Fat Diet (HFD) induces diabetes in Thy1-C/EBPβ transgenic mice

A. Growth curves of 3-month-old wild-type, C/EBPβ transgenic mice, and C/EBPβ/AEP -/- transgenic mice fed with chow diet or HFD. Bodyweight was measured biweekly and expressed as mean ±SEM (n =7–10; * $P < 0.05$, ** $P < 0.01$, WT-HFD versus C/EBPβ-HFD, # $P < 0.05$, ## $P < 0.01$ C/EBPβ-Chow versus C/EBPβ-HFD, one-way ANOVA and Bonferroni's post hoc test). **B.** Insulin tolerance test in wild-type, C/EBPβ transgenic mice, and C/EBPβ transgenic

mice with AEP knockout (6–7 months old) that have been fed with HFD for 12 weeks after overnight fasting. Blood glucose level was monitored at different time intervals after intraperitoneal injection of glucose (2 g/kg). Data present mean ±SEM (n =7-8; * $p < 0.05$, ** $p < 0.01$, WT-HFD versus C/EBPβ-HFD, # $P < 0.05$, ## $P < 0.01$ C/EBPβ-Chow versus C/EBPβ-HFD, one-way ANOVA and Bonferroni's post hoc test). **C.** Glucose tolerance test in wild-type, C/EBPβ transgenic mice, and C/EBPβ transgenic mice with AEP knockout (6–7 months old) that have been fed with HFD for 12 weeks after overnight fasting. Blood glucose level was monitored at different time intervals after intraperitoneal injection of glucose (2 g/kg). Data presented mean ±SEM (n =7-8; * $p < 0.05$, ** $p < 0.01$, WT-HFD versus C/EBPβ-HFD, # $P < 0.05$, ## $P < 0.01$ C/EBPβ-Chow versus C/EBPβ-HFD, one-way ANOVA and Bonferroni's post hoc test). **D&E.** Area under the curve (AUC) for ITT and GTT (n=7-8; * $P < 0.05$, ** $P < 0.01$ one-way ANOVA and Bonferroni's multiple comparison test).

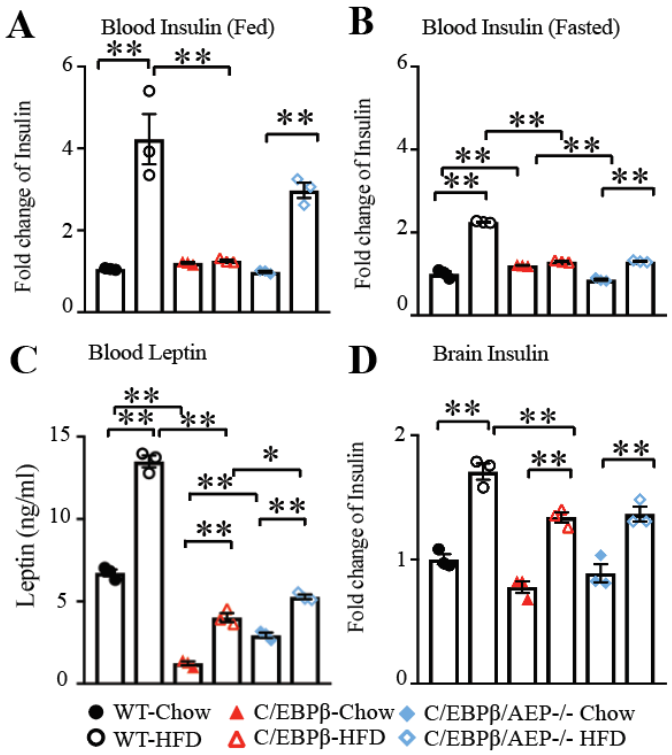

Figure 3.6 Insulin and leptin levels in plasma and brain of Thy1-C/EBPβ transgenic mice

A&B. Circulating insulin concentrations of fed and fasting wild-type, C/EBPβ transgenic mice, and C/EBPβ/AEP -/- mice (6–7 months old) that have been fed with chow diet or HFD for 12 weeks (n = 3). Results were expressed as mean ±SEM (* $P < 0.05$, ** $P < 0.01$; one-way ANOVA and Bonferroni's multiple comparison test). **C.** Serum leptin levels in fed condition (n =3; * $P < 0.05$, ** $P < 0.01$; one-way ANOVA and Bonferroni's multiple comparison test). **D.** Brain insulin levels in fed condition (n =3; * $P < 0.05$, ** $P < 0.01$; one-way ANOVA and Bonferroni's multiple comparison test).

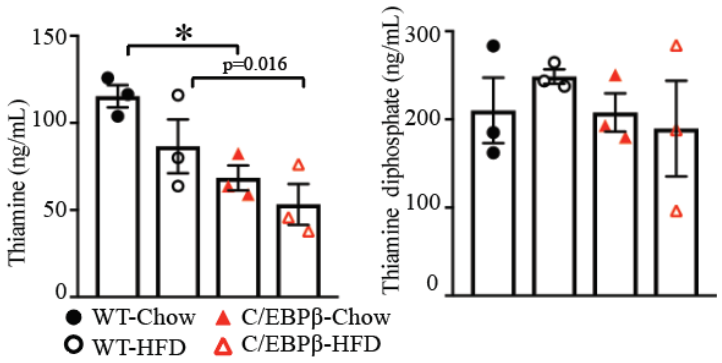

Figure 3.7 Thiamine and Thiamine diphosphate levels in C/EBPβ transgenic mice

Thiamine and Thiamine diphosphate levels in whole blood were collected from wild-type and C/EBPβ transgenic mice fed with chow diet or HFD. (Mean ± SEM, n = 3, one-way ANOVA and Bonferroni's multiple comparison test, * $p < 0.05$, ** $p < 0.01$).

3.2.2 High-Fat Diet (HFD) diminishes AMPK/ACC pathway and impairs insulin signaling in Thy1-C/EBPβ transgenic mice

Adipocyte dysfunction is one of the major factors that trigger insulin resistance. Therefore, we examined diet-induced adipogenesis in C/EBPβ Tg mice. In H&E stained tissue sections, adipocytes in white adipocyte tissue (WAT) of WT mice treated with HFD were bigger than those in chow diet-fed mice. However, the adipocytes in HFD-treated C/EBPβ Tg mice were much larger than in the chow diet-treated group. By contrast, deletion of AEP from C/EBPβ Tg mice reduced the adipocyte size (Figure 3.8A, upper panels). Further, more lipid droplets were found in H&E stained sections of the livers of HFD-treated WT and C/EBPβ Tg mice fed with HFD than in their chow diet control. In contrast, the lipid droplets were less abundant in C/EBPβ/AEP -/- mice (Figure 3.8A, lower panels). These observations were validated using Oil-Red staining (Figure 3.8 B&C). The concentrations of free fatty acid (FFA) and triglyceride (TG) in blood were significantly higher in HFD-fed C/EBPβ Tg mice than those of their chow diet-fed control. Knockout of AEP from C/EBPβ Tg mice abolished these effects.

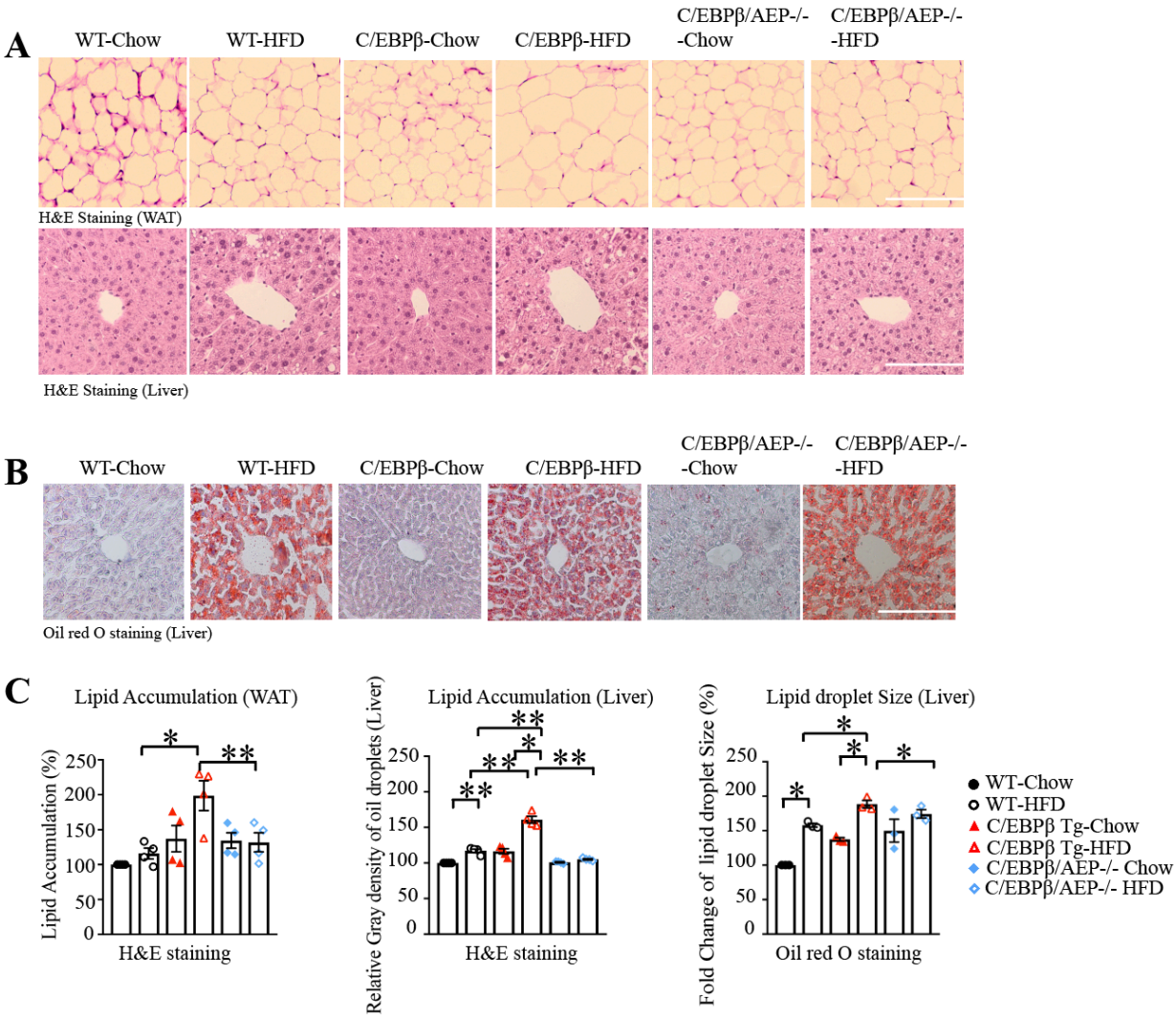

Figure 3.8 HFD enlarges adipocyte size and increases fat deposit into the liver in Thy1-C/EBPβ transgenic mice

A. Hematoxylin-eosin (H&E) staining of inguinal WAT sections (upper panel) and liver sections (lower panel) from wild-type, C/EBPβ transgenic mice, and C/EBPβ/AEP-/- animals (6–7 months old) that have been fed with chow diet or HFD for 12 weeks. Representative results of different mice from each genotype were shown. (Scale bar: 50 μm). **B.** Oil red O (*lower panel*) staining of liver sections collected from wild-type, C/EBPβ transgenic mice, and C/EBPβ/AEP-/- animals that have been fed with chow diet or HFD for 12 weeks. (Scale bar: 50 μm.) A representative result from each genotype is shown. **C.** Quantification of lipid accumulation in

WAT cells and liver from wild-type, C/EBPβ transgenic mice, and C/EBPβ/AEP-/- animals (6–7 months old) that have been fed with chow diet or HFD for 12 weeks. Quantification of lipid accumulation, the density of oil droplets, and inguinal WAT cell area. Results were expressed as mean ± SEM, n=3-4, one-way ANOVA and Bonferroni's multiple comparison test, * $p < 0.05$, ** $p < 0.01$.

Circulating cholesterol levels were highly increased in WT mice after HFD treatment. Though both FFA and TG were elevated in WT mice after HFD feeding compared to the chow diet group, they only displayed the trends but were not statistically significant (Figure 3.9). Moreover, pro-inflammatory cytokines including IL-1β, IL-6, and TNFα were all highly augmented in WT after HFD treatment, which was further elevated in C/EBPβ Tg mice. Notably, the levels of cytokines in C/EBPβ Tg mice were significantly higher than in WT mice even under the chow diet. Again, eradication of AEP from C/EBPβ Tg mice greatly decreased these cytokine concentrations in the blood (Figure 3.10). Hence, HFD strongly increases the lipid deposition, adipocyte size, and inflammation in Thy1-C/EBPβ Tg mice, and deletion of AEP markedly diminishes these effects.

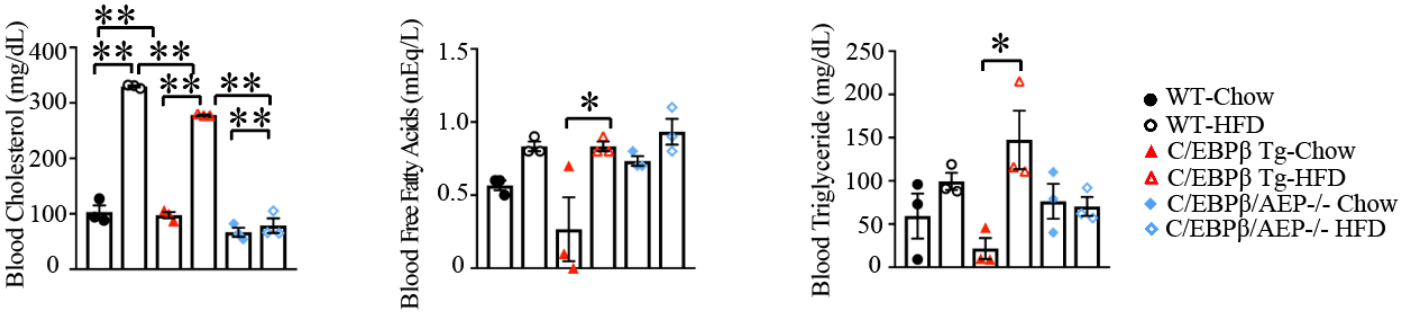

Figure 3.9 Levels of fatty acids and derivatives in the plasma

Serum cholesterol, free fatty acids, and triglyceride levels of wild-type, C/EBPβ transgenic mice, and C/EBPβ/AEP-/- animals that have been fed with chow diet or HFD for 12 weeks**.** Results were expressed as mean ±SEM (*n*=3, * $p < 0.05$, ** $p < 0.01$; one-way ANOVA and Bonferroni's multiple comparison test).

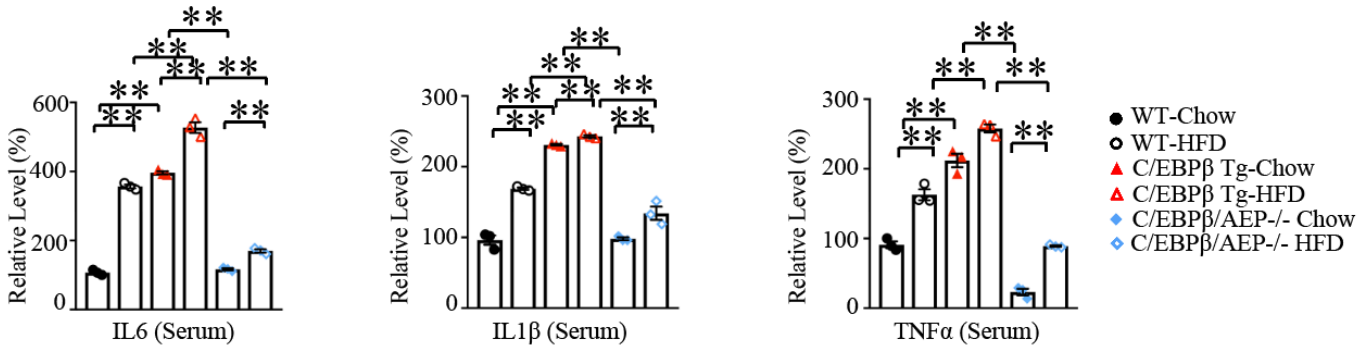

Figure 3.10 HFD induces inflammation in C/EBPβ transgenic mice

Inflammation was enhanced in HFD-treated C/EBPβ transgenic mice. IL-1β, IL-6, and TNFα were quantified by the ELISA from the serum samples. (Mean ± SEM, n = 3; one-way ANOVA and Bonferroni's multiple comparison test, * $p < 0.05$, ** $p < 0.01$).

AMPK (AMP-activated protein kinase) is a fuel-sensing kinase. Activation of AMPK reduces hepatic gluconeogenic gene expression and glucose production, increases fatty acid oxidation, and enhances glucose uptake (152). IB revealed that both p-AMPK and p-Acetyl-CoA carboxylase (ACC) signals were demonstrable in the WAT in WT mice under chow diet, but they were clearly reduced in C/EBPβ Tg mice, though AMPK and ACC total levels in these tissues were comparable. Deletion of AEP from C/EBPβ Tg mice alleviated this suppression. Remarkably, HFD strongly suppressed both p-AMPK and p-ACC activities in WT mice and this antagonistic effect was even stronger in C/EBPβ Tg mice by HFD. Again, the effects were attenuated in C/EBPβ/AEP -/- mice (Figure 3.11A). Similar effects are also observed in BAT (brown adipose tissue), muscle, and liver (Figure 3.11B-D). Hence, AMPK/ACC signaling is decreased in the peripheral tissues in C/EBPβ Tg mice and deletion of AEP alleviates this repressive effect in C/EBPβ/AEP -/- Tg mice. In addition, we monitored insulin signaling in insulin-responsive tissues including muscle and liver. IB showed that p-IR was evidently reduced in C/EBPβ Tg mice muscles as compared to WT mice under chow diet. HFD markedly reduced p-IR activities in WT mice and this inhibitory effect was much more robust in C/EBPβ Tg mice. Knockout of AEP from C/EBPβ Tg mice significantly abrogated this effect. The total levels of IR in muscles from different strains of mice were almost similar, and the ratios of p-IR/IR were quantified. As expected, the downstream effectors p-IRS and p-Akt tightly oscillated with the upstream p-IR activities (Figure 3.12, left). We made the same observations in the liver tissue (Figure 3.12, right). Hence, both insulin signaling and the p-AMPK/p-ACC pathway are impaired in Thy1-C/EBPβ Tg mice under the basal conditions, and HFD treatment further abolishes this metabolic signaling.

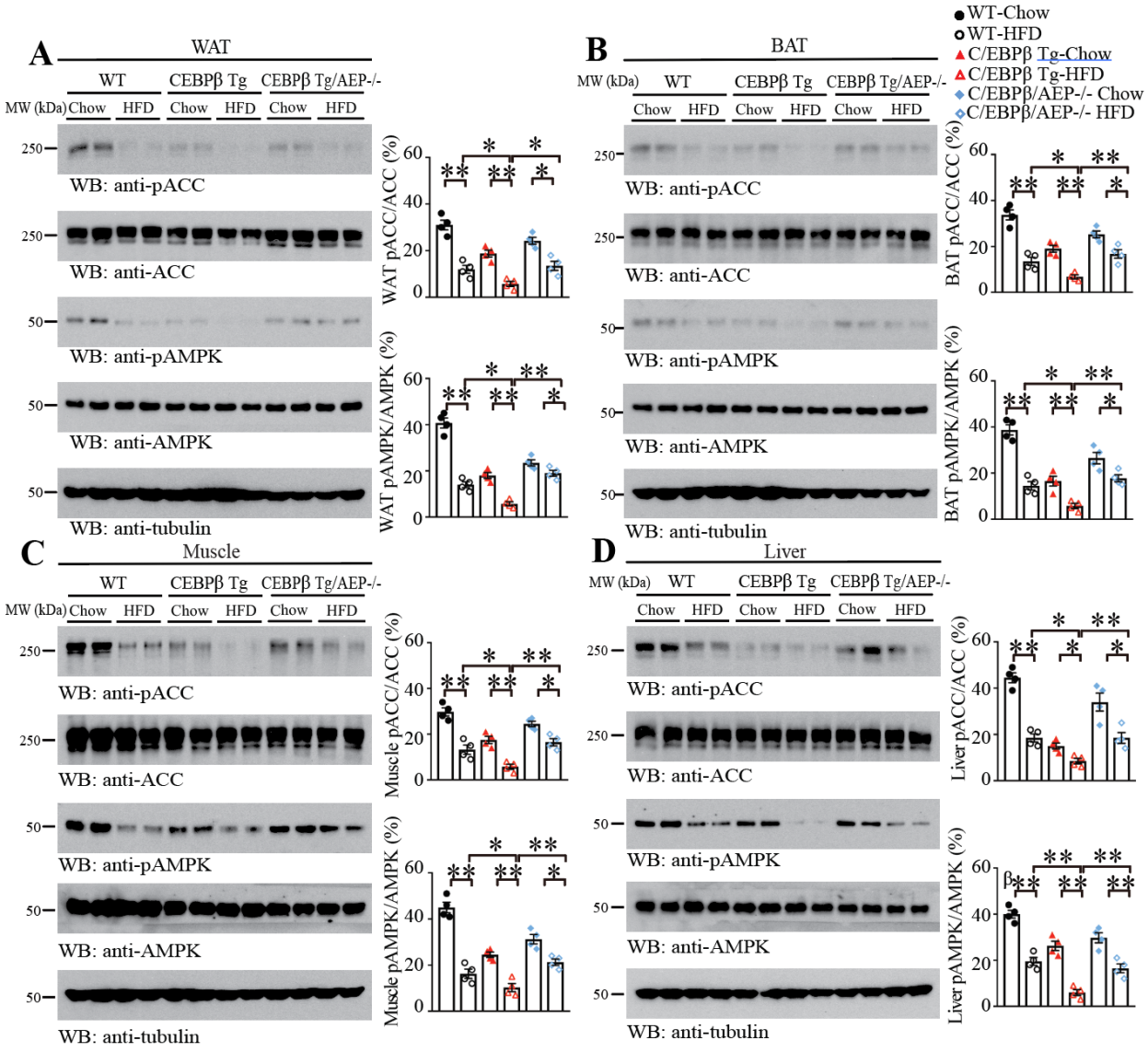

Figure 3.11 High-Fat Diet (HFD) impairs insulin signaling and diminishes AMPK/ACC pathways in Thy1-C/EBPβ transgenic mice

Analysis of AMPK/ACC and insulin signaling pathway in wild-type, C/EBPβ Tg mice and C/EBPβ/AEP -/- mice (6–7 months old) that have been fed with chow diet or HFD for 12 weeks. Extracts of inguinal WAT (**A**), BAT **(B)**, muscle (**C**), and liver (**D**) were prepared and immunoblotted with phosphor–Thr^{172}-AMPK, phosphor–Ser^{79}-ACC, total AMPK, and ACC.

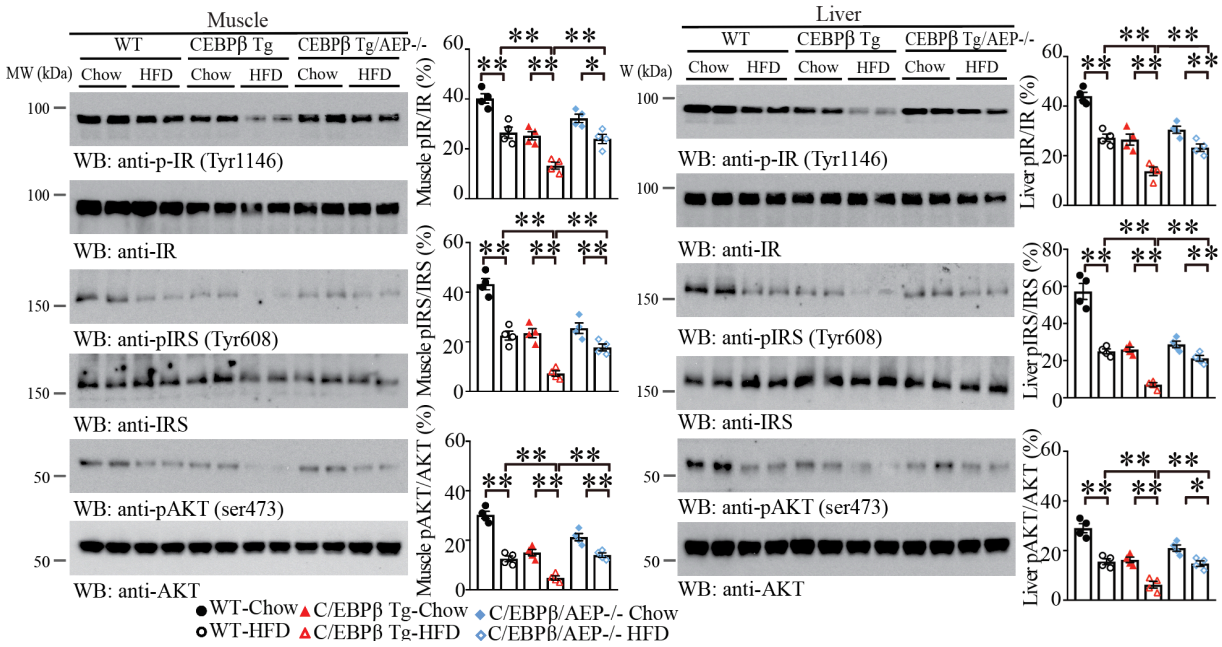

Figure 3.12 High-Fat Diet (HFD) impairs insulin signaling in insulin-responsive tissues

Muscle (**left**) and liver (**right**) IR were further immunoblotted with phosphor-IR (Tyr^{1146}), IRS, phosphor-IRS (Tyr^{608}), AKT, and phosphor-AKT (Ser^{473}) antibodies. (Mean ± SEM, n=4, one-way ANOVA and Bonferroni's multiple comparison test, * $p < 0.05$, ** $p < 0.01$).

3.2.3 Knockout of AEP in Thy1-C/EBPβ transgenic mice alleviates HFD-induced neuro-inflammation and AD pathologies

To assess the impact of neuronal C/EBPβ or HFD on insulin signaling in the brain, we conducted IB with the brain tissues from WT and C/EBPβ Tg mice with or without 12 weeks of HFD treatment. Under chow conditions, p-IR/p-IRS/p-Akt activities were significantly decreased in the brain of C/EBPβ Tg mice as compared to WT mice. Under HFD, this pathway was also reduced in WT mice when compared to the chow diet, and this signaling was further repressed in C/EBPβ Tg mice. However, the deletion of AEP from C/EBPβ Tg mice significantly alleviated this inhibitory effect. A similar pattern of the p-AMPK/p-ACC pathway was detected in the brain (Figure 3.13 A&B). Enzymatic assays revealed that AEP protease activities were increased in the brain of WT mice from chow diet to HFD, which were further enhanced in C/EBPβ Tg mice from chow diet to HFD, and they were eradicated in C/EBPβ/AEP -/- mice (Figure 3.14A). Quantification showed pro-inflammatory cytokines including IL-1β and IL6 but not TNFα displayed similar patterns, and both IL-1β and IL6 were significantly reduced in C/EBPβ/AEP -/- mice under both chow diet and HFD feeding conditions (Figure 3.14 B-D). To explore whether HFD provokes AD pathologies in these mice, we conducted IB and found that C/EBPβ and truncated (active) AEP were escalated in WT mice upon HFD treatment. These events were augmented in the brain of C/EBPβ Tg mice and further elevated by HFD stimulation, accompanied by increased fragmented APP N585 and Tau N368 truncates. Consequently, p-Tau AT8 levels were strongly increased in C/EBPβ Tg mice upon HFD treatment. Notably, both Tau5 and BACE1 total levels were enhanced in C/EBPβ Tg mice by HFD stimulation (Figure 3.15).

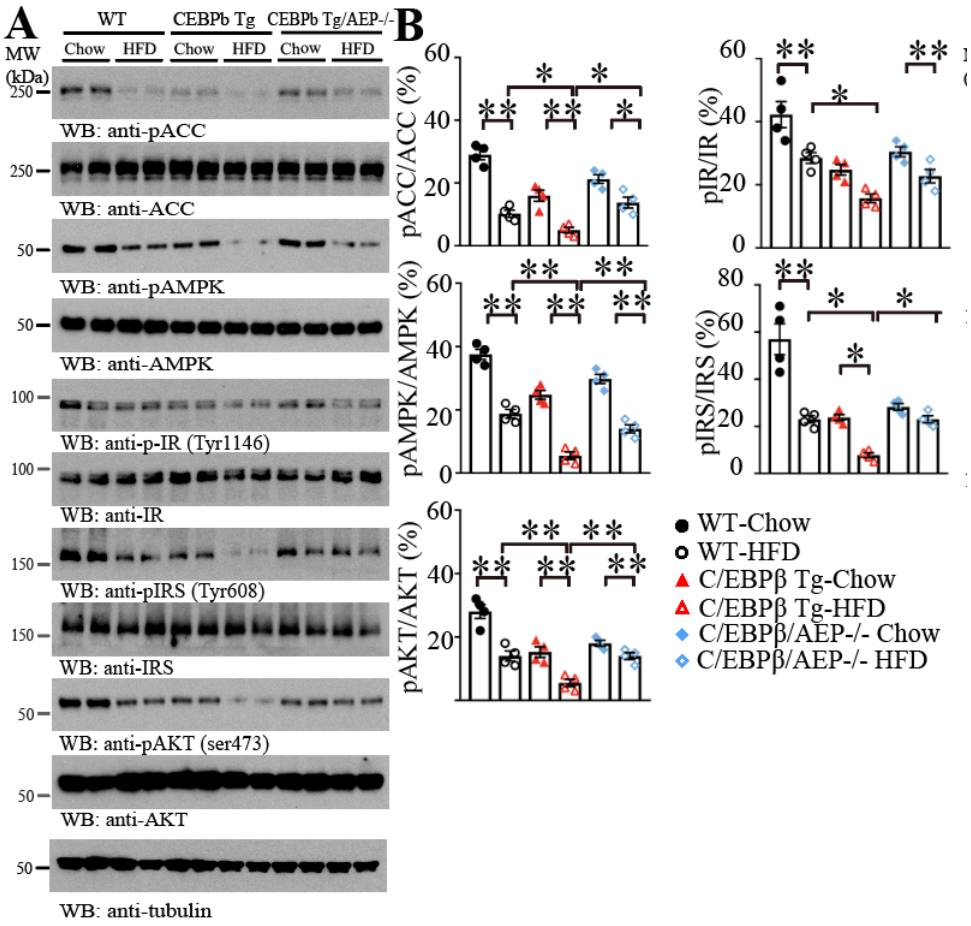

Figure 3.13 Knockout of AEP from Thy1-C/EBPβ transgenic mice alleviates HFD-induced insulin signaling pathway impairment

A&B. Analysis of the insulin signaling pathway in the brain from wild-type and C/EBPβ Tg and C/EBPβ/AEP -/-mice, (6–7 months old) that have been fed with chow diet or HFD for 12 weeks. Extracts of the brain tissues were prepared and immunoblotted with a phosphor–Thr^{172}-AMPK, phosphor–Ser^{79}-ACC, total AMPK, ACC, AMPK (Thr^{172}), IR, phosphor-IR (Tyr^{1146}), IRS, phosphor-IRS (Tyr^{608}), AKT, phosphor-AKT (Ser^{473}), GSK, GSK (Ser^{9}) antibodies. (Mean ± SEM, n=4, one-way ANOVA and Bonferroni's multiple comparison test, * $p < 0.05$, ** $p < 0.01$).

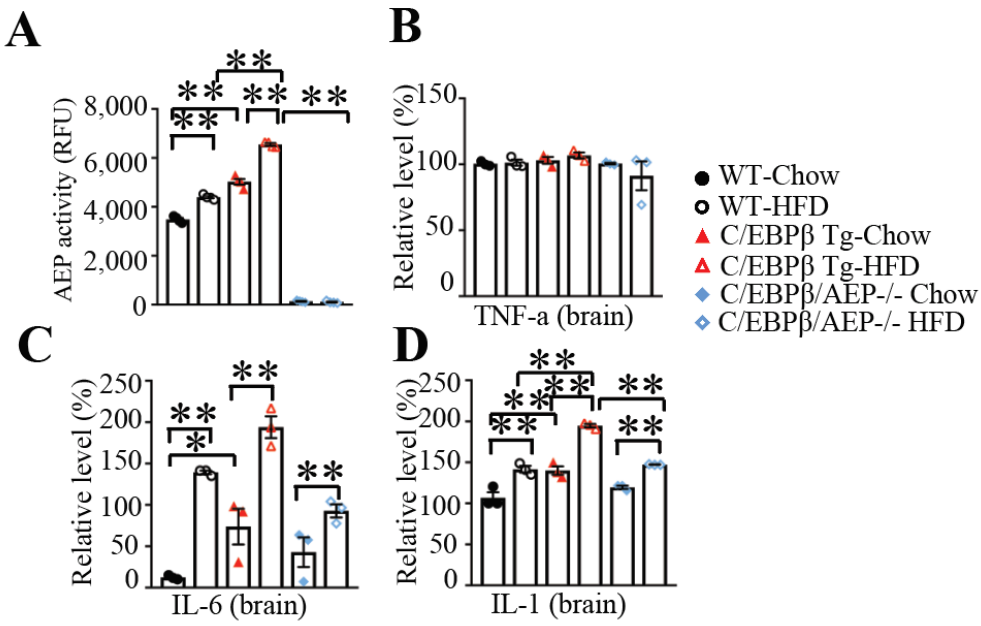

Figure 3.14 Knockout of AEP from Thy1-C/EBPβ transgenic mice alleviates HFD-induced inflammation

A. AEP enzymatic activity assay (Mean ± SEM, n = 3, one-way ANOVA and Bonferroni's multiple comparison test, * $p < 0.05$, ** $p < 0.01$). **B-D.** ELISA analysis of neuroinflammation factors IL-1β, IL-6, TNFα in the brain lysates from the above mice. (Mean ± SEM, n = 3 mice for each group, one-way ANOVA, and Bonferroni's multiple comparison test. * $p < 0.05$, ** $p < 0.01$).

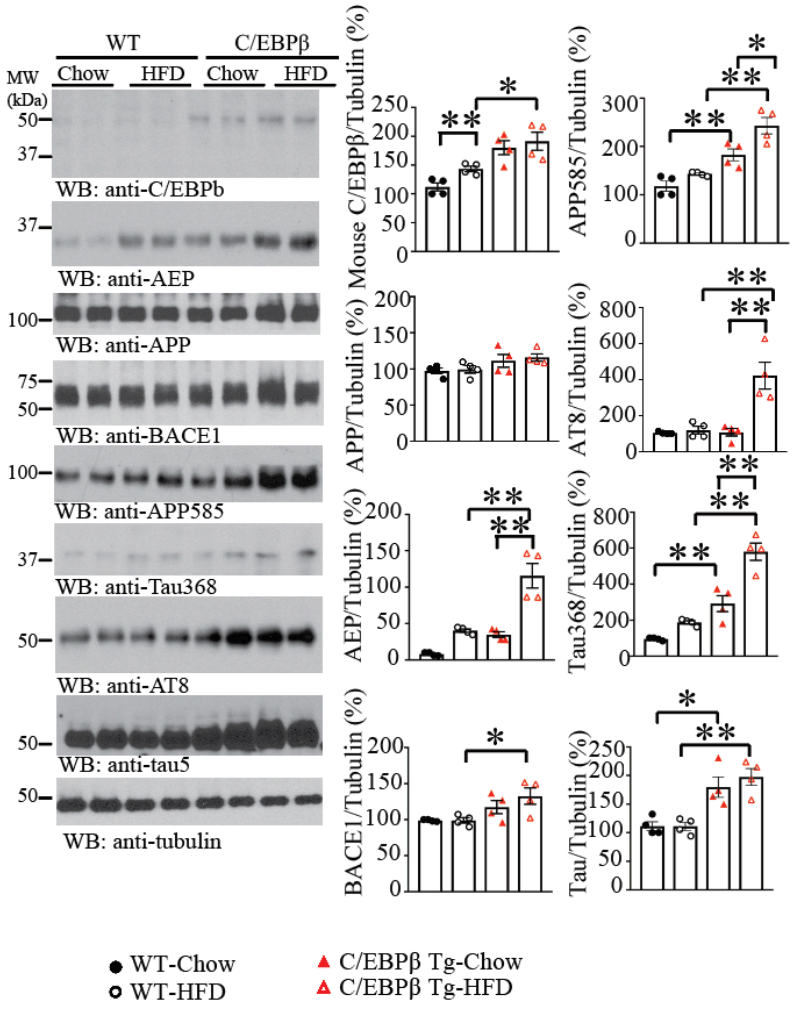

Figure 3.15 HFD induced AD pathology in C/EBPβ Transgenic mice

Western blot assays demonstrated HFD-induced activation of C/EBPβ and C/EBPβ- mediated upregulation of AEP, Tau, and BACE1 in the hippocampus compared to Chow diet treatment. HFD enhanced the levels of C/EBPβ downstream proteins in C/EBPβ Tg mice, leading to cleavages of APP (N585) and Tau (N368) by activating AEP, and tau hyperphosphorylation (AT8). The relative abundance of various indicated proteins was quantified (Mean ± SEM, n = 4, one-way ANOVA and Bonferroni's multiple comparison test, * $p < 0.05$, ** $p < 0.01$).

IF co-staining validated that HFD provoked p-C/EBPβ and AEP escalation in the hippocampus of WT mice as compared to the chow diet. These effects were escalated in C/EBPβ Tg mice but profoundly alleviated in C/EBPβ/AEP -/- mice (Figure 3.16A). Consequently, APP was markedly cleaved by active AEP into APP N585 in the brains of C/EBPβ Tg mice, and knockout of AEP strongly diminished APP fragmentation in C/EBPβ/AEP-/- mice (Figure 3.16B). Moreover, Tau N368 and AEP co-staining revealed that they were increased in C/EBPβ Tg mice as compared to WT mice with HFD. By contrast, these signals were barely detectable in C/EBPβ/AEP-/- mice (Figure 3.16C), supporting the notion that HFD stimulates both APP N585 and Tau N368 cleavage by active AEP via C/EBPβ/AEP signaling.

In alignment with these findings, Iba-1 and Glial Fibrillary Acidic Protein (GFAP) staining showed that microglia and astrogliosis were elevated in the hippocampus of WT mouse brain by HFD treatment versus chow diet. This pattern was greatly aggravated in C/EBPβ Tg mice with prominent Iba-1 and GFAP signals under HFD treatment, and deletion of AEP from C/EBPβ Tg mice selectively eliminated Iba-1 and GFAP activities (Figure 3.17), suggesting that AEP plays a critical role in mediating HFD-triggered neuro-inflammation in C/EBPβ Tg mice.

Immunohistochemistry (IHC) staining of anti-Aβ with monoclonal antibody 4G8 and anti-p-Tau AT8 on the hippocampal sections demonstrated that both Aβ and Tau pathologies were peaked in C/EBPβ Tg mice under HFD treatment, which was significantly abolished in C/EBPβ/AEP -/- mice. Silver staining also validated proteinaceous inclusions accumulated in the hippocampus of C/EBPβ Tg mice upon HFD treatment, which were reduced in C/EBPβ/AEP -/- mice. These signals were quantified (Figure 3.18, top). Quantification revealed that HFD significantly elevated Aβ40 levels in the brains of both WT and C/EBPβ Tg mice versus chow diet, and

depletion of AEP from C/EBPβ Tg mice substantially decreased Aβ40 concentrations. On the other hand, HFD only significantly augmented Aβ42 concentrations in the brains of C/EBPβ Tg mice versus the chow diet. We also observed escalated Aβ42 concentrations in WT and C/EBPβ/AEP -/- mice after HFD, but this effect was not statistically significant (Figure 3.18, bottom). Therefore, HFD elicits insulin resistance and AD pathologies in the brains of C/EBPβ Tg mice, and AEP is indispensable for this effect.

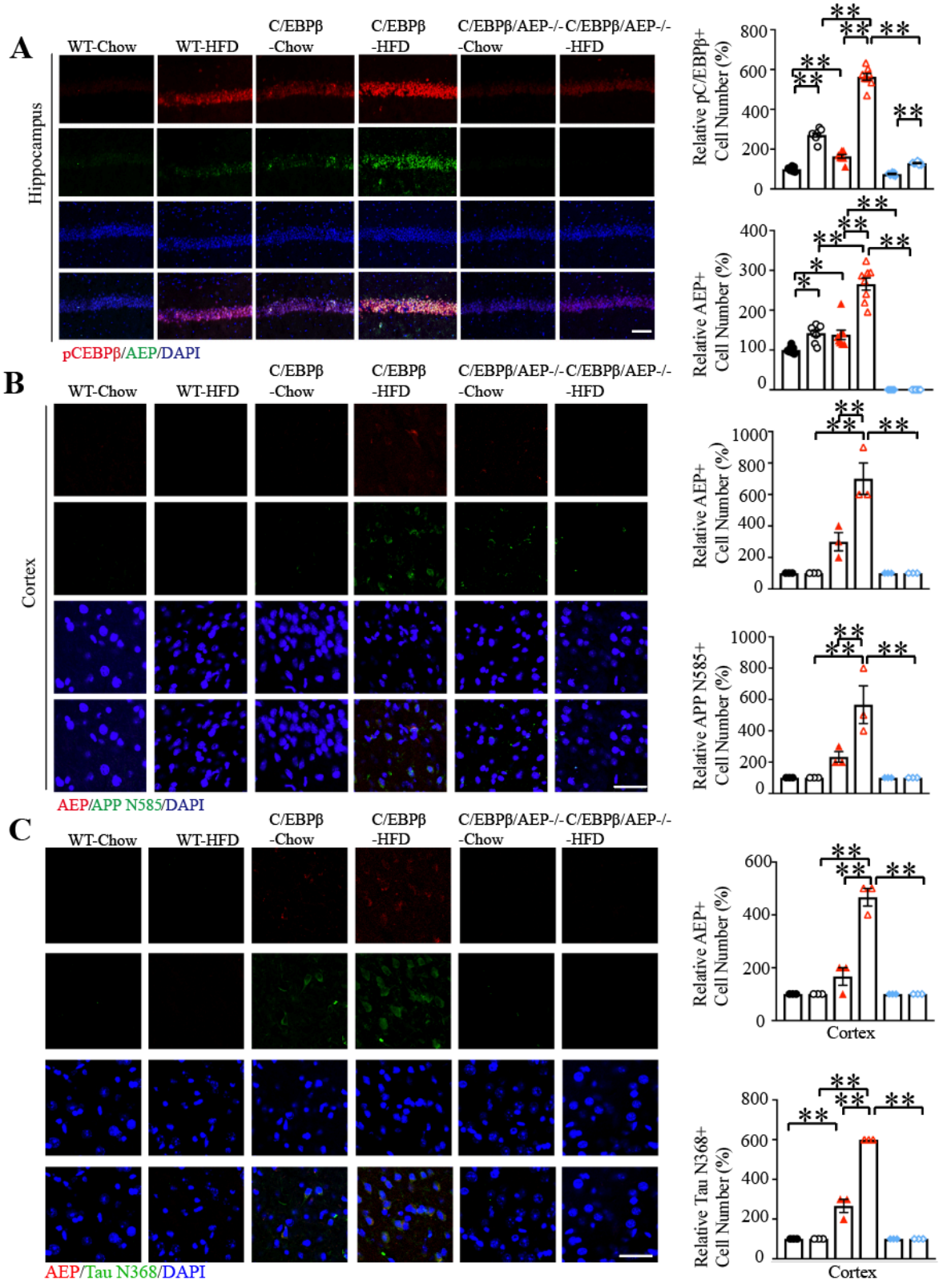
A
WT-Chow
WT-HFD
C/EBPβ -Chow
C/EBPβ -HFD
C/EBPβ/AEP-/- -Chow
C/EBPβ/AEP-/- -HFD
Hippocampus
pCEBPβ/AEP/DAPI
Relative pC/EBPβ+ Cell Number (%)
Relative AEP+ Cell Number (%)
B
Cortex
AEP/APP N585/DAPI
Relative AEP+ Cell Number (%)
Relative APP N585+ Cell Number (%)
C
AEP/Tau N368/DAPI
Relative AEP+ Cell Number (%)
Cortex
Relative Tau N368+ Cell Number (%)
Cortex

Figure 3.16 HFD induces AEP activation, APP and Tau cleavage and neuro-inflammation in the hippocampus and cortex of Thy1-C/EBPβ transgenic mice

A. Immunofluorescent co-staining of AEP and phosphor-C/EBPβ on the hippocampal sections of chow diet or HFD-treated WT, C/EBPβ transgenic mice, and C/EBPβ/AEP-/- mice. Scale bar: 50 μm. The relative abundance of various indicated proteins was quantified. (Mean ± SEM, n = 8, one-way ANOVA and Bonferroni's multiple comparison test, * $p < 0.05$, ** $p < 0.01$). **B.** Immunofluorescent co-staining of AEP and APP N585 on the cortex sections of chow diet or HFD-treated WT, C/EBPβ transgenic mice, and C/EBPβ/AEP-/- mice. AEP and APP N585 immunofluorescent signaling was upregulated in HFD-treated C/EBPβ transgenic mice. Scale bar: 50 μm. The relative abundance of various indicated proteins was quantified. (Mean ± SEM, n = 3, one-way ANOVA and Bonferroni's multiple comparison test, * $p < 0.05$, ** $p < 0.01$). **C.** Immunofluorescent co-staining of AEP and Tau N368 on the cortex sections of chow diet or HFD-treated WT, C/EBPβ transgenic mice, and C/EBPβ/AEP-/- mice. AEP and Tau N368 immunofluorescent signaling increased in HFD-treated C/EBPβ transgenic mice. Scale bar: 50 μm. The relative abundance of various indicated proteins was quantified. (Mean ± SEM, n = 3, one-way ANOVA and Bonferroni's multiple comparison test, * $p < 0.05$, ** $p < 0.01$).

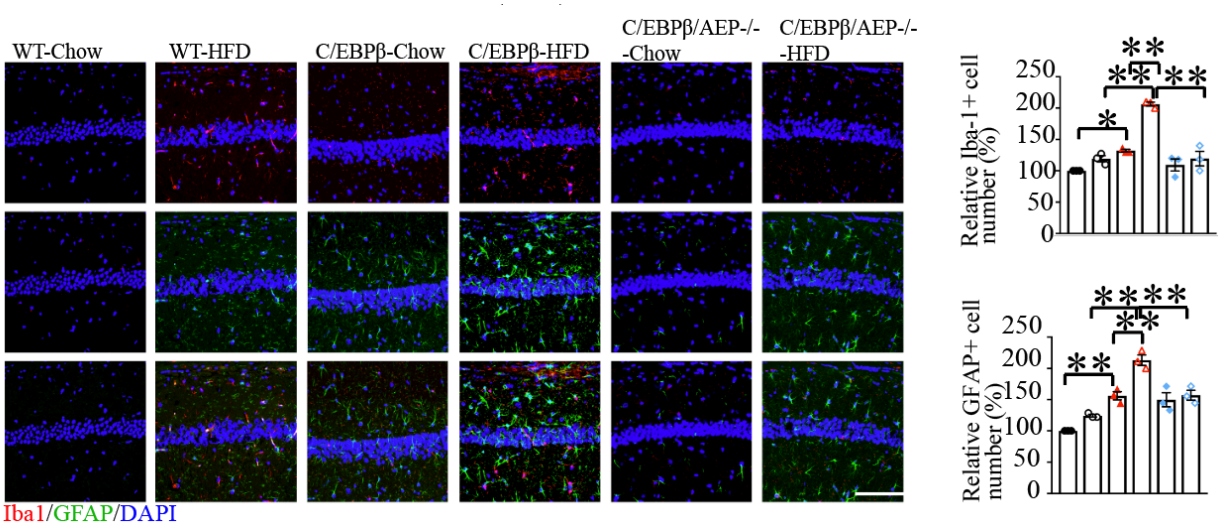

Figure 3.17 AEP deletion from Thy1-C/EBPβ transgenic mice alleviates HFD-induced neuro-inflammation in the cortex

Immunofluorescent co-staining of Iba-1 and GFAP on the hippocampal sections of chow diet or HFD-treated WT, C/EBPβ Tg, and C/EBPβ/AEP -/- mice. Microglia activation and gliosis were highly enriched in HFD-treated C/EBPβ Tg mice. Scale bar: 50 μm. The quantification of Iba-1 and gliosis were analyzed (right). (Mean ± SEM, n = 3, one-way ANOVA and Bonferroni's multiple comparison test, * $p < 0.05$, ** $p < 0.01$).

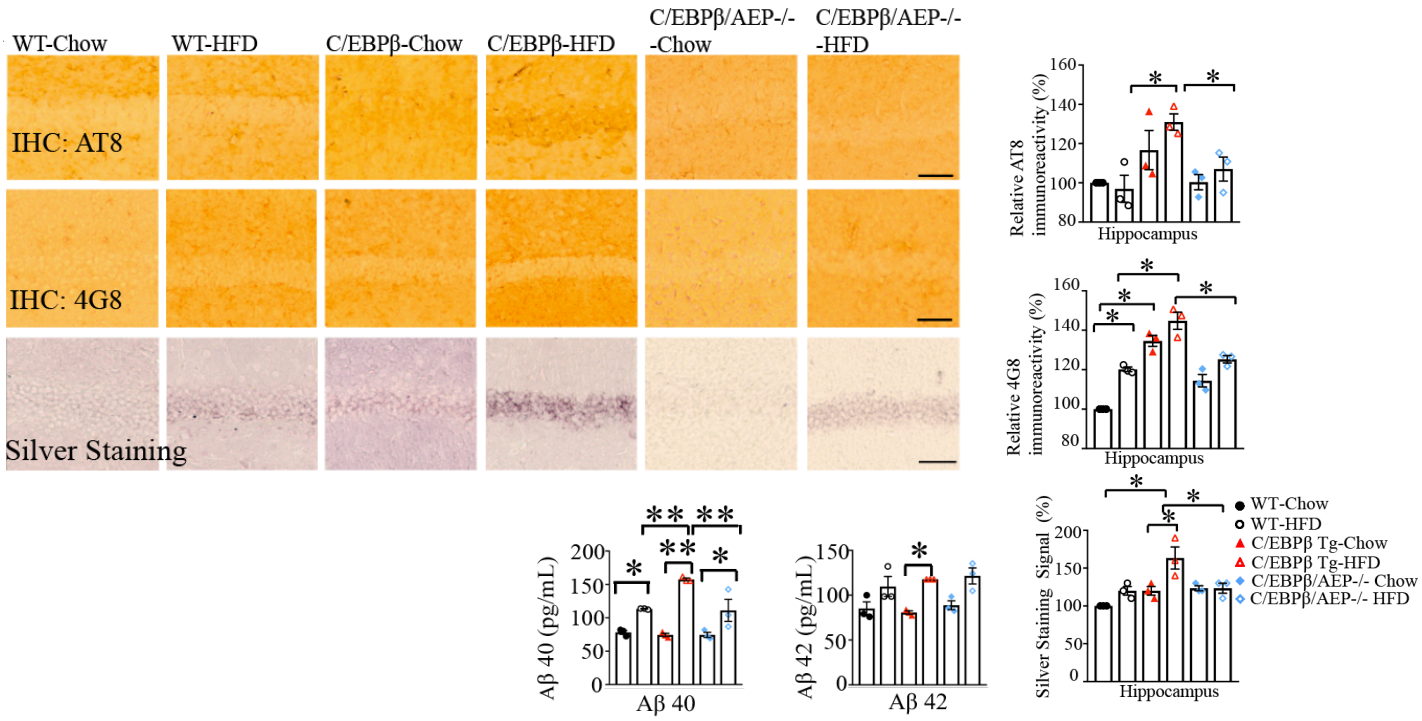

Figure 3.18 Knockout of AEP reduced HFD-induced APP and Tau aggregation in Thy1-C/EBPβ transgenic mice

Immunohistochemistry analysis of hyperphosphorylated Tau (top panel), Aβ (middle panel), and Gallyas-Braak silver staining (lower panel) in the hippocampus of HFD and chow diet-treated WT, C/EBPβ transgenic mice, and C/EBPβ/AEP -/- mice (scale bar: 50 μm). The abundance of hyperphosphorylated Tau, Aβ, and proteinaceous inclusions are quantified (Mean ± SEM, n = 3 mice for each group, one-way ANOVA and Bonferroni's multiple comparison test. * $p < 0.05$, ** $p < 0.01$) ELISA analysis of mouse Aβ40/42 in the brain lysates from the above mice. (Mean ± SEM, n = 3 mice for each group, one-way ANOVA. * $p < 0.05$, ** $p < 0.01$).

CHAPTER 4: HFD-induced diabetes triggers AD pathology through inflammation-activated C/EBPβ/delta-secretase pathway

4.1 Introduction

Previous research has shown that C/EPBβ/AEP promotes the accumulation of amyloid plaques and neurofibrillary tangles (NFTs) and contributes to AD pathogenesis in AD mouse models (122). We expect that mouse models with C/EBPβ overexpression in the brain will develop AD pathology, while the AD pathology might be alleviated by AEP inhibition. In order to confirm the role of inflammation in coupling AD and diabetes, we employed an NSAID (Aspirin) to decrease the level of inflammation, thereby testing whether AD pathology is subsequently alleviated. If NSAID (Aspirin) treatment attenuates AD pathology and cognitive decline in Thy1-C/EBPβ fed with HFD, this will demonstrate the role of inflammation in activating the pathway. We also hypothesize that Thy1-C/EBPβ mice exhibit AD pathology and cognitive impairment upon chronic LPS treatment. LPS is a component of the outer membrane of Gram-negative bacteria, and it is commonly used in animal models to trigger the inflammation process and induce the expression of pro-inflammatory cytokines.

4.2 Results

4.2.1 Deletion of AEP from Thy1-C/EBPβ transgenic mice ameliorates HFD-triggered synaptic degeneration and cognitive dysfunctions

To further examine the effect of HFD on AD pathology in both C/EBPβ Tg mice and C/EBPβ/AEP -/- mice, we conducted IB with brain tissue and found that HFD highly elevated C/EBPβ versus chow diet in C/EBPβ Tg mice, and this effect was abrogated in C/EBPβ/AEP -/- mice. The downstream targets of AEP were greatly escalated by HFD in the brain of C/EBPβ Tg mice, as noted by elevated Tau N368 and APP N585 fragmentation. p-Tau AT8 activities were increased. BACE1 total levels were enhanced in C/EBPβ Tg mice by HFD, and all these biochemical events were substantially blunted in C/EBPβ/AEP -/- mice (Figure 4.1A & B). Golgi staining showed that C/EBPβ Tg mice exhibited reduced neurite processes and dendritic spines compared to WT mice under a chow diet. Sholl analysis for the dendritic crossing and intersection number indicated that C/EBPβ Tg mice displayed the fewest intersection crossings, with HFD fewer than chow diet, which were substantially decreased by HFD treatment. By contrast, deletion of AEP significantly rescued the reductions in dendritic branching and spines in C/EBPβ/AEP -/- mice under both feeding conditions (Figure 4.2). IB showed that HFD treatment elicited pronounced reductions in synaptic proteins in C/EBPβ Tg mice as compared to the chow diet. Deletion of AEP from C/EBPβ Tg mice restored the synaptic proteins, in alignment with dendritic spine augmentation in C/EBPβ/AEP -/- mice. In contrast, the content of synaptic proteins in WT mice remained constant between the chow diet and HFD conditions (Figure 4.3)

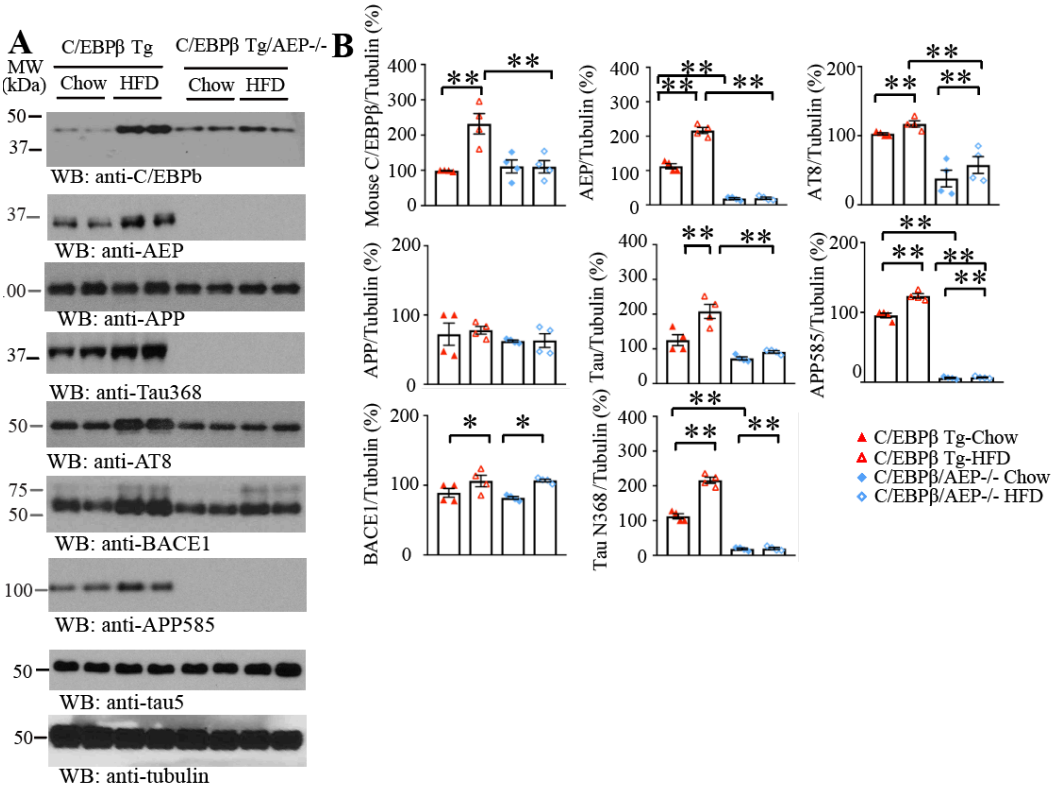

Figure 4.1 Deletion of AEP from Thy1-C/EBPβ transgenic mice ameliorates HFD-triggered AD pathology

A&B. Knockout of AEP in C/EBPβ transgenic mice repressed HFD-triggered the upregulation of AEP, Tau, and BACE1, along with increased APP and Tau fragmentation by active AEP, and hyperphosphorylated Tau (AT8). The relative abundance of various indicated proteins was quantified (Mean ± SEM, n = 4, one-way ANOVA and Bonferroni's multiple comparison test, * $p < 0.05$, ** $p < 0.01$)

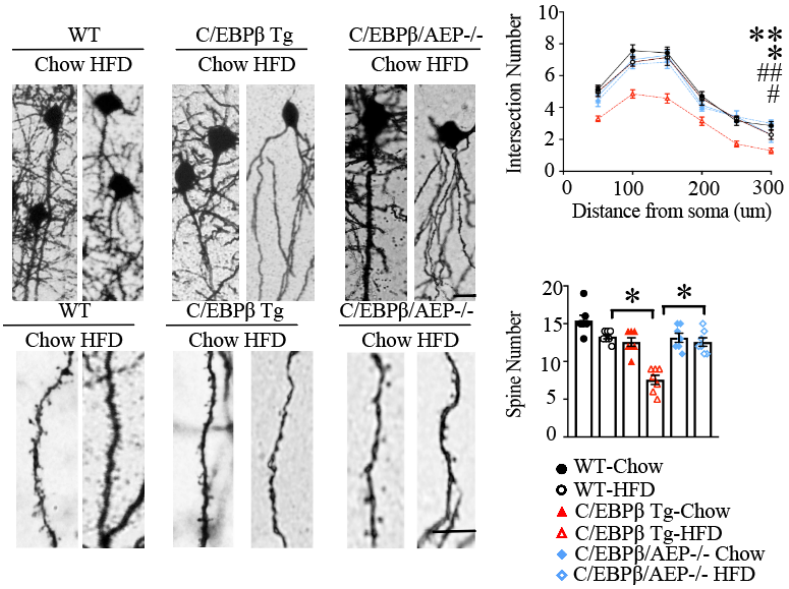

Figure 4.2 Deletion of AEP from Thy1-C/EBPβ transgenic mice ameliorates HFD-triggered synaptic degeneration

Golgi staining showed the neurite crossings and dendritic spines from the apical dendritic layer of the CA1 region. Sholl analysis of the neurites crossing (upper, Scale bar: 5 μm). (top, **P < 0.05 C/EBPβ Tg-HFD versus WT-Chow, *P < 0.05 C/EBPβ Tg-HFD versus C/EBPβ Tg-HFD, # P < 0.05 C/EBPβ Tg-HFD versus C/EBPβ Tg-Chow, ## P < 0.05 C/EBPβ Tg-HFD versus C/EBPβ/AEP-/- Tg-HFD, two-way ANOVA and Bonferroni's post hoc test). Quantitative analysis of the spine density. (bottom, mean ± SEM, n = 6 for each group, one-way ANOVA and Bonferroni's multiple comparison test, * p < 0.05, ** p < 0.01).

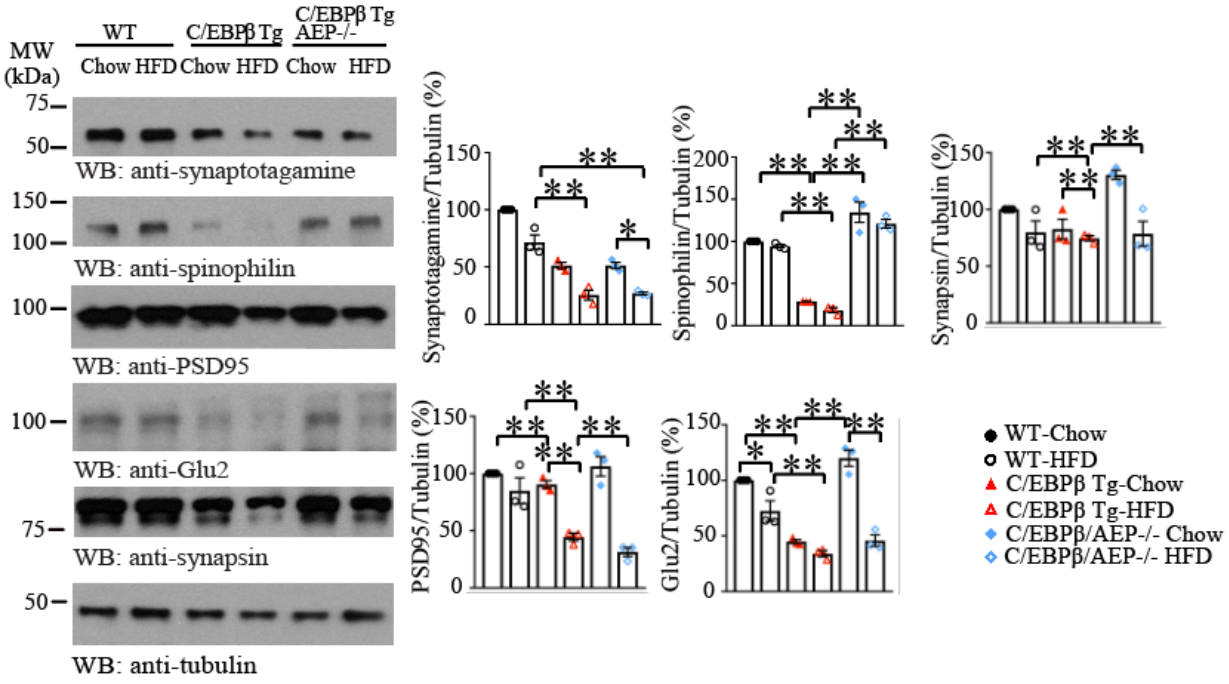

Figure 4.3 AEP knockout restores HFD-elicited reductions in synaptic proteins

Western blot assays demonstrated HFD-induced synaptic proteins downregulation in the hippocampus of C/EBPβ Tg mice. This decline was rescued by AEP KO in the transgenic mice. (Mean ± SEM, n = 3, one-way ANOVA and Bonferroni's multiple comparison test, * $p < 0.05$, ** $p < 0.01$).

In Morris Water Maze (MWM) tests, C/EBPβ Tg mice displayed impaired memory versus WT mice under both feeding conditions. Moreover, HFD strongly reduced the time spent in the platform quadrant by C/EBPβ Tg mice as compared to WT mice. Since some of the C/EBPβ/AEP -/- mice were unable to swim well, their cognitive functions could not be analyzed in the MWM assay (Figure 4.4, top panel). In fear conditioning tests, C/EBPβ Tg mice exhibited prominent cognitive defects versus WT mice under both feeding conditions. HFD significantly impaired cognitive functions in C/EBPβ Tg mice compared to WT mice. Knockout of AEP from C/EBPβ Tg mice restored the cognitive defects triggered by HFD (Figure 4.4, lower panel). Therefore, HFD elicits cognitive dysfunction in Thy1-C/EBPβ Tg mice, and AEP is necessary for this action.

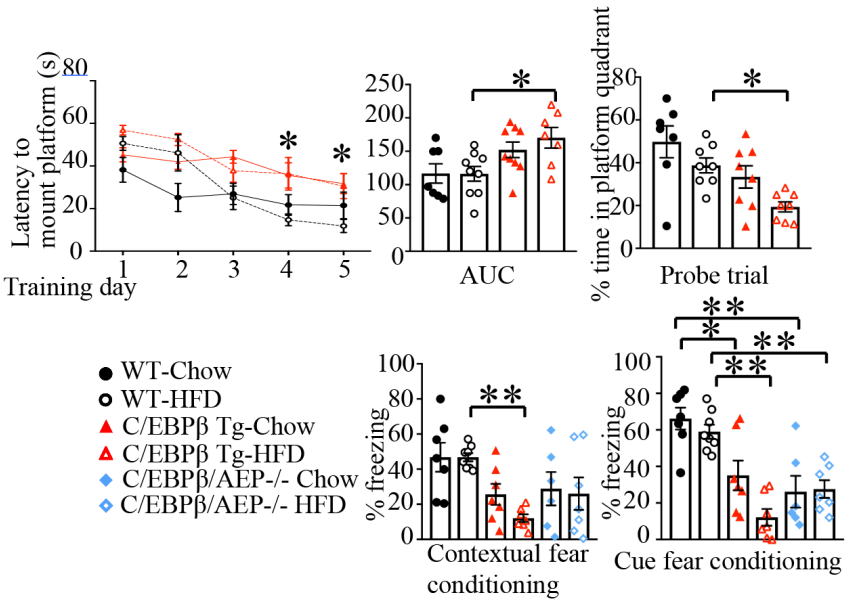

Figure 4.4 Deletion of AEP from Thy1-C/EBPβ transgenic mice ameliorates HFD-triggered cognitive dysfunction

Top panel. E. Morris water maze analysis as the percentage of time spent in the target quadrant in the probe trial (right) and the latency time (left, AUC: area under the curve) to the platform in the training days. (Mean ± SEM, n ≥ 7 mice for each group, * $p < 0.05$, ** $p < 0.01$, WT-HFD versus C/EBPβ-HFD, # $P < 0.05$, ## $P < 0.01$ C/EBPβ/AEP$^{-/-}$-HFD versus C/EBPβ-HFD, one-way ANOVA and Bonferroni's multiple comparison test). **Lower panel.** Fear conditioning tests. Contextual (left) and cued (right) fear conditioning in mice after chow or HFD treatment. (Mean ± SEM, n ≥ 6~7 mice for each group, one-way ANOVA and Bonferroni's multiple comparison test, * $p < 0.05$, ** $p < 0.01$).

4.2.2 LPS triggers APP and Tau cleavage and neuro-inflammation in Thy1-C/EBPβ transgenic mice via activation of C/EBPβ/AEP signaling

HFD induces both diabetes and AD pathology and stimulates learning and memory disorders in C/EBPβ Tg mice, and the C/EBPβ/AEP pathway plays a vital role in these events. Since C/EBPβ and inflammation mutually regulate each other (153), we wondered if HFD-elicited chronic inflammation couples these two diseases and drives the pathogenesis via activating C/EBPβ/AEP signaling. To test this notion, we chronically treated these animals with LPS (lipopolysaccharide), an endotoxin secreted by bacteria, to induce inflammation. Quantitative RT-PCR (qRT-PCR) revealed that transgenic human C/EBPβ mRNA levels remained comparable under both PBS and LPS conditions, whereas mouse C/EBPβ mRNA concentrations were significantly elevated upon LPS stimulation in both WT and C/EBPβ Tg mice but not in C/EBPβ/AEP -/- mice. These findings indicate that C/EBPβ might act as a transcription factor for *APP*, *MAPT,* and *BACE1*, driving the expression of these crucial genes in AD pathogenesis, in addition to mediating reported *LGMN* and *IL-6* genes. IB analysis indicated that LPS upregulated C/EBPβ and increased expression of its downstream targets, AEP, APP, Tau, and BACE1. These effects were highly enhanced in C/EBPβ Tg mice, leading to cleaved (active) AEP, and APP N585 and Tau N368 fragmentation produced by the activated AEP, resulting in elevation of p-Tau AT8 activity. These events were diminished in C/EBPβ +/- mice (Figure 4.5A). AEP enzymatic activities in the brain lysates oscillated with active AEP levels shown in

IB (Figure 4.5B).

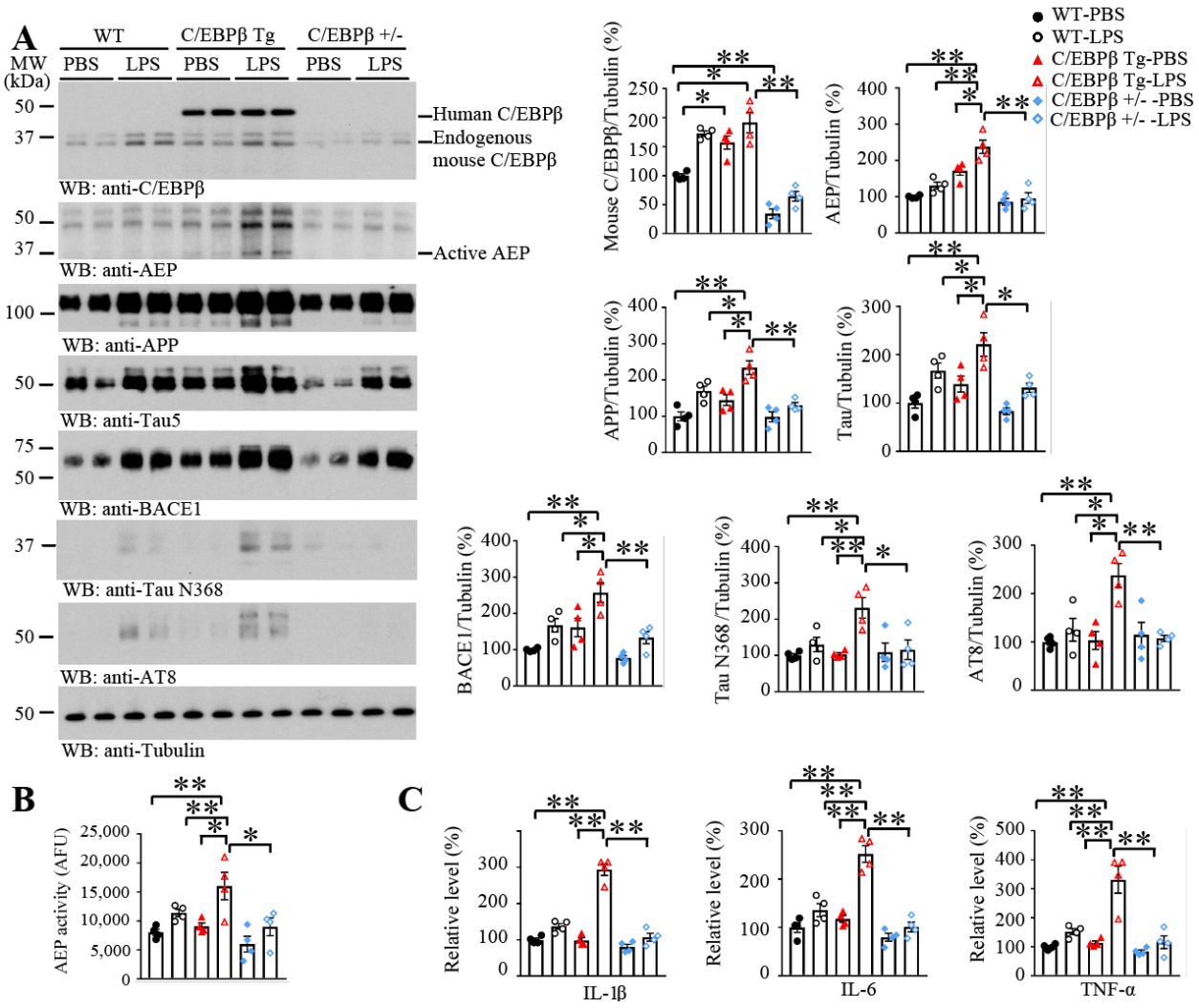

Figure 4.5 LPS triggers APP and Tau cleavage and neuro-inflammation in Thy1-C/EBPβ transgenic mice

A. Western blot assays demonstrated LPS-induced activation of C/EBPβ and C/EBPβ-mediated upregulation of AEP, APP, Tau, and BACE1 in the hippocampus compared to PBS treatment. LPS stimulation enhanced the levels of C/EBPβ downstream proteins, leading to cleavages of APP and Tau (N368) by activated AEP, and tau hyperphosphorylation (AT8) in C/EBPβ transgenic mice. Knockdown of C/EBPβ diminished these events. The relative abundance of

various indicated proteins was quantified (Mean ± SEM, n = 4, one-way ANOVA and Bonferroni's multiple comparison test, * $p < 0.05$, ** $p < 0.01$). **B.** AEP enzymatic activity assay (Mean ± SEM, n = 4, one-way ANOVA and Bonferroni's multiple comparison test, * $p < 0.05$, ** $p < 0.01$). **C.** Neuroinflammation in LPS-treated C/EBPβ transgenic mice. IL-1β, IL-6, and TNFα were quantified by the ELISA from the brain lysates. (Mean ± SEM, n = 4, one-way ANOVA and Bonferroni's multiple comparison test, ** $p < 0.01$).

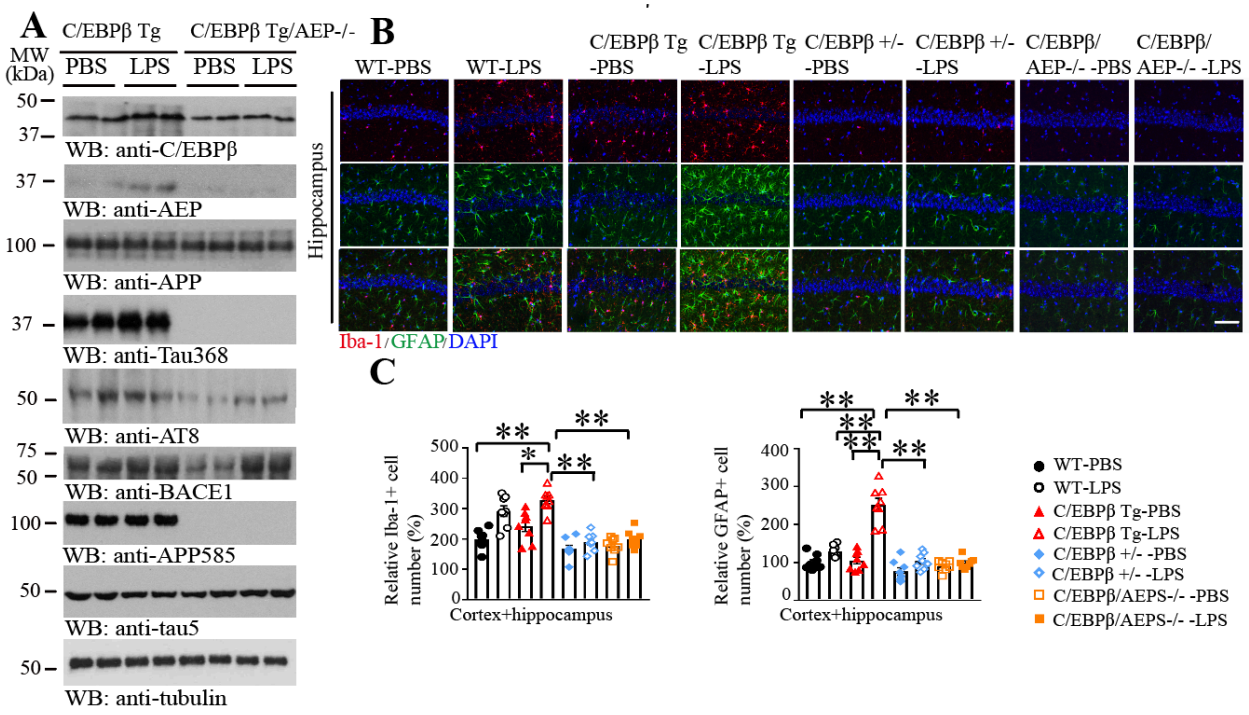

Figure 4.6 Deletion of AEP rescues LPS-triggered APP and Tau cleavage and neuro-inflammation in Thy1-C/EBPβ transgenic mice

A. Immunoblotting analysis of the brain lysates from LPS-treated C/EBPβ transgenic mice. Deletion of AEP from C/EBPβ Tg mice reduced LPS-triggered biochemical effects. **B&C.** Immunofluorescent co-staining of Iba-1 and GFAP on the hippocampal sections of the vehicle or LPS-treated WT, C/EBPβ transgenic mice, C/EBPβ+/- and C/EBPβ/AEP -/- mice. Microglia activation and gliosis were highly enriched in LPS-treated C/EBPβ transgenic mice and reduced in LPS-treated C/EBPβ transgenic mice with AEP knockout (E). Scale bar: 50 μm. The quantification of Iba-1 and gliosis were analyzed (F). (Mean ± SEM, $n \geq 7$, one-way ANOVA and Bonferroni's multiple comparison test, * $p < 0.05$, ** $p < 0.01$).

Quantitative assays of inflammatory cytokines by ELISA demonstrated that expression of IL-1β, IL6, and TNFα were greatly increased in the brains of C/EBPβ Tg mice by LPS as compared to WT or C/EBPβ +/- mice (Figure 4.5C). Moreover, IB analysis demonstrated that these LPS-stimulated biochemical effects in C/EBPβ Tg mice were greatly diminished when AEP was depleted (Figure 4.6A). IF co-staining revealed that LPS treatment robustly increased both Iba-1 and GFAP signals in brains of WT mice as compared to the PBS vehicle. These effects were further amplified in C/EBPβ Tg mice. In contrast, deletion of AEP greatly decreased Iba-1 positive microglia activation and GFAP-positive astrogliosis (Figure 4.6C & D).

To further assess the role of LPS in activating C/EBPβ and neuroinflammation in the hippocampus, we conducted IF co-staining on the brain sections after chronic LPS treatment. Both C/EBPβ and p-C/EBPβ signals were elevated in the hippocampus of WT mice by LPS, accompanied by IL-6 upregulation. These effects were greatly augmented in the hippocampus of C/EBPβ Tg mice. As a control for staining specificity, we employed C/EBPβ +/- mice. The LPS-elicited effects in these mice were greatly abrogated (Figure 5A), supporting the specificity og the anti-C/EBPβ immunofluorescent staining and that C/EBPβ indeed is responsible for the observed IL6 escalation. Quantification of these fluorescent intensity signals is summarized in Figure 4.7 B. Nissl staining revealed LPS-stimulated hippocampal volume reductions in C/EBPβ Tg mice accompanied by brain atrophy, with this effect being ameliorated in C/EBP +/- and C/EBPβ/AEP -/- mice. Consistent with our previous observations, the number of hippocampal neurons was reduced in the hippocampal CA1 and CA3 regions of C/EBPβ Tg mice treated with LPS (Figure 4.7C). Hence, chronic LPS exposure elicits C/EBPβ/AEP signaling activation,

neuroinflammation, and APP and Tau fragmentation in the brains of C/EBPβ Tg mice, and is associated with hippocampal atrophy.

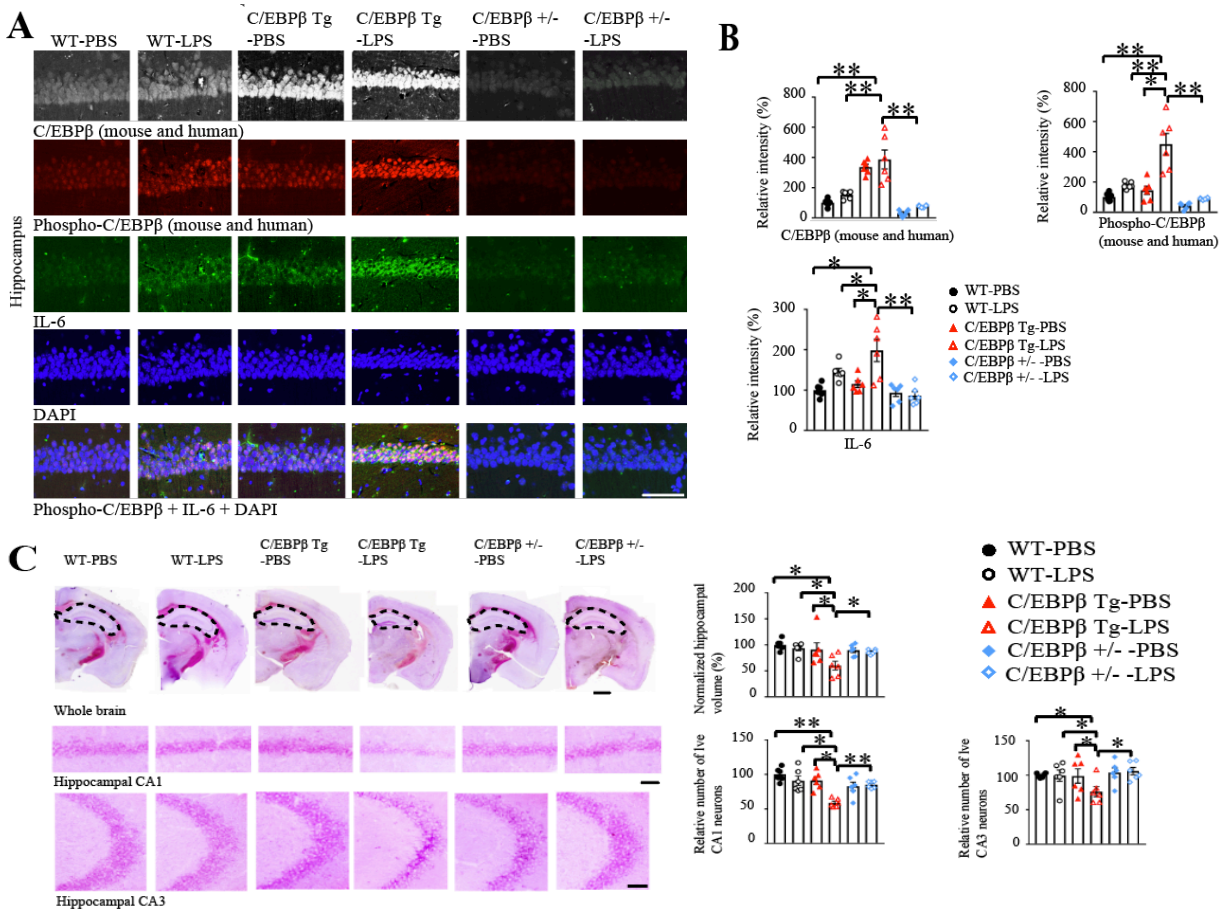

Figure 4.7 LPS triggers C/EBPβ and neuronal loss in Thy1-C/EBPβ transgenic mice

A&B. Immunofluorescent staining showed LPS-elicited p-C/EBPβ and upregulated its downstream readout IL-6 in the hippocampus in C/EBPβ transgenic mice. The relative fluorescent intensities were quantified (Mean ± SEM, n = 6, one-way ANOVA and Bonferroni's multiple comparison test, * $p < 0.05$, ** $p < 0.01$; Scale bar: 50 μm). **C.** Hippocampal neuronal loss and brain volume reduction. Nissl staining was conducted on the brain sections, and the brain volumes and hippocampal neuronal degeneration were quantified (Mean ± SEM, n = 6,

one-way ANOVA and Bonferroni's multiple comparison test, * $p < 0.05$, ** $p < 0.01$; scale bar on the top: 500 μm, scale bars in the middle and at the bottom: 50 μm). The hippocampal area is indicated by the dashed line.

4.2.3 LPS induces AD pathologies and cognitive deficits in Thy1-C/EBPβ transgenic mice

To investigate whether chronic LPS stimulation triggers AD pathologies in the brains of C/EBPβ Tg mice, we performed IHC staining with anti-Aβ (4G8) antibody on the brain sections and found that LPS stimulated formation of extensive Aβ aggregates, which were absent in WT or C/EBPβ +/- mice (Figure 4.8A &B). Co-staining with both anti-Aβ and Thioflavin S (ThS) revealed that the cores of senile plaques were ThS positive, indicating that these aggregated Aβ inclusions might form fibrillary β-sheets. Human Aβ antibody staining yielded no signals, validating that these were mouse Aβ aggregates. However, LPS failed to stimulate Aβ accumulation in C/EBPβ/AEP -/- mice (Figure 4.8C). To characterize Aβ40 and Aβ42 concentrations in the brain, we prepared the insoluble and soluble Aβ fractions with formic acid and diethylamine (DEA), respectively. Quantification indicated that Aβ40 and Aβ42 levels in both fractions were significantly enhanced in C/EBPβ Tg mice by LPS, whereas they remained unchanged in WT, C/EBPβ +/- or C/EBPβ/AEP -/- mice (Figure 4.8D). IHC staining with antibody AT8 demonstrated that chronic LPS stimulation elicited Tau hyperphosphorylation in the hippocampus in WT mice, which was markedly aggravated in C/EBPβ Tg mice. Knockout of either C/EBPβ or AEP alleviated these pathological effects (Figure 4.9A & B). Notably, co-staining revealed that AT8 positive neurons were also ThS positive, suggesting NFT (neurofibrillary tangle) accumulation in these neurons in the hippocampus of C/EBPβ Tg mice, which was further confirmed by silver staining (Figure 4.9C).

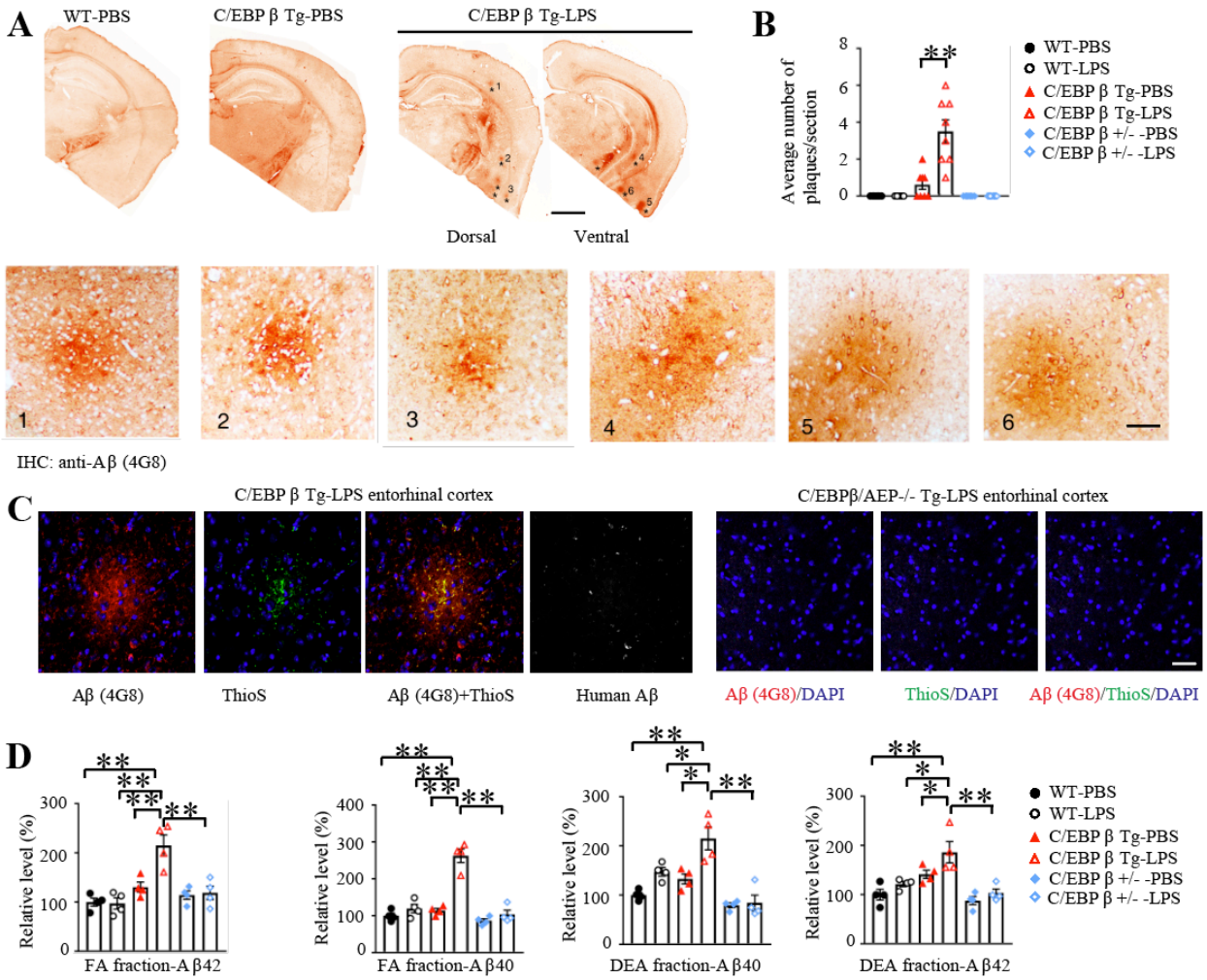

Figure 4.8 LPS induces senile plaques in Thy1-C/EBPβ transgenic mice

A. Immunohistochemistry analysis of Aβ in the cortex and hippocampus of LPS-treated C/EBPβ transgenic mice. Numerous senile plaques were identified in both the dorsal and ventral brain sections. Arrowhead indicated intracellular Aβ around the plaques (Scale bar on the top: 500 μm; scale bar at the bottom: 50 μm). **B**. Quantitative analysis of average senile plaques in the vehicle

or LPS-treated WT, C/EBPβ transgenic mice, and C/EBPβ+/- mice. (Mean ± SEM, n = 8, one-way ANOVA and Bonferroni's multiple comparison test, ** $p < 0.01$). **C**. Immunofluorescent co-staining of brain sections with anti-Aβ and Thioflavin S. Scale bar: 50 μm. **D.** Quantification of Aβ40 and 42 from the formic acid (FA, insoluble fractions) and diethylamine (DEA, soluble fractions) fractions from the animals. (Mean ± SEM, n = 4, one-way ANOVA and Bonferroni's multiple comparison test, * $p < 0.05$, ** $p < 0.01$).

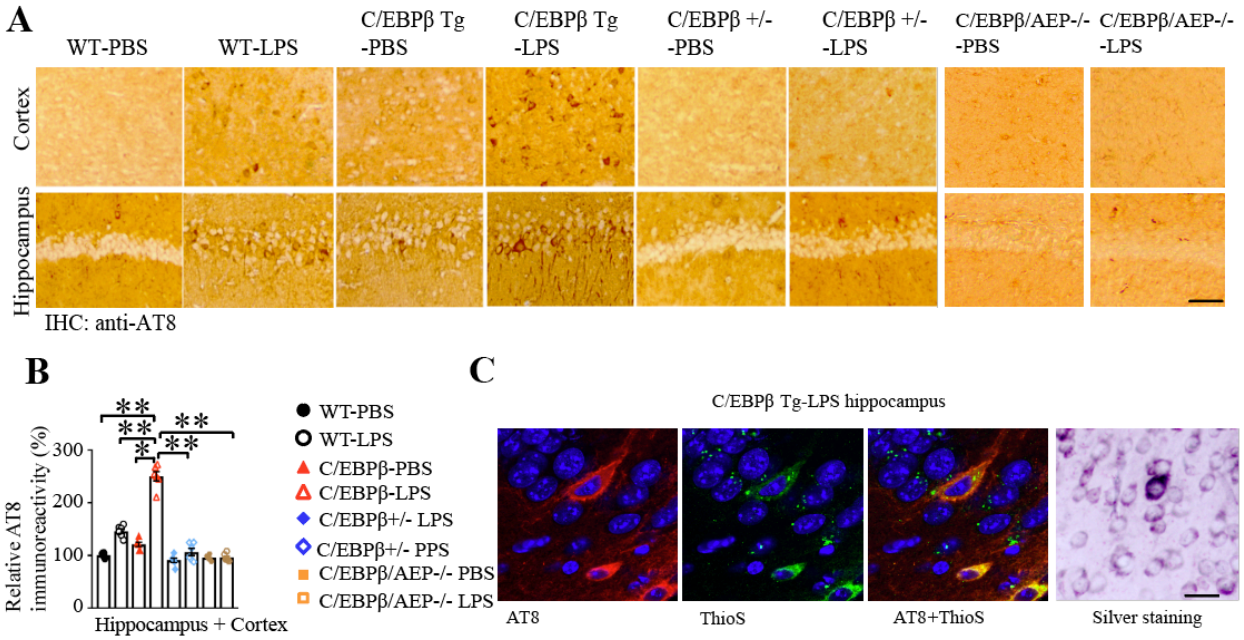

Figure 4.9 LPS elicits tau phosphorylation in Thy1-C/EBPβ transgenic mice

A&B. Immunohistochemistry of hyperphosphorylated Tau in the cortex and hippocampus of animals. Tau phosphorylation was analyzed with anti-AT8 (E). The intraneuronal NFT signals were quantified (F). (Mean ± SEM, n = 4, one-way ANOVA and Bonferroni's multiple comparison test, * $p < 0.05$, ** $p < 0.01$, scale bar: 50 μm). **C.** Immunofluorescent staining and Silver staining. LPS-triggered AT8 and ThS co-staining in the hippocampus of C/EBPβ Tg mice. Silver staining revealed the proteinaceous inclusions.

Sholl analysis showed that dendritic branching and process crossing were substantially diminished in C/EBPβ Tg mice upon LPS chronic treatment as compared to WT mice. Moreover, Golgi staining revealed that the dendritic spines were significantly reduced in C/EBPβ Tg mice as compared to WT mice. Deletion of C/EBPβ or knockout AEP from C/EBPβ Tg mice alleviated these effects (Figure 4.10A&B).

IB analysis demonstrated that expression of synaptic proteins was clearly decreased in C/EBPβ Tg mice after chronic LPS treatment, which was alleviated in C/EBPβ/AEP -/- mice (Figure 4.11A), underscoring that LPS triggers synaptic degeneration in C/EBPβ Tg mice, for which AEP is necessary. Quantitative analysis revealed that LPS strongly increased expression of inflammatory cytokines, including IL-1β and IL-6 in WT mice. These were further enhanced by LPS in C/EBPβ Tg mice, and TNFα levels were also robustly elevated in these mice. As expected, this stimulatory effect was abrogated in C/EBPβ/AEP -/- mice (Figure 4.11B).

MWM results were consistent with the idea that chronic LPS stimulation triggered learning and memory deficits in C/EBPβ Tg mice without impairing the motor functions because these mice exhibited comparable swimming speeds (Figure 4.12A-C). Fear conditioning tests showed that LPS triggered dramatic cognitive deficits in C/EBPβ Tg mice as compared to WT mice, but C/EBPβ/AEP -/- or C/EBPβ +/- mice were resistant to LPS stimulation (Figure 4.12D&E). Hence, these results support the notion that LPS treatment stimulates both AD pathologies and cognitive dysfunctions in C/EBPβ Tg mice, with AEP being required for this effect.

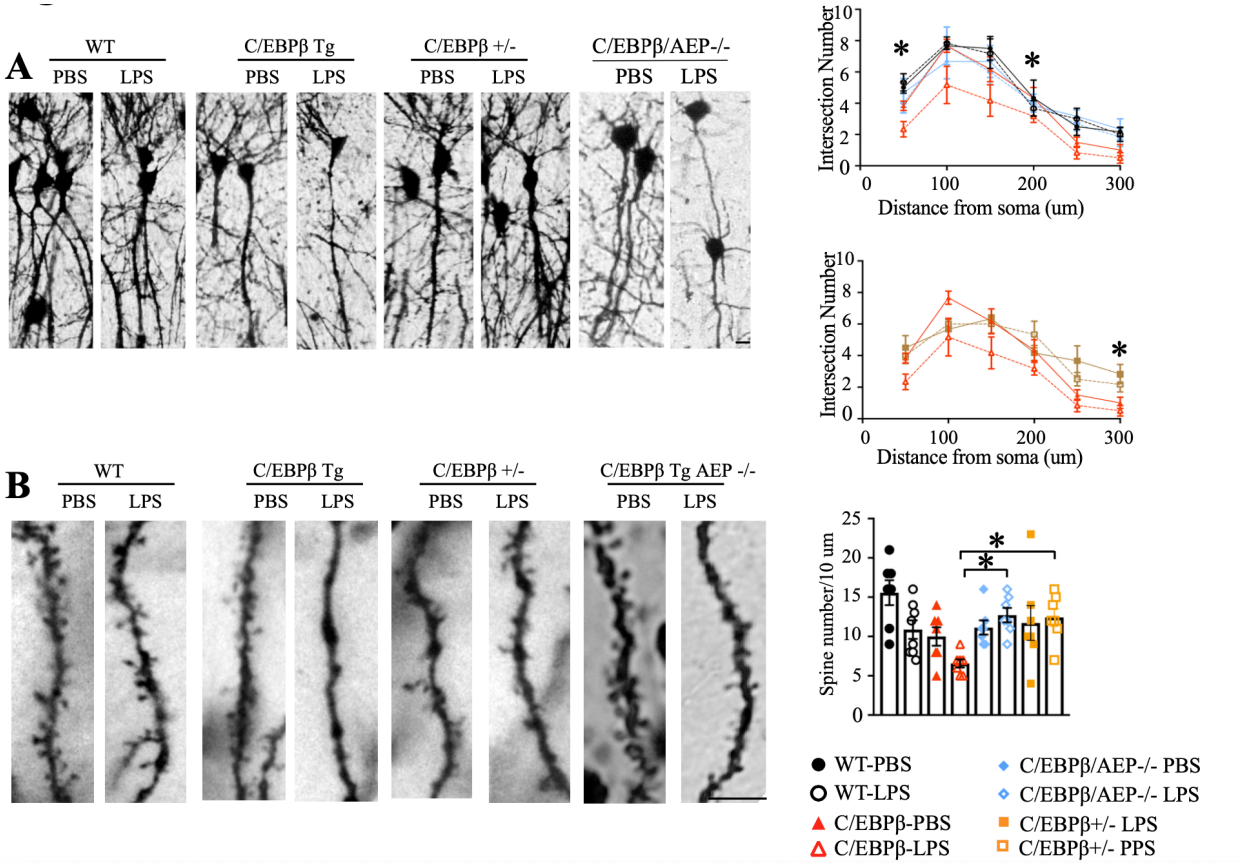

Figure 4.10 LPS reduces neurite crossings and dendritic spines in C/EBPβ Tg mice

A&B. Golgi staining showed the neurite crossing and dendritic spines from the apical dendritic layer of the CA1 region. (Left, Scale bar: 5 μm). Sholl analysis revealed the synaptic arborization reduction in LPS-treated Thy1-C/EBPβ transgenic mice (Scale bar: 5 μm). Quantitative analysis of the intersection crossing in these animals (Middle, mean ± SEM, n = 6 for each group, * $p < 0.05$, ** $p < 0.01$, WT-LPS versus C/EBPβ-LPS, # $p < 0.05$, ## $p < 0.01$ C/EBPβ/AEP$^{-/-}$-LPS versus C/EBPβ-LPS, one-way ANOVA and Bonferroni's post hoc test) (A).

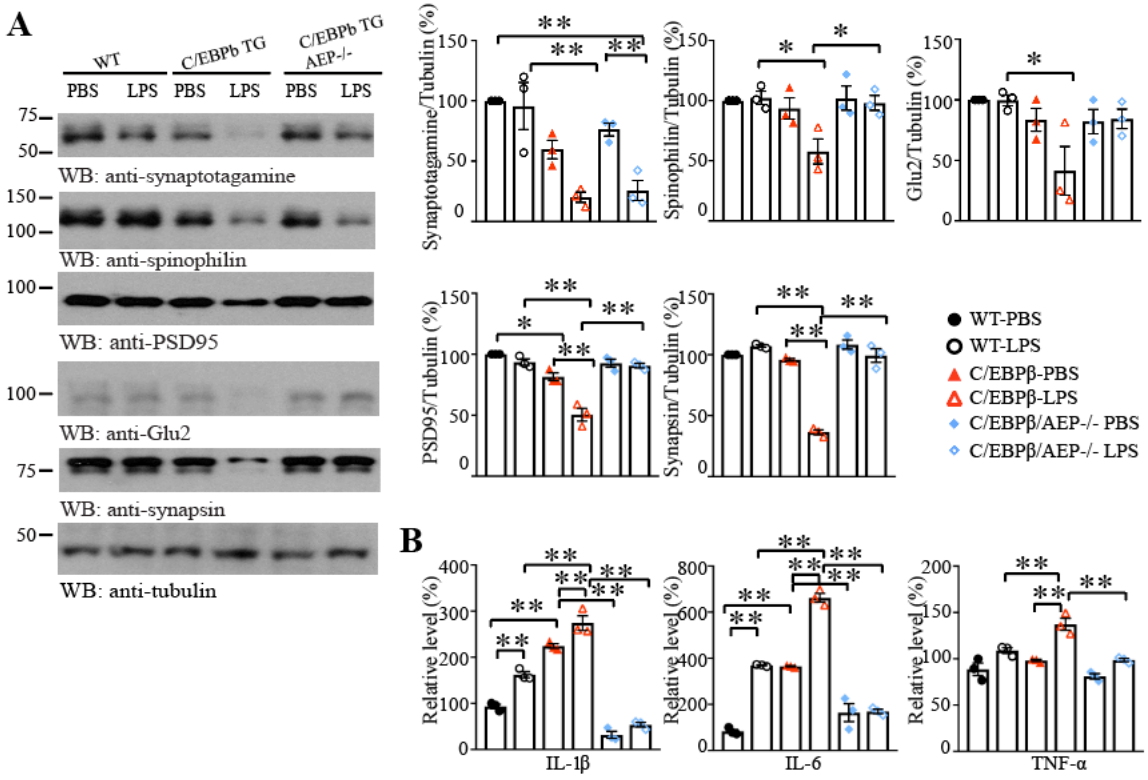

Figure 4.11 Deletion of AEP rescues LPS-reduced synaptic proteins

A. Western blot assays demonstrated LPS-induced downregulation of synaptic proteins in the hippocampus of C/EBPβ Tg mice compared to PBS treatment. This decline was rescued in C/EBPβ/AEP KO mice. (Mean ± SEM, n = 3, one-way ANOVA and Bonferroni's multiple comparison test, * $p < 0.05$, ** $p < 0.01$). **B.** Quantification of LPS-induced neuroinflammation. ELISA analysis of neuroinflammation factors IL-1β (left), IL-6 (middle), TNFα (right) in the serum from wild-type, C/EBPβ transgenic mice, and C/EBPβ/AEP -/- mice (6–7 months old) that have been treated with PBS or LPS. (Mean ± SEM, n = 3 mice for each group, one-way ANOVA, and Bonferroni's multiple comparison test. * $p < 0.05$, ** $p < 0.01$).

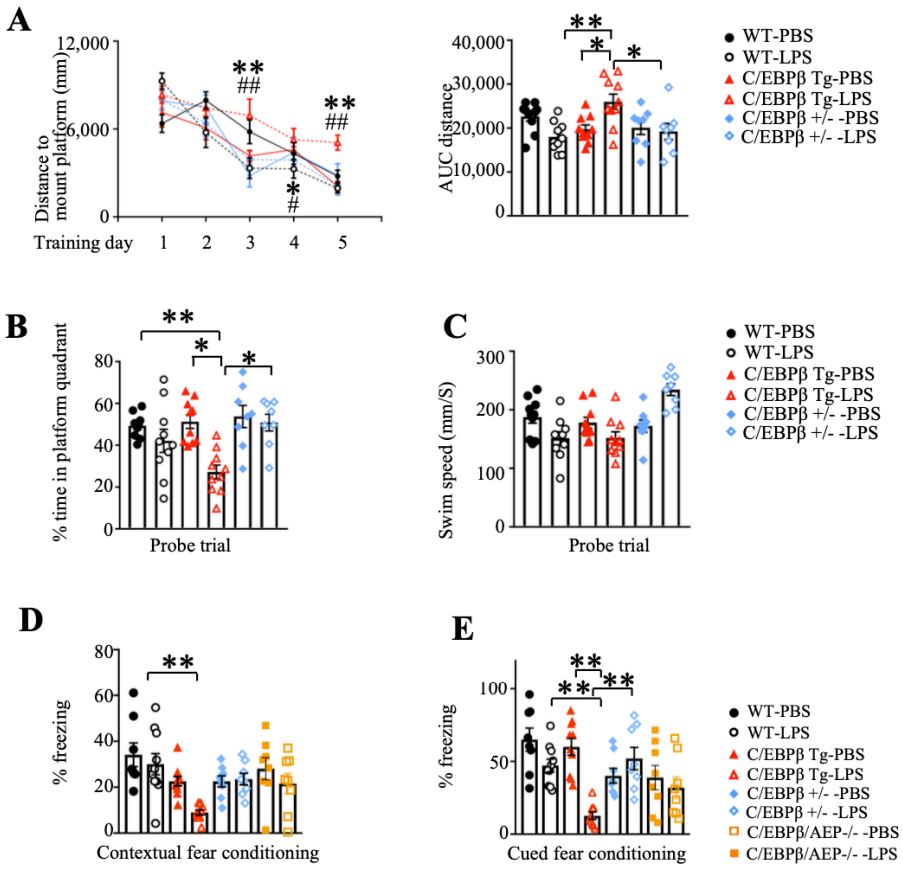

Figure 4.12 Deletion of AEP from Thy1-C/EBPβ transgenic mice alleviates LPS-induced cognitive defects

A-C. Morris Water Maze cognitive-behavioral test. Chronic LPS administration impaired the learning and memory in C/EBPβ transgenic mice (Mean ± SEM, n = 8-10 mice for each group, ** * $p < 0.05$, ** $p < 0.01$, WT-LPS versus C/EBPβ-LPS, # $p < 0.05$, ## $p < 0.01$ C/EBPβ$^{+/-}$-LPS versus C/EBPβ-LPS, one-way ANOVA and Bonferroni's post hoc test for A; one-way ANOVA and Bonferroni's multiple comparison test for B and C, * $p < 0.05$, ** $p < 0.01$). The swimming speeds among the groups remained comparable with each other (C). **D&E.** Fear conditioning tests. Contextual and cued fear conditioning was impaired in C/EBPβ transgenic mice upon chronic LPS treatments (Mean ± SEM, n = 7-10 mice for each group, one-way ANOVA and Bonferroni's multiple comparison test, * $p < 0.05$, ** $p < 0.01$).

4.2.4 NSAID aspirin abrogates HFD-induced inflammation, diabetes, and AD pathologies in Thy1-C/EBPβ transgenic mice

As shown above, HFD or LPS-induced chronic inflammation triggers neuronal C/EBPβ/AEP signaling activation, leading to AD pathogenesis and cognitive defects in Thy1-C/EBPβ Tg mice. To ascertain whether chronic inflammation is indeed driving this effect, we pretreated WT or C/EBPβ Tg mice with HFD for 2 months, followed by the non-steroid anti-inflammatory drug (NSAID) aspirin and HFD co-treatment for 1 month. At the end of the treatment, we examined the expression of pro-inflammatory cytokines in the serum and the brains. We found that aspirin greatly diminished inflammation in these tissues from both WT and C/EBPβ Tg mice as compared to vehicle control, and also significantly blunted AEP enzymatic activities in both mice (Figure 4.13). In alignment with neuro-inflammation reduction, Iba-1 and GFAP co-staining revealed that HFD-triggered microglia activation and astrogliosis were markedly suppressed by aspirin (Figure 4.13). IB analysis showed that aspirin also substantially reduced HFD-provoked C/EBPβ/AEP signaling. Consequently, AEP-truncated APP N585 and Tau N368 fragmentation was robustly antagonized, leading to AT8 activities decrease (Figure 4.14). IHC staining indicated that HFD-elicited mouse Aβ aggregates (4G8) and mouse Tau hyper-phosphorylation (AT8) were attenuated by aspirin (Figure 4.17 A&B). IF co-staining showed that HFD-induced C/EBPβ/AEP signaling activation and subsequent APP N585 and Tau N368 cleavage by active AEP were inhibited by aspirin (Figure 4.17 C&D, Figure 4.18). On the other hand, insulin signaling pathways, including p-IR/p-IRS/p-Akt/p-GSK3β in the brain of C/EBPβ Tg mice, were repressed by HFD as compared to WT mice. Aspirin treatment significantly alleviated this inhibitory effect (Figure 4.15), indicating that HFD-induced insulin resistance in C/EBPβ Tg mice in the brain is assuaged by aspirin. Sholl analysis and Golgi staining supported

that the neurite crossing and the dendritic spine reduction in C/EBPβ Tg mice induced by HFD were restored by aspirin as compared to vehicle (Figure 4.19). Accordingly, cognitive-behavioral tests demonstrated that HFD-triggered learning and memory defects in C/EBPβ Tg mice were greatly rescued by the aspirin treatment (Figure 4.16). Together, these data support that the NSAID aspirin blocks HFD-induced neuroinflammation in C/EBPβ Tg mice and attenuates insulin resistance and AD pathologies, restoring cognitive functions.

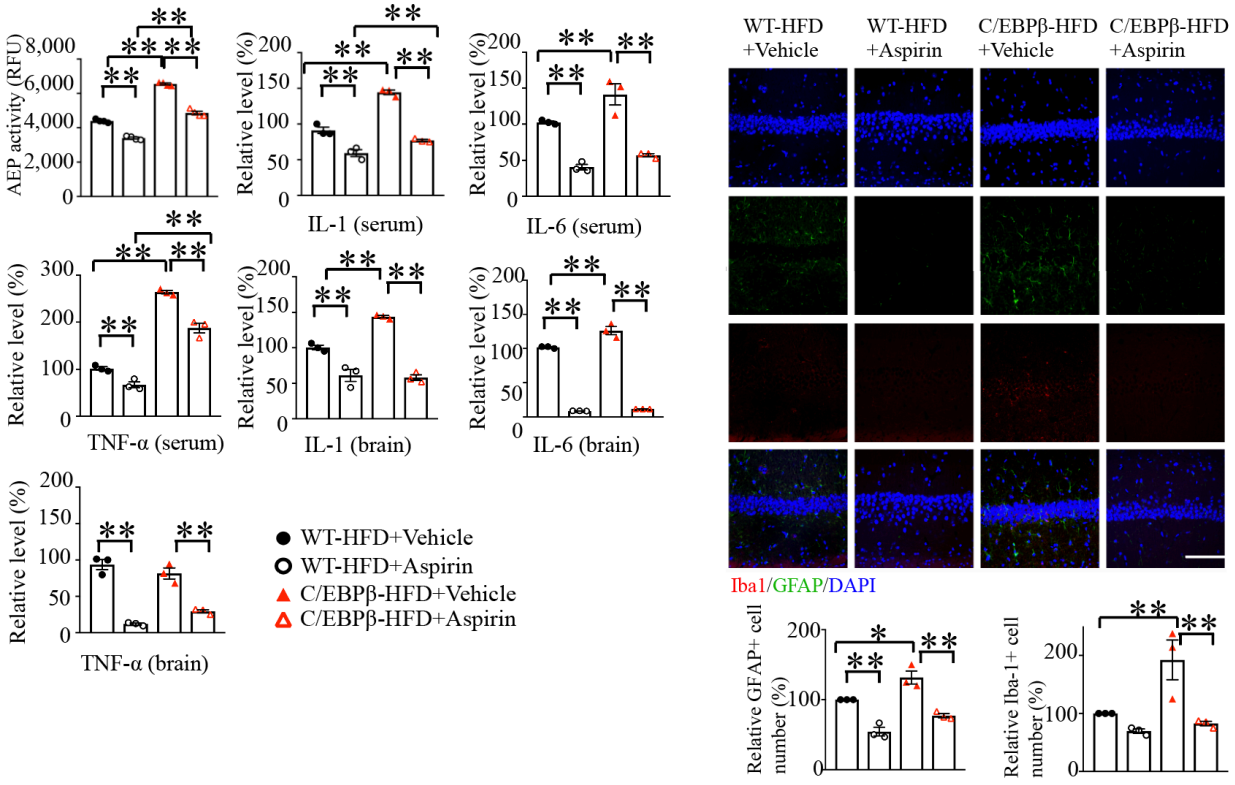

Figure 4.13 NSAID aspirin abrogates HFD-induced inflammation in Thy1- C/EBPβ transgenic mice

Left. AEP enzymatic activity assay (Mean ± SEM, n = 3, one-way ANOVA and Bonferroni's multiple comparison test, * $p < 0.05$, ** $p < 0.01$). ELISA analysis of neuroinflammation factors IL-1β, IL-6, TNFα in the serum and brain lysates from wild-type and C/EBPβ transgenic mice (6–7 months old) that have been fed HFD for 12 weeks and administered with either aspirin or vehicle in the last 4 weeks of the 12-week HFD. (Mean ± SEM, n = 3 mice for each group, one-way ANOVA, and Bonferroni's multiple comparison test. * $p < 0.05$, ** $p < 0.01$). **Right.** Immunofluorescent co-staining of Iba-1 and GFAP on the hippocampal sections of chow diet or HFD or HFD with aspirin-treated or vehicle WT and C/EBPβ transgenic mice. Scale bar: 50 μm. The quantification of Iba-1 and gliosis were analyzed. (Mean ± SEM, n = 3, one-way ANOVA and Bonferroni's multiple comparison test, * $p < 0.05$, ** $p < 0.01$).

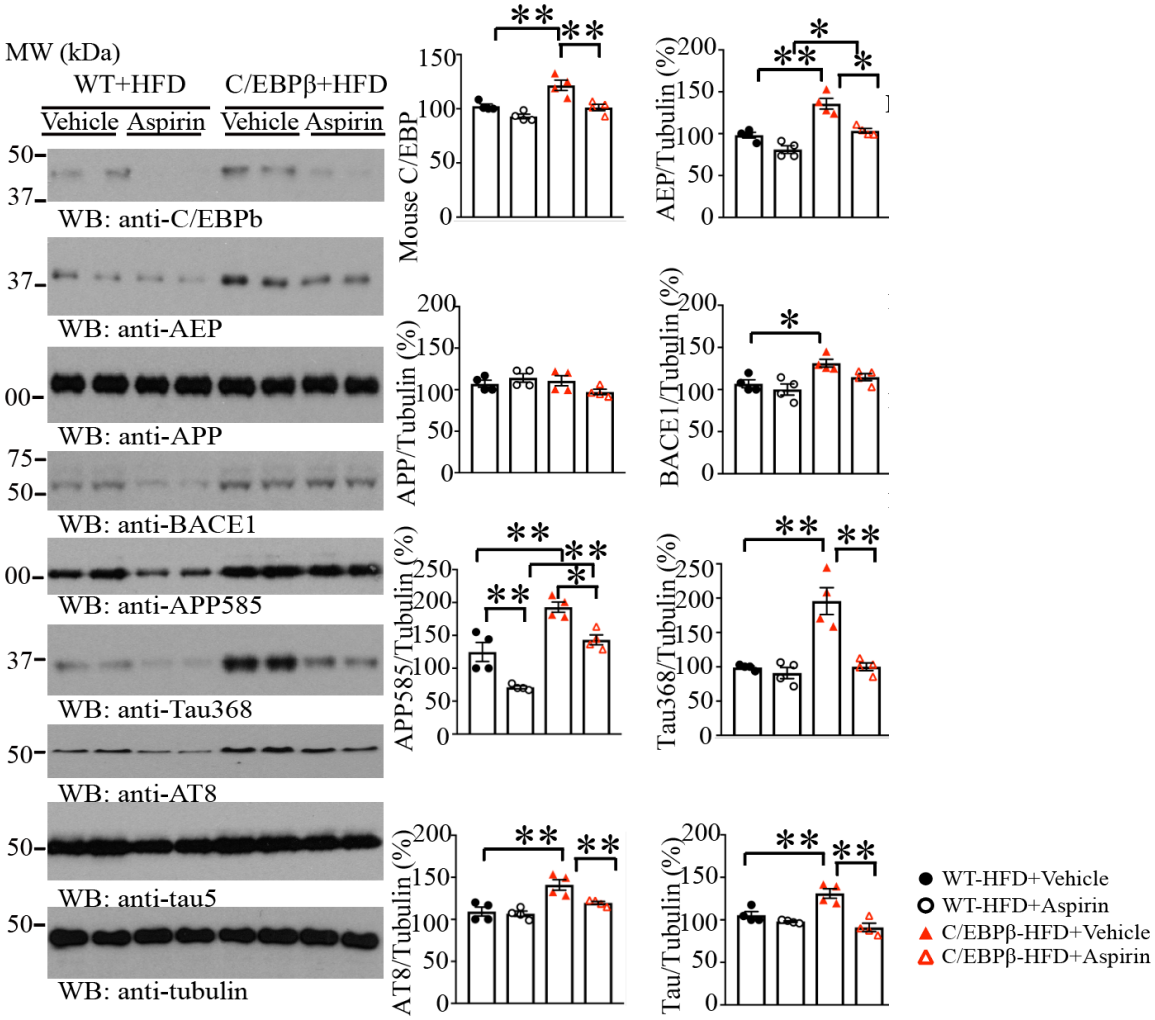

Figure 4.14 Aspirin abrogates HFD-induced APP and tau fragmentation in Thy1- C/EBPβ transgenic mice

Western blot assays demonstrated reduced activation of C/EBPβ and C/EBPβ- mediated downregulation of AEP, APP, Tau, and BACE1 in the hippocampus from HFD-fed mice treated with aspirin. Reductions of C/EBPβ in the hippocampus decreased the levels of C/EBPβ downstream proteins, leading to decreased cleavage of APP (N585) and Tau (N368) by AEP, and tau hyperphosphorylation (AT8). The relative abundance of various indicated proteins was

quantified (Mean ± SEM, n = 4, one-way ANOVA and Bonferroni's multiple comparison test, * $p < 0.05$, ** $p < 0.01$).

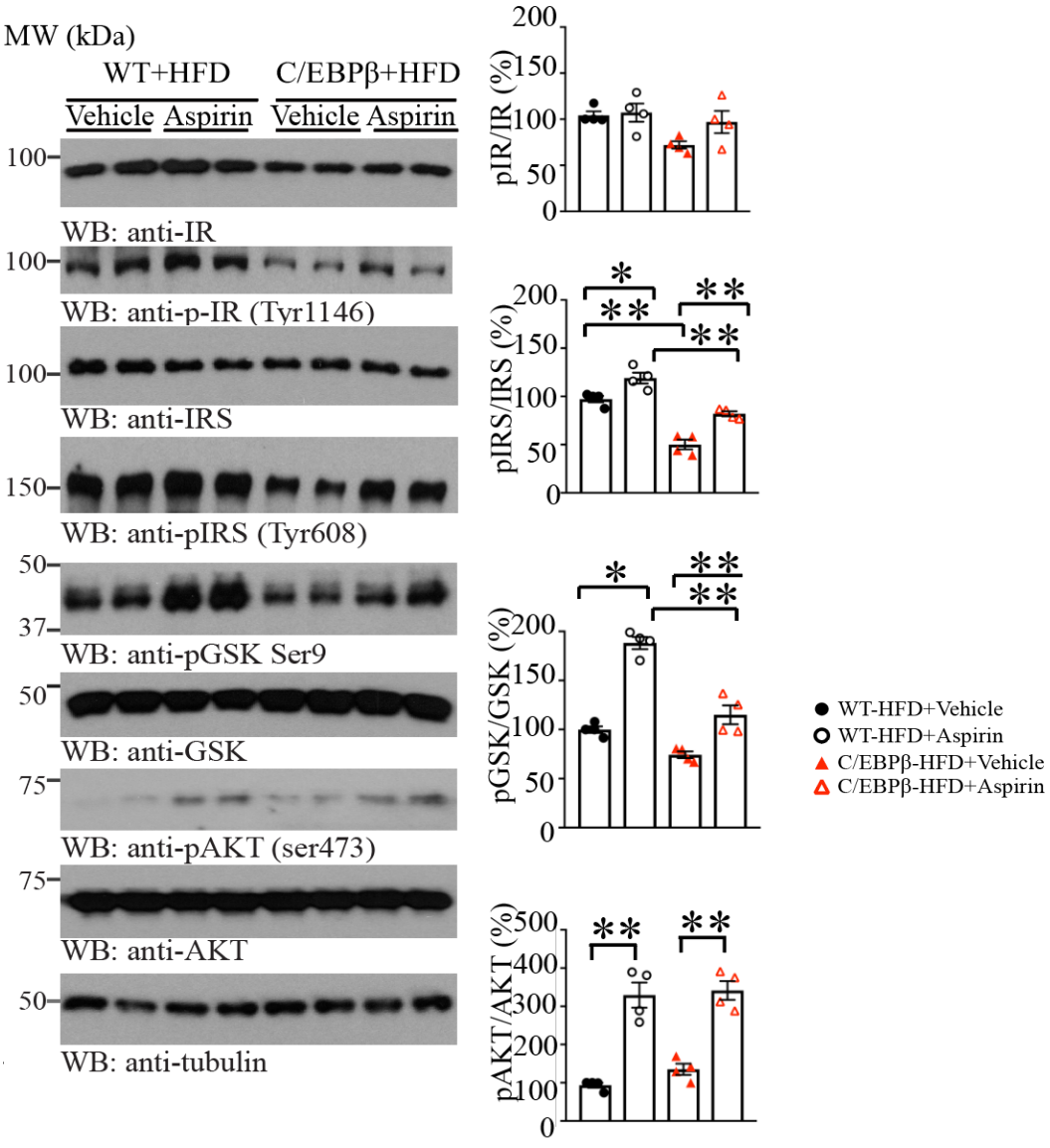

Figure 4.15 Aspirin restores HFD-induced insulin signaling impairment in Thy1- C/EBPβ transgenic mice

Analysis of insulin signaling pathway in the hippocampus of HFD or chow-diet fed wild-type and C/EBPβ transgenic mice with either vehicle or aspirin treatment. Extracts of brain tissues

were prepared and immunoblotted with IR, phosphor-IR (Tyr^{1146}), IRS, phosphor-IRS (Tyr^{608}), AKT, phosphor-AKT (Ser^{473}) antibodies. The relative abundance of various indicated proteins was quantified (Mean ± SEM, n = 4, one-way ANOVA and Bonferroni's multiple comparison test, * $p < 0.05$, ** $p < 0.01$).

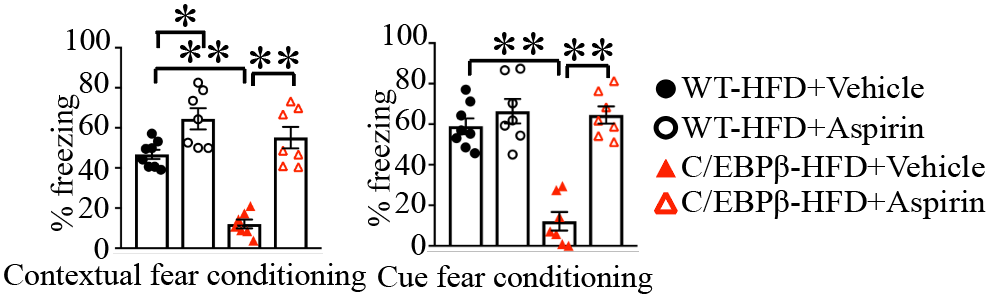

Figure 4.16 Aspirin alleviates HFD-triggered cognitive decline in Thy1- C/EBPβ transgenic mice

Fear conditioning tests. Contextual (left) and cued (right) fear conditioning in the animals. (Mean ± SEM, n ≥ 7 mice for each group, one-way ANOVA and Bonferroni's multiple comparison test, * $p < 0.05$, ** $p < 0.01$).

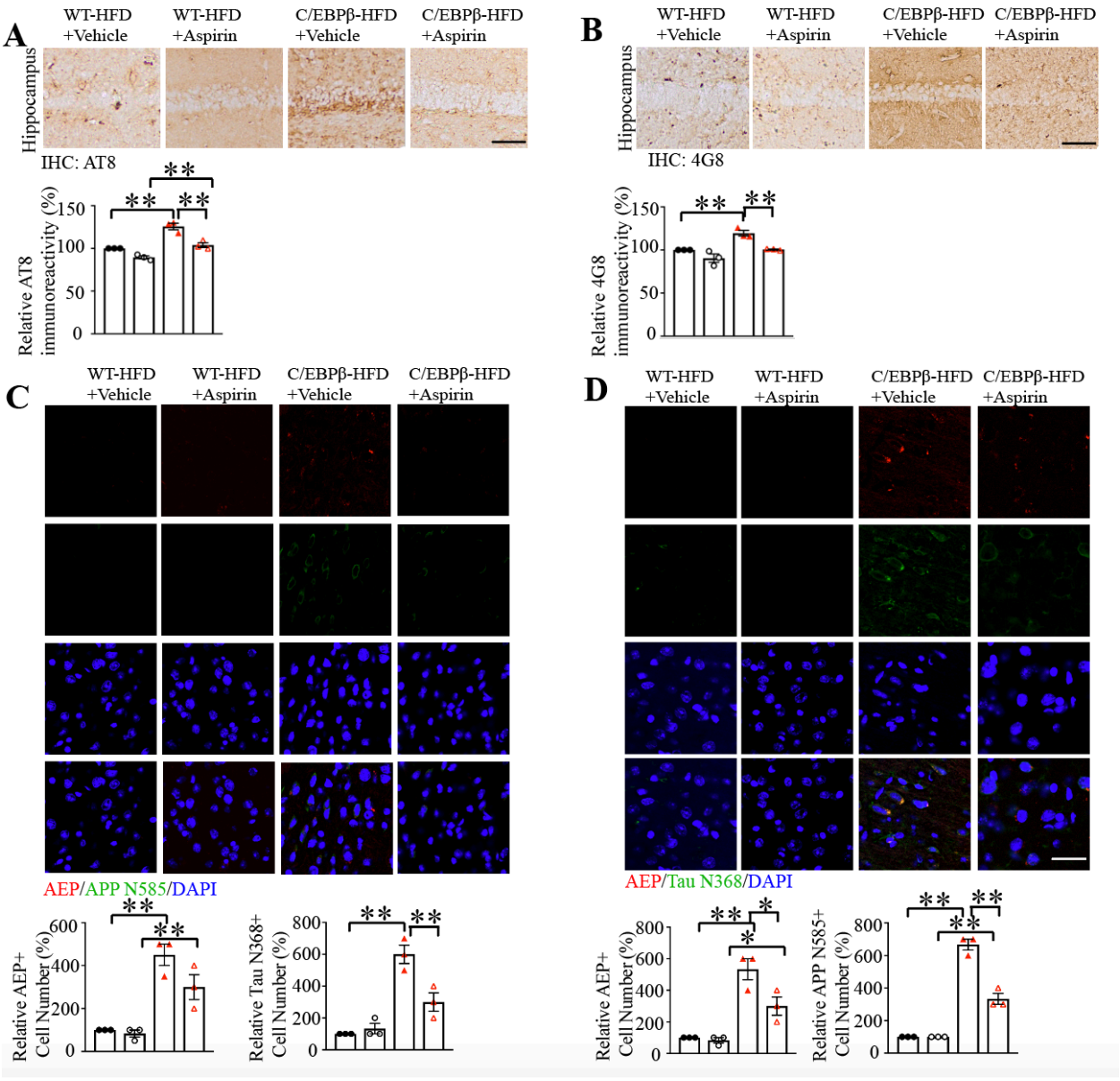

Figure 4.17 Aspirin diminishes HFD-induced APP and Tau cleavage

A. Immunohistochemistry of hyperphosphorylated Tau in the hippocampus of animals. Tau phosphorylation was analyzed with anti-AT8. The intraneuronal NFT signals were quantified. (Mean ± SEM, n = 3, one-way ANOVA and Bonferroni's multiple comparison test, ** $p < 0.05$, ** $p < 0.01$, scale bar: 50 μm). **B.** Immunohistochemistry analysis of Aβ (4G8) in the cortex of HFD-C/EBPβ transgenic mice and HFD-wild-type mice with vehicle or aspirin treatment. The

relative abundance of 4G8 was quantified (Mean ± SEM, n = 3, one-way ANOVA and Bonferroni's multiple comparison test, * $p < 0.05$, ** $p < 0.01$). **C.** Immunofluorescent co-staining of AEP and APP N585 on the cortex sections of HFD-treated WT and C/EBPβ transgenic mice with either vehicle or aspirin treatment. AEP and APP N585 signals were upregulated in HFD-treated C/EBPβ transgenic mice but reduced by aspirin. The relative abundance of various indicated proteins was quantified (Mean ± SEM, n = 3, one-way ANOVA and Bonferroni's multiple comparison test, * $p < 0.05$, ** $p < 0.01$). **D.** Immunofluorescent co-staining of AEP and Tau N368 on the cortex sections of HFD-treated WT and C/EBPβ transgenic mice either with or without aspirin treatment. AEP and Tau N368 signals were upregulated in HFD-treated C/EBPβ transgenic mice but reduced by aspirin. The relative abundance of various indicated proteins was quantified (Mean ± SEM, n = 3, one-way ANOVA and Bonferroni's multiple comparison test, * $p < 0.05$, ** $p < 0.01$).

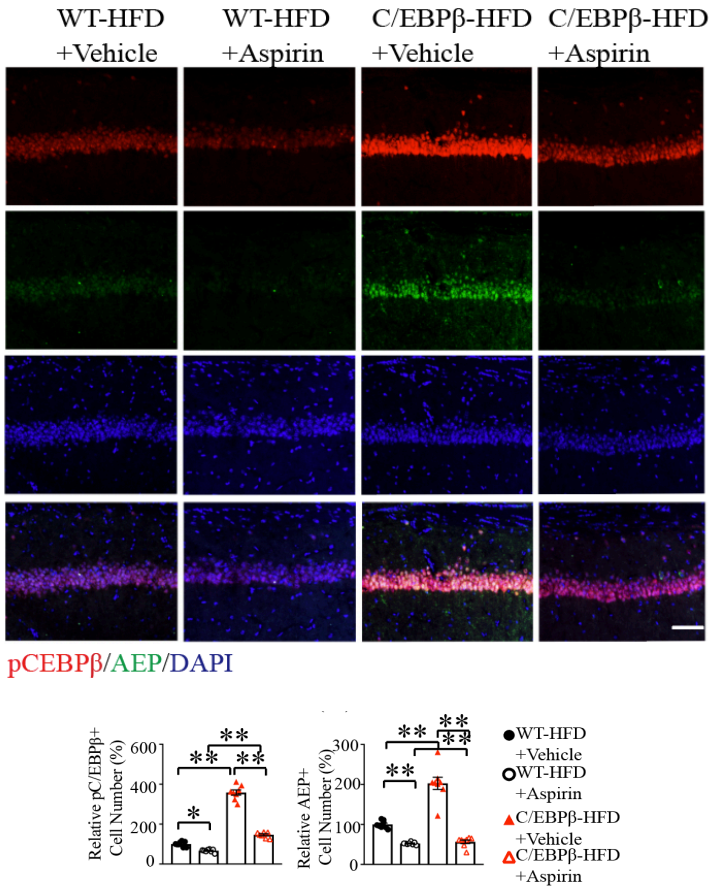

Figure 4.18 Aspirin abrogates HFD-induced C/EBP**β**/AEP signaling activation

Immunofluorescent co-staining of AEP and phosphor-C/EBPβ on the hippocampal sections of aspirin or HFD-treated WT and C/EBPβ transgenic mice. AEP and p-C/EBPβ signals were upregulated in HFD-treated C/EBPβ transgenic mice, which were suppressed by aspirin. Scale bar: 50 μm. The relative abundance of various indicated proteins was quantified. (Mean ± SEM, n = 8, one-way ANOVA and Bonferroni's multiple comparison test, * $p < 0.05$, ** $p < 0.01$).

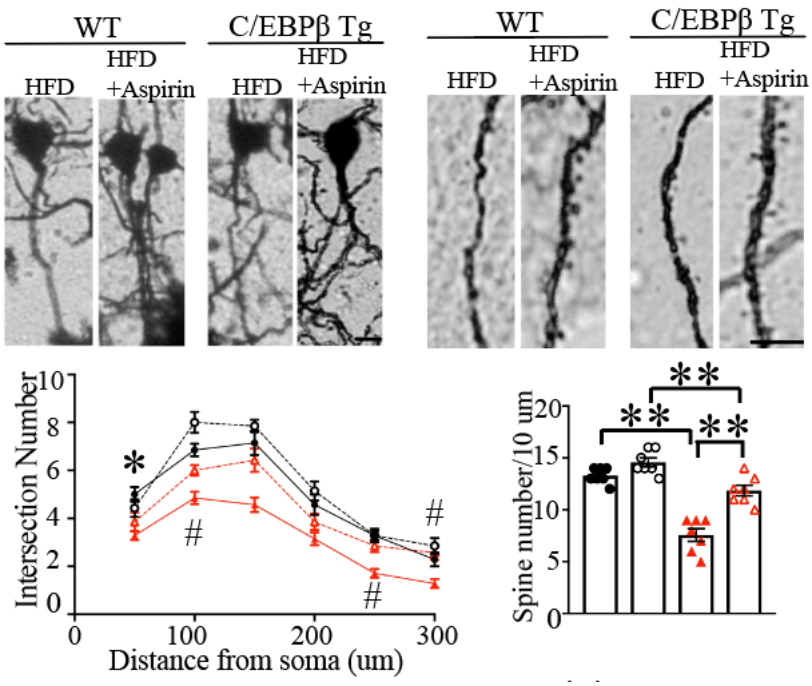

Figure 4.19 Aspirin restores neurite crossings elicited by HFD in Thy1-5 C/EBPβ Tg mice Golgi staining and Quantitative analysis of the intersection crossing in these animals (* $p < 0.05$, ** $p < 0.01$, WT-HFD versus C/EBPβ-HFD, # $p < 0.05$, ## $p < 0.01$ C/EBPβ-HFD versus C/EBPβ-HFD-Aspirin, one-way ANOVA and Bonferroni's post hoc test). Golgi staining showed the dendritic spines from the apical dendritic layer of the CA1 region. (Scale bar: 5 μm). Quantitative analysis of the spine density. (Right, mean ± SEM, n = 6 for each group, one-way ANOVA and Bonferroni's multiple comparison test, * $p < 0.05$, ** $p < 0.01$).

CHAPTER 5: Conclusion and Discussion

5.1 Conclusion and discussion of the dissertation study

This dissertation study aimed to examine the role of inflammation-activated C/EBPβ/AEP in AD-diabetes coupling. The findings of this study suggest that HFD induces diabetes and impairs insulin signaling in Thy1-C/EBPβ transgenic mice whereas knockout of AEP partially alleviates this effect. This study also showed that HFD induces AD pathology including neuroinflammation, synaptic degeneration, and cognitive deficits in Thy1-C/EBPβ transgenic mice. Deletion of AEP from Thy1-C/EBPβ transgenic mice alleviates HFD-induced AD pathology. Moreover, LPS triggers AD pathology in Thy1-C/EBPβ transgenic mice through C/EBPβ/AEP signaling pathway. NSAID aspirin reduced HFD-elicited inflammation, diabetes, and AD pathologies in Thy1-C/EBPβ mice. Taken together, these data indicate that HFD-elicited inflammation is the major activator of the C/EBPβ/AEP pathway that links diabetes and AD. Multiple lines of evidence highlight the importance of peripheral inflammation and its link to neuroinflammation, which leads to neurodegenerative diseases including AD and Parkinson's disease (PD) (94). In the current study, we demonstrate that HFD treatment induces diabetes in Thy1-C/EBPβ Tg mice (Figure 1-3), accompanied by demonstrable neuroinflammation that is manifested by extensive gliosis and microglial activation in the brain. Employing pro-inflammatory LPS and the anti-inflammatory drug aspirin, we found that diabetes-associated inflammation activates neuronal C/EBPβ, which subsequently upregulates APP and Tau expression levels that are cleaved by augmented AEP and BACE1 (Figure 5-7). Consequently, mouse Aβ and phosphorylated mouse Tau are accumulated and aggregated into proteinaceous inclusions that are associated with diminished dendritic spines with simplified dendritic arbor morphology, resulting in cognitive defects (Figure 5 & 6). Notably, deletion of AEP from Thy1-C/EBPβ Tg mice not only abolishes HFD-induced obesity and diabetes but also abrogates AD-

like pathologies and cognitive deficits. It remains unclear why C/EBPβ Tg/AEP -/- mice are abnormal in swimming, although other aspects of their locomotor function appear normal. Hence, we cannot use MWM tests to evaluate their cognitive performance. As expected, depletion of AEP markedly decreased HFD or LPS-triggered inflammation and C/EBPβ activation in the brains, underscoring that inflammation links diabetes to AD via activating neuronal C/EBPβ/AEP signaling. This observation is further enforced by the observation that aspirin, which robustly antagonized HFD-induced neuroinflammation and AD-like pathologies in C/EBPβ Tg mice, restored insulin signaling and cognitive function.

AMPK is the master sensor for energy status and is responsible for the metabolic homeostasis (154). Once activated, AMPK initiates a concomitant inhibition of energy-consuming biosynthetic pathways and activation of ATP-producing pathways such as fatty oxidation in mitochondria (155). One of the functions of AMPK is to switch off fatty acid synthesis via p-ACC. In alignment with the obese phenotype in WT mice upon HFD treatment, p-AMPK/p-ACC signaling is reduced in WT mice. Notably, p-AMPK/p-ACC is further repressed in C/EBPβ Tg mice after HFD treatment. The decreased p-AMPK and p-ACC in the WAT of Thy1-CEBPβ Tg mice lead to lipid accumulation and adipocytes hyperplasia upon HFD treatment (Figure 3.9). This finding also indicates that neuronal C/EBPβ somehow exacerbates the inhibitory actions of HFD feeding on these enzymes in the peripheral tissues. Deletion of AEP in C/EBPβ Tg mice alleviates the inhibitory activities of HFD (Figure 3.4, Figure 3.5), indicating that AEP plays an essential role in mediating HFD's antagonistic effect on the AMPK/ACC pathway. Remarkably, the p-AMPK/p-ACC pathway and insulin signaling display the same activation format in both the brain and peripheral tissues (Figure 3.4, Figure 3.5, Figure 3.9A). Interestingly, like C/EBPβ -/- mice, Thy1-C/EBPβ Tg mice are also lean in body weight as compared to WT littermates

(Figure 3.6A). Though HFD progressively increases the bodyweight of Thy1-C/EBPβ Tg mice, they are still substantially lighter than their WT counterparts, albeit their food intakes remain comparable (Figure 3.5). It has been reported that a change in neuronal AMPK signaling enhances energy expenditure via the sympathetic nervous system. For instance, thyroid hormone suppresses AMPK activity in the hypothalamus, which leads to the activation of UCP1 expression in the BAT, causing an increase of whole-body energy expenditure (156). Because a decrease in p-AMPK/p-ACC signaling was detected in the brain of Thy1-C/EBPβ Tg mice (Figure 3.13A), this may elicit energy expenditure escalation, leading to bodyweight reduction in CEBPβ Tg mice. Although AMPK inhibition in the hypothalamus suppressed hepatic glucose production, the relationship between neuronal AMPK activity and peripheral insulin signaling has not been clearly established (157). Hence, it remains unknown how impaired the AMPK/ACC pathway in the brain of Thy1-C/EBPβ Tg mice alters the insulin signaling in their peripheral tissues. In alignment with the crosstalk between neuronal overexpressed C/EBPβ and AMPK in peripheral tissues, previous studies show that C/EBPβ is phosphorylated by CK2 (casein kinase 2) under AMPK suppression and ER stress, worsening the pathological condition of type 2 diabetes, such as decreased insulin secretion and apoptosis of pancreatic β cells(158). Moreover, C/EBPβ is suppressed by the AMPK-activator AICAR or constitutively active AMPK, while dominant-negative AMPK increases the C/EBPβ expression (159).
C/EBPβ knockout mice are resistant to HFD-induced obesity, exhibit decreased serum triacylglycerol and cholesterol concentrations, and also exhibit lower hepatic triacylglycerol concentrations compared to their wild-type littermates (130). Moreover, the expression of hepatic lipogenic genes is downregulated, while the expression of β-oxidation genes in brown adipose tissue is increased (130). In Figure 2E and F, HFD treatment prominently reduces p-IR,

p-IRS, and p-Akt in both muscle and liver in C/EBPβ Tg mice, leading to insulin resistance in C/EBPβ Tg mice versus WT mice, which is supported by the GTT data (Figure 2.6C). Remarkably, downregulation of IR/IRS/Akt signaling in the brain can only be found in 16-month-old CEBPβ Tg mice but not in younger mice under chow diet (Figure 3.5A), suggesting that increased expression of C/EBPβ in neurons in the brain *per se* does not change the IR signaling, but that other factors/stresses during aging are needed to trigger the insulin resistance, thereby fitting with the observation that the impaired IR signaling is only detected in HFD-fed C/EBPβ Tg mice (Figure 2.12, Figure 2.13, Figure 2.14). Previous studies demonstrate that insulin regulates the expression of C/EBPβ in various peripheral tissues (160, 161). Moreover, insulin triggers expression of numerous stress-responsive genes via inducing C/EBPβ (162). C/EBPβ is also implicated in mediating IGF-1 and IR expression via binding to their promoters (129, 163, 164). Nevertheless, accumulating evidence shows that C/EBPβ in the liver and the pancreas negatively regulates insulin levels (165). Moreover, C/EBPβ is accumulated in the pancreatic islets of diabetic animal models because of ER stress before the onset of hyperglycemia. Transgenic overexpression of C/EBPβ specifically in β cells of mice reduces β cell mass and lowers plasma insulin levels, resulting in the development of diabetes. Conversely, genetic ablation of C/EBPβ in the β cells of leptin receptor-deficient (Lepr -/-) mice, a mouse model of diabetes, increases β cell mass and ameliorates hyperglycemia. Thus, the accumulation of C/EBPβ in pancreatic β cells contributes to β cell failure in mice by enhancing susceptibility to ER stress (165). Mounting evidence supports that the brain coordinates the aging process by acting as a primary sensor of physiological and environmental stressors through the action of conserved signaling pathways. Conceivably, neuronal C/EBPβ overexpression in Thy1-

C/EBPβ transgenic mice mediates neural endocrine effects that may affect peripheral insulin signaling.

C/EBPβ performs diverse functions, participating in the regulation of genes that contribute to the acute phase response, glucose metabolism, and tissue differentiation, including adipogenesis and hematopoiesis. C/EBPβ is important in the differentiation and maturation of adipocytes (130). C/EBPβ is also activated in proinflammatory conditions (108). It feeds back and elevates the expression of various proinflammatory genes (111). Accordingly, C/EBPβ deletion completely blunts the HFD-induced inflammation (166). In obesity, adipose tissue macrophages are polarized into pro-inflammatory M1 macrophages and secrete many pro-inflammatory cytokines capable of impairing insulin signaling, therefore promoting the progression of insulin resistance (70). Consequently, we observed insulin signaling reduction in Thy1-C/EBPβ Tg mouse brains, associated with p-IRS/p-Akt attenuation in an age-dependent manner (Figure 3.13A, Figure 3.5A). Moreover, HFD treatment induces pronounced insulin resistance in Thy1-C/EBPβ Tg mice, revealed by ITT and GTT assays, accompanied by blunted insulin signaling (Figure 3.6, Figure 3.7, Figure 3.12). Accordingly, both gliosis and microglial activation is highly elevated in Thy1-C/EBPβ Tg mice by HFD, suggesting that neuroinflammation is greatly augmented in the brains of C/EBPβ Tg mice. As expected, the downstream targets of C/EBPβ, APP, Tau, AEP, and BACE1 are robustly escalated in the brains. Consequently, APP N585 and Tau N368 are profoundly increased by AEP fragmentation, which is associated with augmented Aβ production and p-Tau (Figure 4.6, Figure 4.7, Figure 3.13, Figure 3.14, Figure 3.15). These findings, consistent with previous studies in HFD-induced AD animal models, have shown that brain insulin resistance in these animals leads to the accumulation of Aβ and the reduction in GSK-3β phosphorylation which promotes Tau phosphorylation to cause AD (167, 168).

Cognitive decline is a major hallmark of aging and is exacerbated in patients with neurodegenerative diseases. Impairments in cerebral glucose utilization and energy metabolism are the early abnormalities that precede (or are concurrent with) the initial stages of cognitive impairment. However, the cause of cerebral regional glucose hypometabolism remains unclear. Thiamine-dependent enzymes, the critical components of glucose metabolism, are reduced in the brains of AD patients and also by thiamine decline, and it is possible that a decrease in the levels of these enzymes could account for the reduction in glucose metabolism (169). Thiamine-dependent processes are critical in glucose metabolism and are diminished in the brains of AD patients at autopsy. Further, the reductions in thiamine-dependent processes are highly correlated to the decline in clinical dementia rating scales. In animal models, thiamine deficiency exacerbates plaque formation, promotes phosphorylation of Tau, and impairs memory. In contrast, treatment of mouse models of AD with the thiamine derivative, benfotiamine, diminishes plaque formation, decreases phosphorylation of tau, and reverses memory deficits (170). Accordingly, we monitored thiamine and its major metabolite thiamine diphosphate (TDP) in the blood from chow and HFD-treated Thy1-C/EBPβ Tg mice and found that thiamine but not TDP is significantly reduced in C/EBPβ Tg mice as compared to WT mice under both feeding conditions (Figure 3.8), indicating that glucose metabolism is severely attenuated in the brains of C/EBPβ Tg mice and fitting with the severe impairment of insulin signaling (Figure 3.12, Figure 3.13, Figure 3.14, Figure 3.15).

Previous studies show that C/EBPβ is age-dependently escalated in the hippocampal neurons (171). We reported that C/EBPβ can act as a crucial transcription factor for *LGMN* and temporally dictates AEP expression in the neurons (122). To interrogate the biological roles of neuronal C/EBPβ escalation in AD pathogenesis, we develop the neuronal-specific Thy1-

C/EBPβ Tg mice. C/EBPβ is readily activated by inflammation triggered by HFD or LPS (Figure 3.14, Figure 4.5), and to assess the pathological role of inflammation in coupling diabetes to AD, we treated the Thy1-C/EBPβ mice with aspirin as an NSAID while feeding HFD. As expected, aspirin strongly abrogates the inflammation and ameliorates the AD-like pathologies, restoring learning and memory (Figure 4.14, Figure 4.15, Figure 4.16, Figure 4.17, Figure 4.18, Figure 4.19). Oxidative arachidonic acid (AA) metabolism is a major hallmark of neuroinflammation (172). Following its release from the cell membrane, AA is metabolized via cyclooxygenases (COX-1, 2) and 5-lipoxygenase (5-LOX) into prostaglandins (PGs) and leukotrienes (LTs), respectively. These bioactive lipids are potent mediators of inflammation. The AA metabolic pathway is not only the core network of inflammation but also the main cause of working memory impairment in AD pathogenesis (43, 173). Aspirin reduces inflammation by acting as a potent inhibitor of Cox enzymes(174). Consequently, aspirin treatment diminished p-C/EBPβ/AEP signaling in the brain, alleviating AD pathology, and increasing cognitive functions.

We also employed AEP-/- mice fed with chow diet and HFD as additional control groups to monitor the effects of AEP deletion. WT and AEP-/- mice exhibited comparable body weights under the chow diet. HFD administration increase body weights in both groups, but the bodyweight of AEP-/- mice with HFD is slightly lower when compared with the WT-HFD mice (Figure 5.1A). As expected, enzymatic assays show that AEP protease activities were abolished in AEP -/- mice (Figure 5.1B). Quantification demonstrated that HFD enhanced levels of pro-inflammatory cytokines including IL-1β and IL6, in the serum and brain in both WT and AEP -/- mice. TNFα is increased in the serum, but not in the brain, of both animals under HFD (Figure 5.1 C&D). This might be explained by the fact that C/EBPχ was originally identified as IL6-

dependent DNA-binding protein, thereby having a lesser effect on TNFα generation (175). HFD fed WT and AEP -/- show slightly increased blood glucose levels but the difference is not statistically significant (Figure 5.2 A&B). However, HFD treatment increases insulin levels in both animal groups under HFD, and AEP deletion slightly diminishes this effect (Figure 5.2 C&D). This is consistent with a previous study that reported high mRNA levels of *LGMN* after pancreatectomy (142). WT mice exhibit significantly increased blood cholesterol levels after HFD treatment, but this effect is drastically alleviated by AEP knockout (Figure 5.2 E). Free fatty acids and triglycerides levels are comparable between animal groups with different diets (Figure 5.2 F&G). Additionally, AEP-/- mice show comparable baseline lipid droplet size comparable to WT under chow diet. HFD treatment increase the mean size of droplets AEP-/- but it is still slightly smaller than WT-HFD (Figure 5.3).

Together, our study supports that diabetes-associated chronic inflammation triggers C/EBPβ/AEP signaling activation, leading to AD pathogenesis in Thy1-C/EBPβ transgenic mice. Conceivably, the management of diabetes, assisted by anti-inflammatory aspirin treatment, may ameliorate AD onset and progression in the general population.

This study was published in *Molecular Psychiatry* in May 2022.

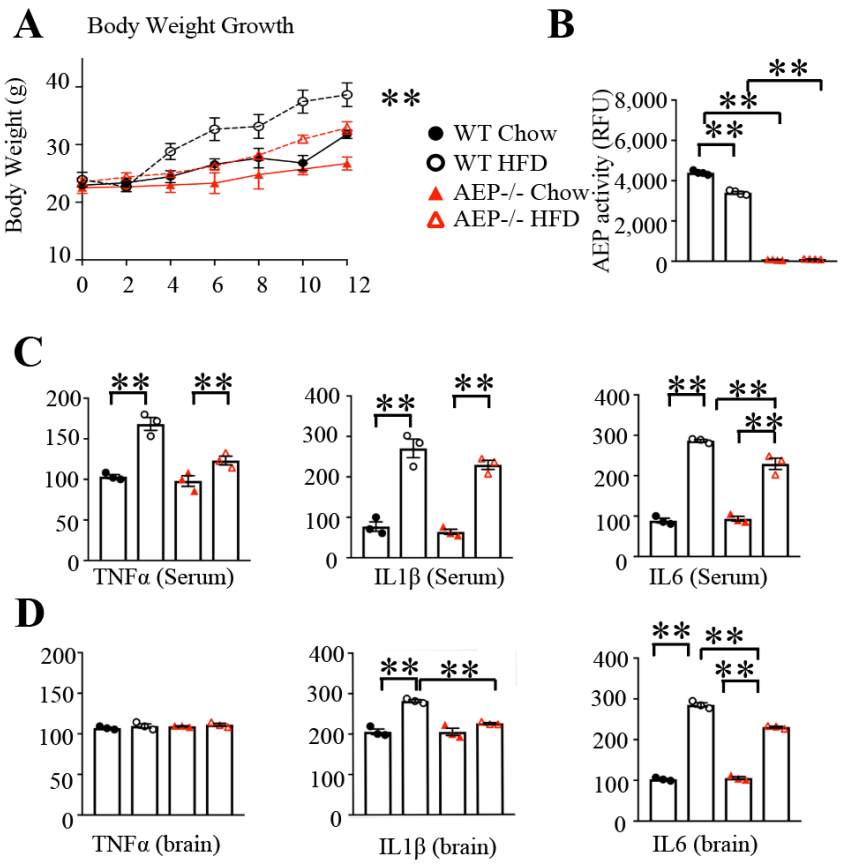

Figure 5.1 Deletion of AEP partially restores HFD-induced inflammation in WT mice

A. Growth curves of 3-month-old wild-type and AEP -/- transgenic mice fed with chow diet or HFD. Bodyweight was measured biweekly and expressed as mean ±SEM (n =7–10; * $P < 0.05$, ** $P < 0.01$, WT-HFD versus AEP-/-, one-way ANOVA and Bonferroni's post hoc test). B. AEP enzymatic activity assay (Mean ± SEM, n = 3, one-way ANOVA and Bonferroni's multiple comparison test, * $p < 0.05$, ** $p < 0.01$). C&D. Inflammation was diminished in HFD-treated AEP-/- transgenic mice. IL-1b, IL-6, and TNFa were quantified by the ELISA from the serum

samples. (Mean ± SEM, n = 3; one-way ANOVA and Bonferroni's multiple comparison test, * p < 0.05, ** p < 0.01).

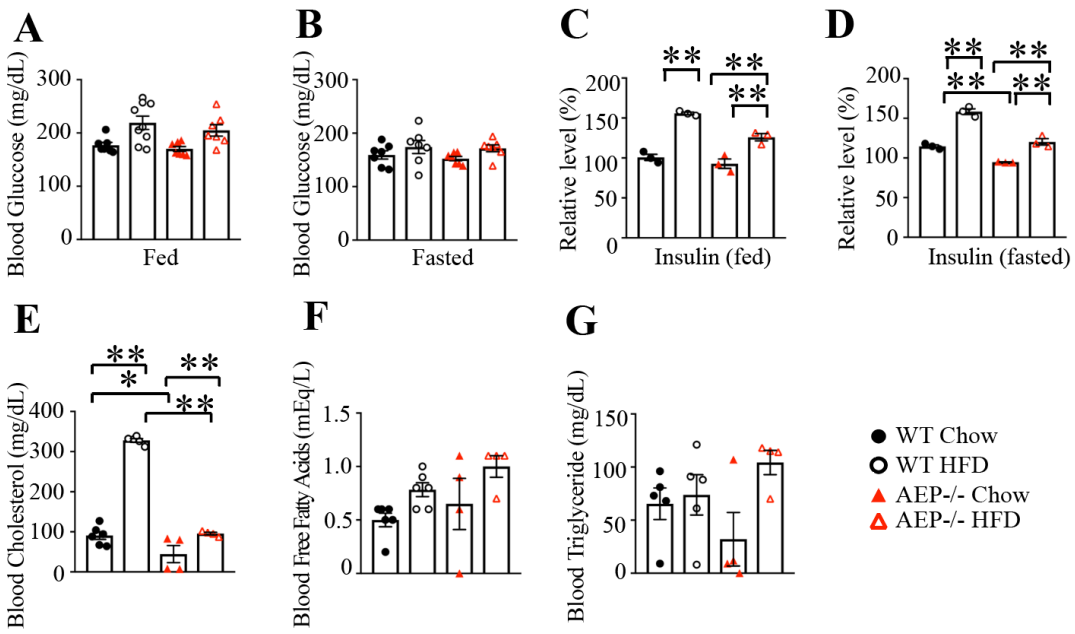

Figure 5.2 Deletion of AEP partially restores HFD-induced insulin elevation in WT mice

A&B. Blood glucose level of fed and fasting wild-type and AEP -/- mice (6–7 months old) that have been fed with chow diet or HFD for 12 weeks (n = 3). Results were expressed as mean ±SEM (* $P < 0.05$, ** $P < 0.01$; one-way ANOVA and Bonferroni's multiple comparison test). **C&D.** Circulating insulin concentration of fed and fasting wild-type and AEP -/- mice (6–7 months old) that have been fed with chow diet or HFD for 12 weeks (n = 3). Results were expressed as mean ±SEM (* $P < 0.05$, ** $P < 0.01$; one-way ANOVA and Bonferroni's multiple comparison test). **E-G**. Serum cholesterol, free fatty acids, and triglyceride levels of wild-type and AEP-/- animals that have been fed with chow diet or HFD**.** Results were expressed as mean ±SEM (n=3, * p < 0.05, ** p < 0.01; one-way ANOVA and Bonferroni's multiple comparison test).

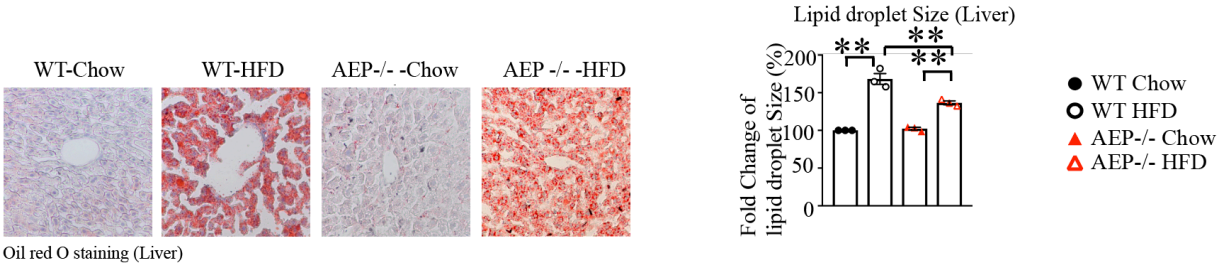

Figure 5.3 Knockout of AEP alleviates lipid droplet expansion triggered by HFD in WT mice

Oil red O staining of liver sections collected from wild-type and AEP-/- animals that have been fed with chow diet or HFD for 12 weeks. (Scale bar: 50 μm.) A representative result from each genotype is shown. Quantification of the lipid droplet size is shown on the right.

5.2 AEP's role in provoking pathogenesis in Alzheimer's disease

The following sections briefly discuss AEP's role in promoting AD pathology through its phosphorylation by Serine/threonine-protein kinase (SRPK2) and cleavage of TrkB receptors.

5.2.1 AEP phosphorylation by SRPK2 enhances its enzymatic activity, provoking pathogenesis in Alzheimer's disease

Serine-arginine protein kinase 2 (SRPK2) belongs to a small protein kinase family that specifically phosphorylates serine residues of the serine-arginine (SR)-rich motif on substrates (176, 177). It has been previously reported that SRPK2 modulates the activity of the pre-mRNA alternative splicing machinery (178-180). A cell-cycle signal induces nuclear translocation of SRPK2 at the G2/M boundary (181). Akt-mediated phosphorylation of SRPK2 at T492 controls the expression of cell-cycle regulators, thus coupling cell-cycle regulation and cell death machinery in the nervous system. Consequently, activation of SRPK2 in neurons leads to cell-cycle progression, DNA synthesis, and, eventually, apoptosis (182). Moreover, our lab has previously shown that apoptosis can be triggered when SRPK2 is cleaved by caspase 3 (183). Interestingly, SRPK2 can also be activated by Aβ, and activated SRPK2 phosphorylates tau, which leads to suppressed tau-dependent microtubules polymerization dynamics and inhibiting axonal growth in neurons. In the neurons of Alzheimer's disease (AD) mice and patients, SRPK2 activity is elevated, implicating its importance in AD etiology and pathogenesis (184).

We have demonstrated that AEP expression level and activity are enhanced in AD pathology, but how this critical protease is regulated post-translationally during aging and AD pathogenesis

remains poorly understood. Here we show that SRPK2 selectively phosphorylates delta-secretase on serine 226 and facilitates its activation, elevating its enzymatic activity in human AD brains. Expression of a non-phosphorylatable mutant (S226A) in 5XFAD mice attenuates the AD pathology, restoring cognitive dysfunction. On the other hand, expression of the phosphorylation mimetic S226D in young 3xTg mice leads to an earlier onset of senile plaque and NFT formation, accelerating cognitive dysfunction.

We found that SRPK2 phosphorylates serine 226 of delta-secretase not only *in vivo* and *in vitro*, but also in human AD brains. To understand whether Aβ activates SRPK2 to phosphorylate AEP in primary neurons, we performed immunofluorescent (IF) staining to find that Aβ induced SRPK2 T492 is positively correlated with delta-secretase S226 phosphorylation (Figure 5.4 A&B). Aβ treatment results in the subcellular co-localization of these two proteins (Figure 5.4 C&D). To understand if SRPK2 is essential in phosphorylating delta-secretase in neurons, we used lentivirus-mediated expression of shRNA to knockdown SRPK2, followed by different doses of Aβ treatment overnight. We found that Aβ triggered SRPK2 T492 phosphorylation, which is a marker for its activation (182). Knockdown of SRPK2 abolished T492 phosphorylation by Aβ. As expected, incubation with Aβ also resulted in delta-secretase fragmentation and S226 phosphorylation, which was inhibited with SRPK2 knockdown (Figure 5.4E, top to 4th panel). As a result, we saw an increase in the cleavage of downstream targets of delta-secretase, such as APP N585 and Tau N368. The extent of cleavage was reduced by SRPK2 knockdown (Figure 5.4E, 5th to bottom panels). These findings suggests that Aβ triggers SRPK2 activation in primary neurons, which subsequently phosphorylates delta-secretase, inducing its proteolytic activity.

Turning now to the experimental evidence in our study using human brain samples, we found a high level of S226 phosphorylation of delta-secretase (associated with its active fragments) in AD brains. Conversely, delta-secretase was barely cleaved or phosphorylated in healthy controls brains. Delta-secretase S226 phosphorylation correlated well with SRPK2 phosphorylation, as well as with the phosphorylation of SRPK2 substrates such as p-Tau S214 and p-Acinus S422 (185) (Figure 5.4F).

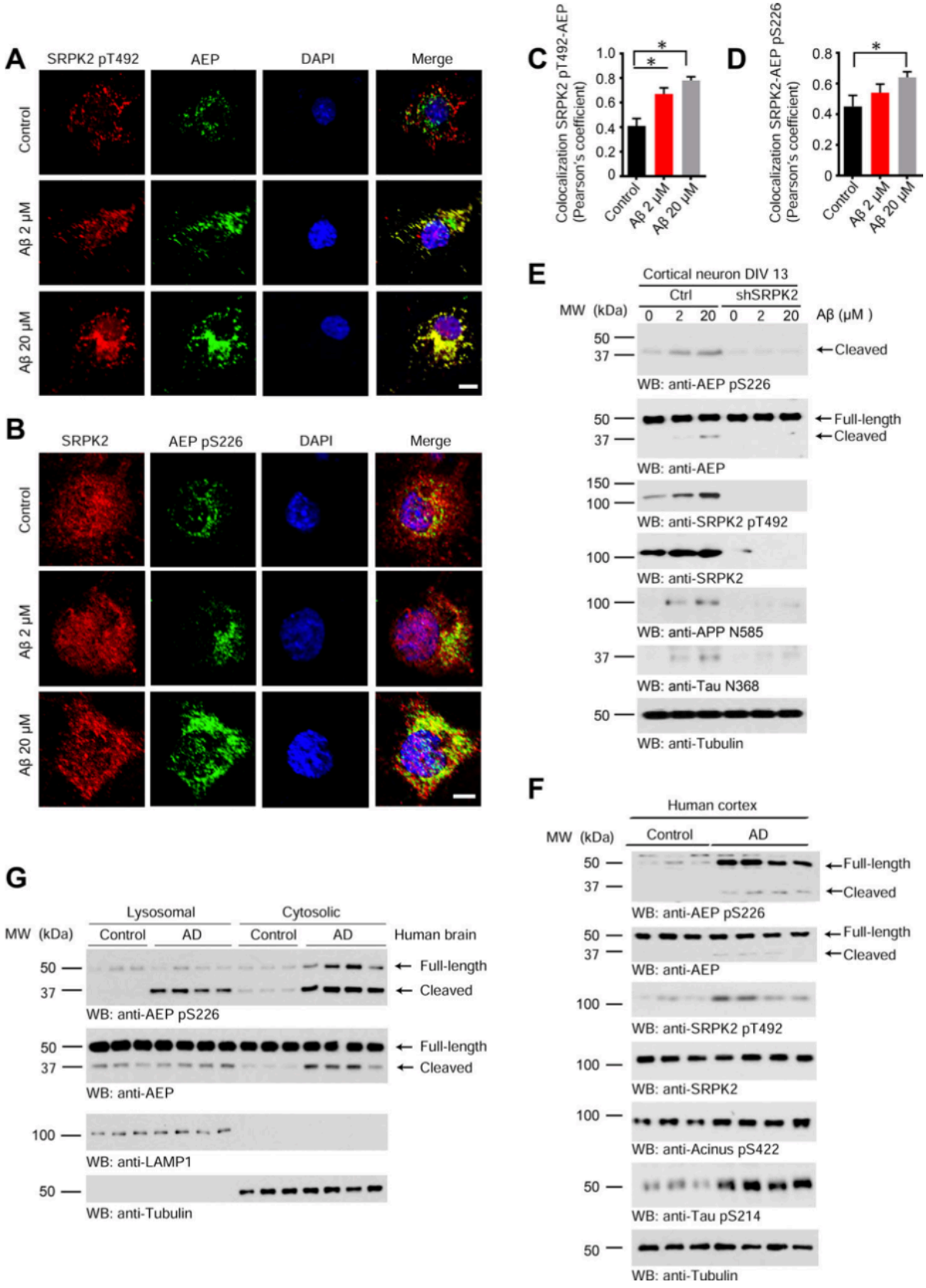
A
SRPK2 pT492
AEP
DAPI
Merge
Control
Aβ 2 μM
Aβ 20 μM
B
SRPK2
AEP pS226
DAPI
Merge
Control
Aβ 2 μM
Aβ 20 μM
C
Colocalization SRPK2 pT492-AEP (Pearson's coefficient)
1.0
0.8
0.6
0.4
0.2
0
*
*
Control
Aβ 2 μM
Aβ 20 μM
D
Colocalization SRPK2-AEP pS226 (Pearson's coefficient)
0.8
0.6
0.4
0.2
0
*
Control
Aβ 2 μM
Aβ 20 μM
E
Cortical neuron DIV 13
Ctrl
shSRPK2
MW (kDa)
0 2 20 0 2 20
Aβ (μM)
50
37
←Cleaved
WB: anti-AEP pS226
50
37
←Full-length
←Cleaved
WB: anti-AEP
150
100
WB: anti-SRPK2 pT492
100
WB: anti-SRPK2
100
WB: anti-APP N585
37
WB: anti-Tau N368
50
WB: anti-Tubulin
F
Human cortex
MW (kDa)
Control
AD
50
37
←Full-length
←Cleaved
WB: anti-AEP pS226
50
37
←Full-length
←Cleaved
WB: anti-AEP
100
WB: anti-SRPK2 pT492
100
WB: anti-SRPK2
100
WB: anti-Acinus pS422
50
WB: anti-Tau pS214
50
WB: anti-Tubulin
G
Lysosomal
Cytosolic
MW (kDa)
Control
AD
Control
AD
Human brain
50
37
← Full-length
← Cleaved
WB: anti-AEP pS226
50
37
← Full-length
← Cleaved
WB: anti-AEP
100
WB: anti-LAMP1
50
WB: anti-Tubulin

Figure 5.4 Delta-secretase phosphorylation by SRPK2 in neurons and AD brains

A. Co-localization between SRPK2 pT492 and delta-secretase in rat primary cortical neurons (DIV 15) treated with 2 or 20 μM of pre-aggregated Aβ for 16 h. **B.** Co-localization between SRPK2 and delta-secretase pS226 in rat primary cortical neurons (DIV 15) treated with 2 or 20 μM of pre-aggregated Aβ for 16 h. **A-B.** Confocal pictures showed co-localization. Scale bars, 5 μm. **C-D.** Quantification of SRPK2 pT492 with delta-secretase (C) and SRPK2 with delta-secretase pS226 (D) co-localization. Data shown as mean ± s.e.m. (n=20–28 cells per group; *P<0.05; student's t-test). **E.** Knockdown of SRPK2 reduces delta-secretase phosphorylation on S226 induced by Aβ. Western blot was conducted from primary cultures infected with virus expressing control or SRPK2 shRNA. **F-G.** Western blot analysis of phosphorylated delta-secretase and SRPK2 in AD brains compared with age-matched healthy controls. Western blot data in **E-G** are representative of three independent experiments.

It has been reported that AEP (delta-secretase) is a lysosomal cysteine protease that is translocated from neuronal lysosomes to the cytoplasm when activated in the AD brain (143). To determine whether S226 phosphorylation is involved in this process, we conducted a subcellular fractionation. Interestingly, the levels of mature and active delta-secretase in the brains of AD patients were higher than those of healthy controls in both cytosolic and lysosomal fractions. In addition, AEP was highly phosphorylated on S226 in AD, compared with healthy controls.

To understand how S226 phosphorylation affects delta-secretase enzymatic activity, we conducted delta-secretase enzymatic assay on HEK293 cells lysates with mGST-SRPK2 (WT or kinase-dead, KD) and Myc-delta-secretase co-transfected. Results show that SRPK2 overexpression increased delta-secretase enzymatic activity while expression of KD SRPK2 reduced delta-secretase enzymatic activity, compared with control (Figure 5.5A). Next, we analyzed endogenous delta-secretase enzymatic activity with transfection of SRPK2. WT SRPK2 expression also elevated endogenous delta-secretase activity (Figure 5.5B). We also extended our studies into the delta-secretase S226D and S226A mutants and found that the phosphorylation mimetic S226D displayed higher enzymatic activity than wild-type, and as expected, S226A mutant possessed the lowest enzymatic activity among all three (Figure 5.5C). The evidence together suggests that delta-secretase S226 phosphorylation enhances its autocatalytic process and enzymatic activity

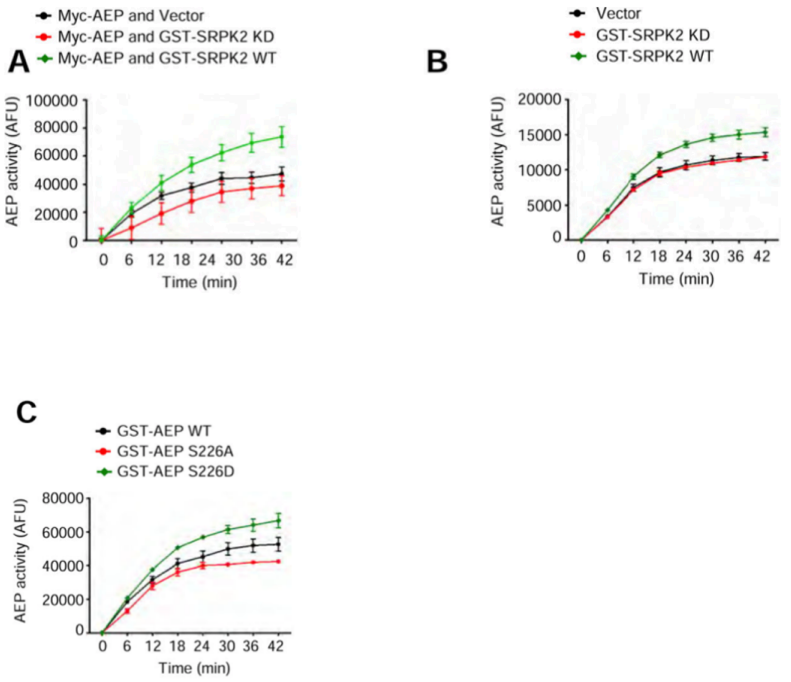

Figure 5.5 Delta-secretase phosphorylation on S226 by SRPK2 increases its enzymatic activity

A-C. Delta-secretase activity assay of HEK293 cell lysates. HEK293 cells were co-transfected with delta-secretase and SRPK2 WT/KD (A) or transfected with SPRK2 WT/KD (B), or WT and mutated delta-secretase (C). Data are shown as mean ± s.e.m. of three independent experiments.

Finally, we demonstrated that delta-secretase S226D facilitates AD pathologies in young 3XTg transgenic mice (APP Swedish, MAPT P301L, and PSEN1 M146V), stimulating cognitive dysfunctions. 3XTg-AD mice progressively develop amyloid plaques in the hippocampus at 6 months old and NFT at 12-month (184). To understand whether the expression of phosphorylated delta-secretase may facilitate the early onset of AD pathology, we injected the hippocampus of 2-month-old wild-type mice and age-matched 3XTg mice with lentivirus expressing control, wild-type delta-secretase, or the S226D mutant (Figure 5.6A). Very few plaques were found in control vector-treated animals in the same hippocampal region (Figure 5.6B). Aβ levels remained comparable in wild-type mice regardless of delta-secretase wild-type or S226D expression (Figure 5.6 C&D). To determine the physiological role of p-S226 on delta-secretase in this process, we used an electron microscope (EM) to show that, when WT or S226D delta-secretase was overexpressed in 3XTg mice, the abundance of synapses gradually diminished. We observed that in 3XTg/S226D mice, significantly fewer synapses were found than 3XTg/control or wild-type/S226D mice. Conversely, synapse numbers are comparable in all wild-type mice, regardless of WT or S226D (Figure 5.6E).

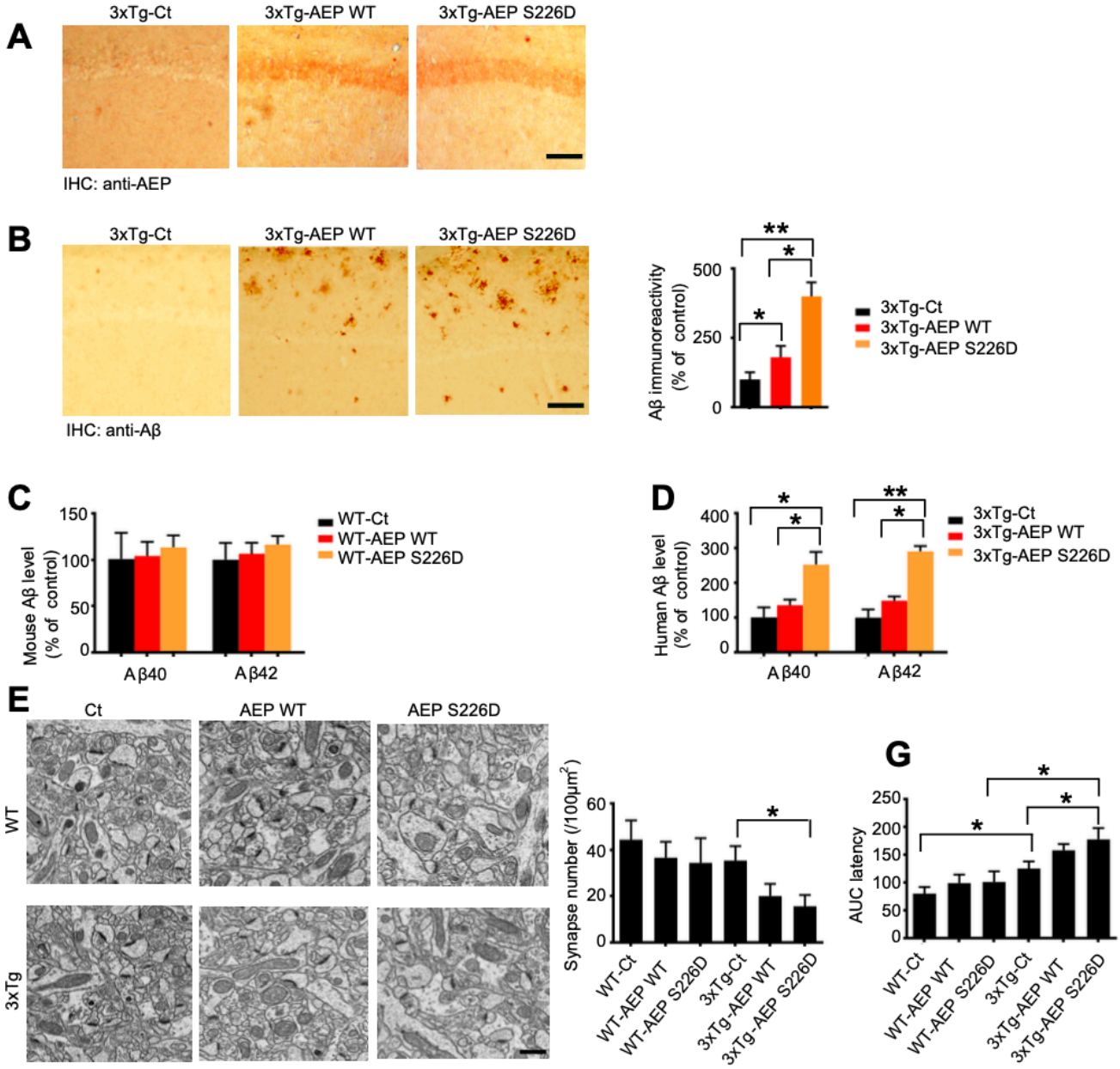

Figure 5.6 Delta-secretase S226D expression in young 3xTg mice accelerates Aβ pathogenesis and synapse loss, exacerbating cognitive impairment

A. Delta-secretase virus expression in the hippocampal CA1 of 3xTg AD mice. Immunohistochemistry staining showing the expression of WT and delta-secretase S226D in mouse CA1 (n = 3 mice per group). Scale bar, 50 μm. B. IHC staining of Aβ in CA1 (left panels,

scale bar, 50 μm). Quantitative analysis of Aβ immunoreactivity (right panel). Data represent mean ±s.e.m. of 10–13 sections from 3 mice in each group (*P < 0.05, **P < 0.01, one-way ANOVA). C-D. Measurements of Aβ levels by ELISA. Aβ ELISA is the representative of the mean ± s.e.m. from 3 mice per group (*P < 0.05, **P < 0.01, one-way ANOVA). E. S226D mutant decreases the number of synapses in CA1. Electron microscopy analysis of synapses (left panels, n = 3 mice per group). Scale bar, 1 μm. Quantitative analysis of synapses in CA1 (right panels, mean±s.e.m.; n =3 mice per group; *P < 0.05, one-way ANOVA)

To investigate the pathological role of S226 phosphorylation in AD pathogenesis, we injected lentivirus expressing WT delta-secretase or the S226A mutant into the hippocampus of 2 months old mice. Tau N368 and APP N585 levels were higher in wild-type delta-secretase-treated mice than in control and S226A-expressing mice (Figure 5.7A). Enzymatic activity was markedly increased in WT delta-secretase overexpressing brains, but not in brains with S226A expression. Consistent with the degree of delta-secretase cleavage, enzymatic activity was higher in 5XFAD mice than in wild-type (Figure 5.7B). When comparing WT delta-secretase injected hippocampi to the controls, thioflavin S staining and IHC staining with anti-Aβ revealed that amyloid plaque deposition was increased. In 5XFAD mice, overexpression of the S226A mutant resulted in a reduction in the development of amyloid plaques (Figure 5.7 C&D). S226A mutant expression significantly increased spine density compared to controls while overexpression of wild-type delta-secretase resulted in lower spine density (Figure 5.7 E). Long-term potentiation (LTP) was diminished when delta-secretase was overexpressed while LTP was restored when S226A was expressed. The paired-pulse ratios were lower in 5XFAD/wild-type participants animals than in 5XFAD/control subjects. 5XFAD/S226A subjects restored the deficit, suggesting that delta-secretase inactivation compensates synaptic dysfunctions (Figure 5.7 F).

The MWM was then used to assess spatial memory in 5-month-old 5XFAD, 5XFAD/AEP, and 5XFAD/S226A mice. Overexpression of delta-secretase wild-type considerably increased the latency to platform compared to control, but S226A greatly reduced it (Figure 5.7 G). In the probe trial, the S226A group spent more time in the target quadrant than the control, demonstrating better learning and memory. In contrast, wild-type AEP expression spent less time in the quadrant (Figure 5.7 H). Cued fear conditioning test also demonstrated that S226A expression can rescue the cognitive defects in 5XFAD mice (Figure 5.7 I). These findings

strongly suggest that overexpression of a non-phosphorylatable delta-secretase mutant accelerates AD pathogenesis in 5XFAD mice, reversing the cognitive impairment shown in this paradigm.

In conclusion, to further understand AEP's role in AD pathogenesis, we found that SRPK2 phosphorylates serine 226 on delta-secretase and enhances its enzymatic activity. Phosphorylated AEP elicits AD-like pathology while unphosphorylated AEP alleviates cognitive functions (Figure 5.8). This work has been published in *Molecular Cell* (186).

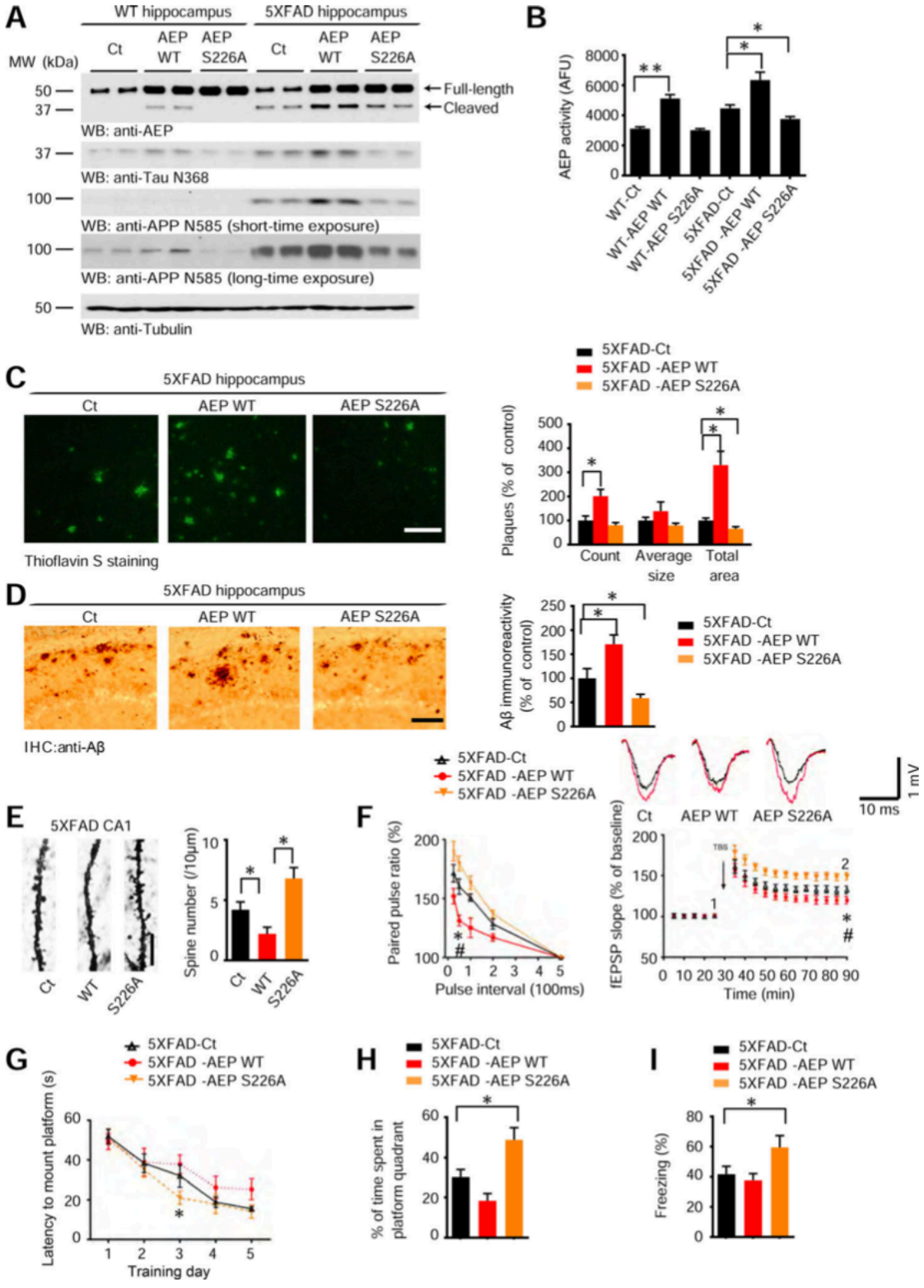
A
WT hippocampus
5XFAD hippocampus
Ct
AEP WT
AEP S226A
MW (kDa)
50
37
Full-length
Cleaved
WB: anti-AEP
WB: anti-Tau N368
100
WB: anti-APP N585 (short-time exposure)
WB: anti-APP N585 (long-time exposure)
WB: anti-Tubulin
B
AEP activity (AFU)
WT-Ct
WT-AEP WT
WT-AEP S226A
5XFAD-Ct
5XFAD -AEP WT
5XFAD -AEP S226A
C
Thioflavin S staining
Plaques (% of control)
Count
Average size
Total area
D
IHC:anti-Aβ
Aβ immunoreactivity (% of control)
E
5XFAD CA1
Spine number (/10μm)
F
Paired pulse ratio (%)
Pulse interval (100ms)
fEPSP slope (% of baseline)
Time (min)
TBS
10 ms
1 mV
G
Latency to mount platform (s)
Training day
H
% of time spent in platform quadrant
I
Freezing (%)

Figure 5.7 Delta-secretase S226A ameliorates the pathologies and behavioral defects in 5XFAD mice

A. S226A mutation reduces delta-secretase and APP and Tau fragments cleaved by delta-secretase. Hippocampal CA1 tissues from lentivirus (control, WT, or delta-secretase S226A) injected 5XFAD mice were analyzed by immunoblotting with various antibodies (n = 4 mice per group). The molecular weight of no-tagged exogenous delta-secretase is similar to endogenous delta-secretase. **B.** S226A mutation reduces delta-secretase enzymatic activity. Data represent mean ± s.e.m. of 3 mice per group (*P < 0.05, **P < 0.01, one-way ANOVA). **C-D.** S226A mutant decreases amyloid plaques and Aβ in 5XFAD mice CA1. **C.** Quantification of number and surface area of amyloid plaques (right panels). Plaque analysis data represent mean ± s.e.m. of 13–15 sections from 3 mice in each group (*P < 0.05, **P < 0.01, one-way ANOVA). Scale bar, 50 μm. **D.** IHC staining of Aβ in the hippocampus (left panels, scale bar, 50 μm). Quantitative analysis of Aβ immunoreactivity (right panel). Data represent mean ± s.e.m. of 12–16 sections from 3 mice in each group (*P < 0.05, one-way ANOVA). **E.** S226A mutant increases the spine density. Scale bar, 5 μm. Golgi staining was conducted on brain sections from CA1 regions of 5XFAD mice (mean ± s.e.m.; n = 5; *p < 0.05, one-way ANOVA). **F.** Electrophysiology analysis. S226A mutant increased ratio of paired pulses (left) and rescued the LTP defects in 5XFAD mice (right) (mean ± s.e.m.; n = 6 in each group; *P < 0.05 5XFAD-S226A vs. 5XFAD-Ct, # P < 0.05 5XFAD-S226A vs. 5XFAD-WT, one-way ANOVA). Shown traces are representative fEPSPs recorded before (black) and 60 minutes after (red) TBS. **G-I,** Morris Water Maze (G&H) and Conditional Fear Conditioning (CFC) analysis of cognitive functions. S226A mutant in CA1 rescues the learning and memory impairments in 5XFAD mice (mean ± s.e.m.; n =9–10 mice per group; *P< 0.05, one-way ANOVA). See also Figure 4.11.

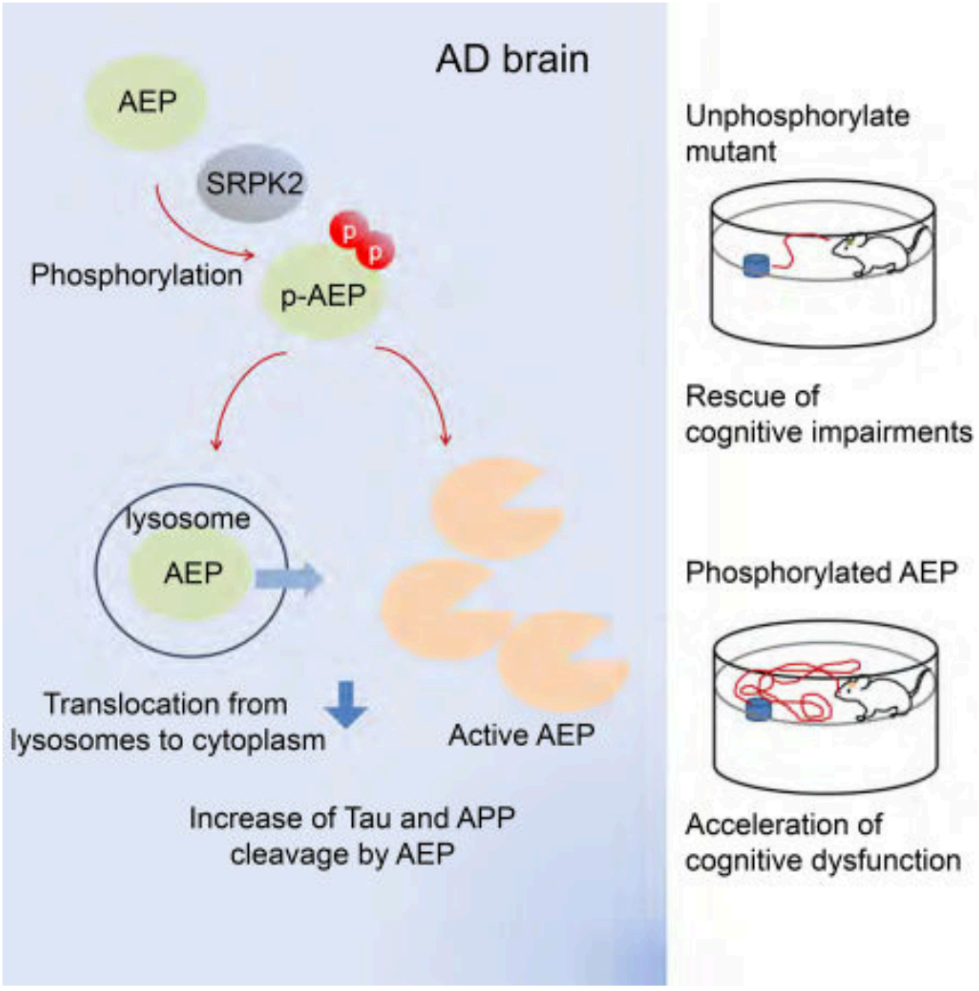

Figure 5.8 A schematic illustration of delta-secretase phosphorylation by SRPK2 provoking pathogenesis in Alzheimer's disease

5.2.2 AEP cleavage of TrkB receptor abolishes its phosphorylation of APP, aggravating Alzheimer's disease pathologies

Neurotrophins (such as NGF, BDNF, NT3) regulate many neuronal functions such as survival, development, and even learning and memory. Major receptors for these neurotrophic factors are tropomyosin-related kinase (Trk) receptor type A, B, C (TrkA, TrkB, TrkC), and p75NTR (187). Neurotropic factors deregulation plays an essential role in AD pathology (188). The levels of mature NGF and BDNF decrease in the brain of AD animal models and patients, thereby leading to cell atrophy and reduced nerve fibers density. Brains of AD patients show decreased levels of BDNF (188-190). BDNF reduces Aβ generation in primary neuronal cultures while BDNF administration improves learning and memory (191, 192).

It has been established that BDNF/TrkB signaling is reduced in AD but the specific mechanism of how the signaling mediates AD diseases is unknown. In this section, we show that the TrkB receptor binds to and phosphorylates APP, lowering amyloid formation, which is inhibited by TrkB cleavage by AEP in Alzheimer's disease.

BDNF stimulates TrkB to phosphorylate APP Y687 residue that accumulates APP in the TGN (Trans-Golgi Network) and diminishes its amyloidogenic cleavage. Delta-secretase cleaves TrkB at N365 and N486/489 residues and abrogates its neurotrophic activity, downregulating p-APP Y687 and altering its subcellular trafficking. Notably, both TrkB and APP are robustly cleaved by δ-secretase in AD brains, accompanied by mitigated TrkB signaling and reduced p-Y687.

We found that AEP-uncleavable TrkB N486/489A attenuates AD pathologies in 5xFAD mice, rescuing the learning and memory. TrkB N486 and AEP activation was barely detectable in mice with TrkB WT and with N486/489A mutant but robust in the mice with the control virus. p-APP Y687 is the strongest in mice with TrkB N 486/489 A mutants, correlated with consequently low

AEP-cleaved APP N585 level (Figure 5.9A). As expected, AEP activity is the lowest in TrkB N 486/489 A samples, along with low levels of Aβ 40 and 42 (Figure 5.9 B). IHC and Thioflavin S (ThS) co-staining show that Aβ plaques are significantly diminished in TrkB N486/489A and TrkB WT mice (Figure 5.9C). The number of dendritic spines is restored in TrkB N486/489A mice (Figure 5.9C). Similar patterns are also observed in MWM cognitive behavioral assays and fear conditioning tests. These data together suggest that blockade of TrkB from AEP cleavage attenuates AD pathology in 5XFAD mice.

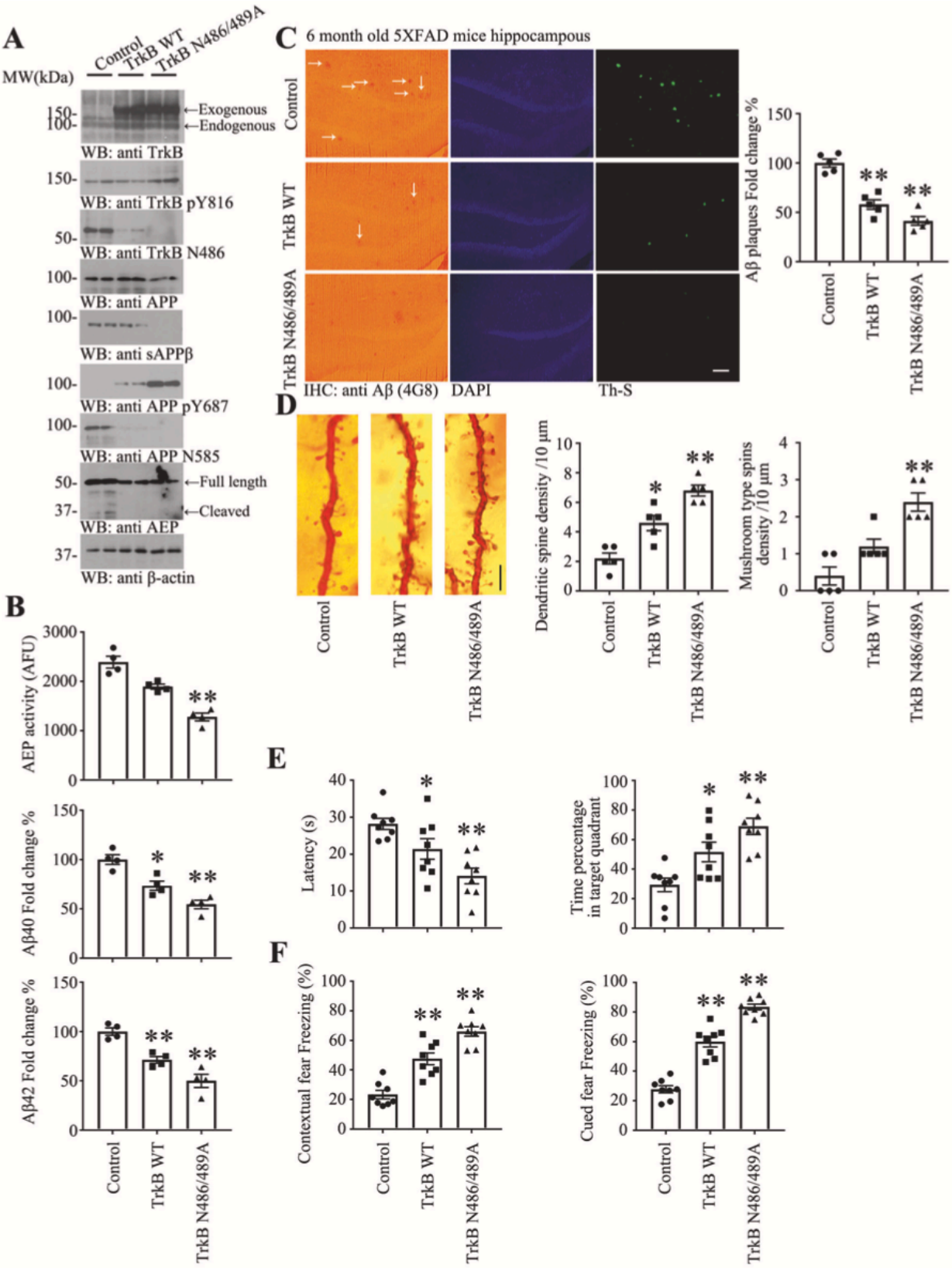
A
Control
TrkB WT
TrkB N486/489A
MW(kDa)
150-
100-
←Exogenous
←Endogenous
WB: anti TrkB
150-
WB: anti TrkB pY816
50-
WB: anti TrkB N486
100-
WB: anti APP
100-
WB: anti sAPPβ
100-
WB: anti APP pY687
100-
WB: anti APP N585
50-
←Full length
37-
←Cleaved
WB: anti AEP
37-
WB: anti β-actin
C
6 month old 5XFAD mice hippocampous
Control
TrkB WT
TrkB N486/489A
IHC: anti Aβ (4G8)
DAPI
Th-S
Aβ plaques Fold change %
D
Dendritic spine density /10 μm
Mushroom type spins density /10 μm
B
AEP activity (AFU)
Aβ40 Fold change %
Aβ42 Fold change %
E
Latency (s)
Time percentage in target quadrant
F
Contextual fear Freezing (%)
Cued fear Freezing (%)

Figure 5.9 δ-secretase-resistant TrkB N486/489 A mutant attenuates AD pathologies in 5xFAD mice

A. Uncleavable TrkB N486/489 A inhibits δ-secretase activation. Western blot analysis of TrkB, APP, δ- secretase cleavage in 6-month old 5xFAD mice CA1 infected with lentivirus expressing TrkB FL or δ-secretase-uncleavable TrkB mutant (N486/489 A) for 3 months. Blocking of TrkB cleavage by δ-secretase reduced δ-secretase itself cleavage. B. Uncleavable TrkB N486/489 A decrease AEP activity and Aβ production. δ-secretase activity was decreased in uncleavable TrkB-expressed 5XFAD mice. Data represent mean ± SEM. ($n = 4$, $^{**}p < 0.01$, compared with control, one-way ANOVA and Bonferroni's multiple comparison test). Aβ level was decreased in TrkB N486/489A-expressed 5XFAD mice. Quantification of Aβ40 and Aβ42 levels by ELISA represents mean ± SEM ($n = 4$, $^{*}p<0.05$, $^{**}p<0.01$, compared with control, one-way ANOVA, and Bonferroni's multiple comparison test). C. Aβ plaques in the hippocampus were decreased with overexpression of TrkB N486/489 A. Immunohistochemistry (IHC) staining of Aβ (left) and Thioflavin S staining (right) showed the Aβ plaques in the hippocampus (Scale bar: 100 μm), arrows showed the Aβ plaques. Quantification of Aβ plaques showed amyloid plaques were decreased in TrkB N486/489A- expressed 5XFAD mice. (mean ± SEM; $n = 5$, $^{**}p < 0.01$, compared with control, one-way ANOVA and Bonferroni's multiple comparison test). D. Blocking TrkB cleavage by δ-secretase rescues the loss of dendritic spine density. Left, Golgi staining was conducted on brain sections from TrkB WT or N486/489 A expressed apical dendritic layer of the CA1 region (Scale bar: 10 μm). Right, quantification of spine density and mushroom type spine density, represents mean ± SEM of 9–12 sections from 5 mice in each group. ($^{*}p < 0.05$, $^{**}p < 0.01$, compared with control, one-way ANOVA and Bonferroni's multiple comparison test). E. Morris Water Maze analysis of cognitive functions. Uncleavable

TrkB expression in the CA1 reversed the learning and memory dysfunctions in 5XFAD mice (mean ± SEM.; n =8 mice per group; *p<0.05, **p<0.01, compared with control, one-way ANOVA and Bonferroni's multiple comparison test). F. Fear condition tests. Contextual and cued fear memory was rescued in uncleavable TrkB expressed mice (mean ± SEM; n = 8 mice per group; **p<0.01, compared with control, one-way ANOVA, and Bonferroni's multiple comparison test).

On the other side, viral expression of TrkB 1-486 fragment in the hippocampus of APP/PS1 mice accelerates AD pathologies in APP/PS1 mice which usually display AD pathology at age of 12-month. We injected the AAV virus expressing green fluorescent protein (GFP)-tagged TrkB 1-486 or FL into the hippocampus of 2-month-old APP/PS1 mice, and conduct the experiments after 4 months. p-APP Y687 is highly elevated in TrkB WT brain but not in TrkB 1-486 samples. Levels of APP N585, AEP, and sAPPβ are inversely correlated with p-APP Y687 signals (Figure 5.10A). As expected, similar patterns are observed in levels of Aβ 40, Aβ 42, and Aβ plaques (Figure 5.10B&C). Dendritic spines in TrkB 1-486 show a decrease in numbers and arborizations, and TrkB 1-486 mice show poor performance in behavioral tests assessing learning and memory. Hence, TrkB 1-486 overexpression reduces BDNF/TrkB neurotrophic signaling and activates delta-secretase, contributing to decreased phosphorylation of APP Y687 and APP N585 fragmentation. Therefore, the evidence listed in this section demonstrates that AEP cleaves TrkB and blunts its phosphorylation of APP at Y687, facilitating AD pathogenesis. This work was published in *Molecular Psychiatry*. (193)

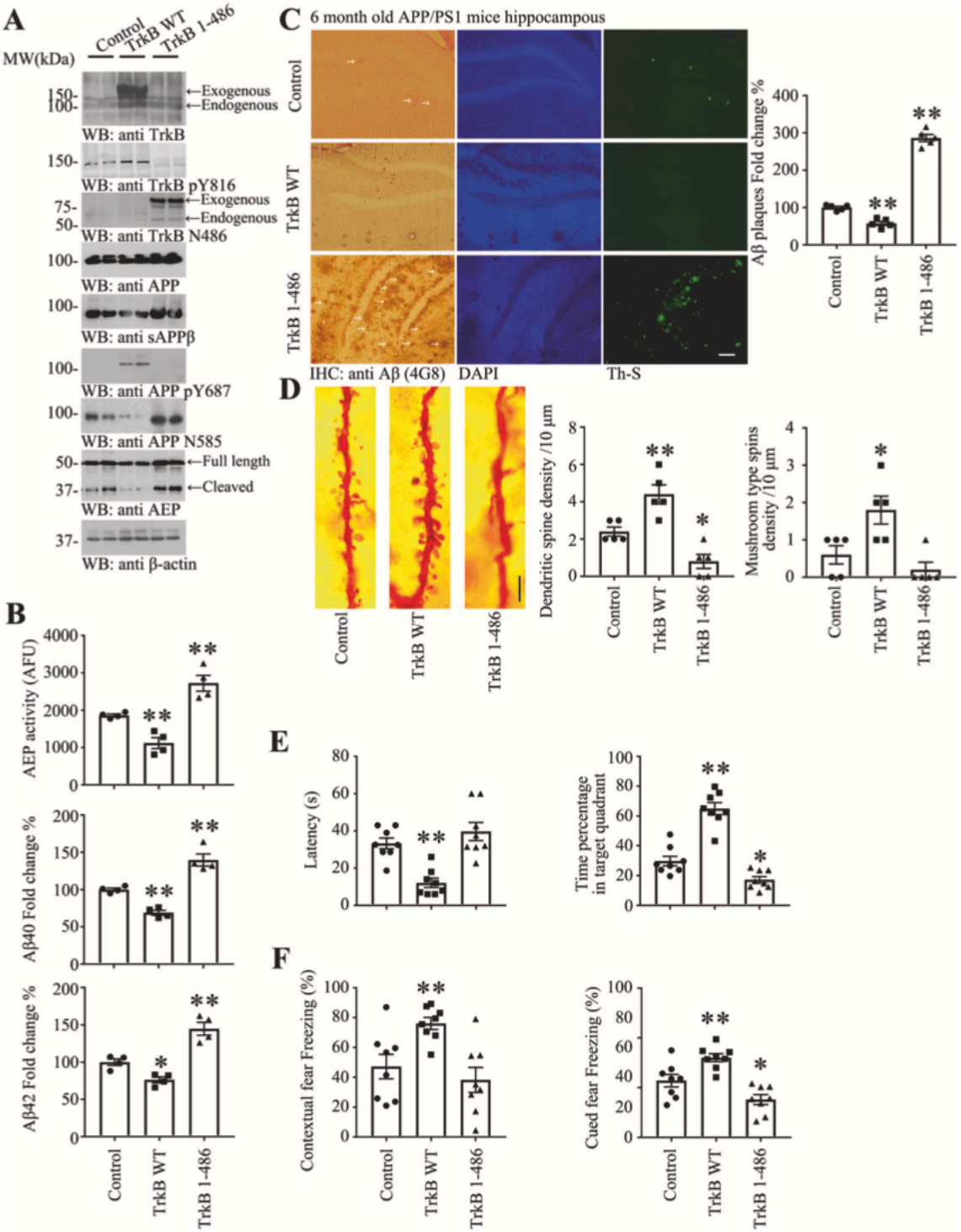
A
Control
TrkB WT
TrkB 1-486
MW(kDa)
150-
100-
←Exogenous
←Endogenous
WB: anti TrkB
150-
WB: anti TrkB pY816
75-
50-
←Exogenous
←Endogenous
WB: anti TrkB N486
100-
WB: anti APP
100-
WB: anti sAPPβ
100-
WB: anti APP pY687
100-
WB: anti APP N585
50-
37-
←Full length
←Cleaved
WB: anti AEP
37-
WB: anti β-actin
B
AEP activity (AFU)
Aβ40 Fold change %
Aβ42 Fold change %
Control
TrkB WT
TrkB 1-486
C
6 month old APP/PS1 mice hippocampous
Control
TrkB WT
TrkB 1-486
IHC: anti Aβ (4G8)
DAPI
Th-S
Aβ plaques Fold change %
D
Dendritic spine density /10 μm
Mushroom type spins density /10 μm
E
Latency (s)
Time percentage in target quadrant
F
Contextual fear Freezing (%)
Cued fear Freezing (%)

Figure 5.10 TrkB 1-486 fragment from δ-secretase cleavage accelerates AD pathologies in APP/PS1 mice

A. TrkB 1-486 expression induces δ-secretase activation and APP cleavage. Western blot analysis of TrkB, APP, and AEP cleavage by δ-secretase in 6-month old APP/PS1 mice CA1 infected with lentivirus expressing TrkB WT or fragment for 3 months. δ-secretase-cleaved TrkB fragment stimulated δ- secretase cleavage in the brains. B. AEP enzymatic and Aβ ELISA assays. δ-secretase activity was increased in TrkB 1-486-expressed APP/PS1 mice CA1. Truncated TrkB escalated δ-secretase activities. Data represent the mean±SEM of 4 mice in each group (**p<0.01, compared with control, one-way ANOVA, and Bonferroni's multiple comparison test). Truncated TrkB escalated Aβ level. Quantification of Aβ40 and Aβ42 levels by ELISA represents mean ± SEM (n = 4, *p < 0.05, **p < 0.01, compared with control, one-way ANOVA and Bonferroni's multiple comparison test). C. Immunohistochemistry (IHC) staining of Aβ (left) and Thioflavin S staining (right) showed the Aβ plaques in the hippocampus (Scale bar: 100 μm.), arrows showed the Aβ plaques. Quantification of Aβ plaques showed amyloid plaques were increased in TrkB 1-486-expressed APP/PS1 mice. (mean± SEM; n=5, **p<0.01, compared with control, one-way ANOVA, and Bonferroni's multiple comparison test). D. TrkB cleavage by δ- secretase decreases the dendritic spine density. Left, Golgi staining was conducted on brain sections from TrkB WT or 1-486 expressed apical dendritic layer of the CA1 region (Scale bar: 10 μm). Right, quantification of spine density and mushroom type spine density, represents mean ± SEM of 9–12 sections from 5 mice in each group. (*p < 0.05, **p < 0.01, compared with control, one-way ANOVA and Bonferroni's multiple comparison test). E. Morris Water Maze analysis of cognitive functions. TrkB 1-486 overexpression in the CA1 exacerbated the learning and memory dysfunctions in APP/PS1 mice (mean ± SEM; n = 8 mice

per group; *p < 0.05, **p < 0.01, compared with control, one-way ANOVA, and Bonferroni's multiple comparison test). F. Fear condition tests. Contextual and cued fear memory was reduced in AEP-truncated TrkB expressed mice (mean ± SEM; n = 8 mice per group; **p < 0.01, compared with control, one-way ANOVA, and Bonferroni's multiple comparison test).

5.3 Limitations and Future Directions

The studies presented in this dissertation aimed to understand the mechanisms coupling diabetes and AD through inflammation-activated C/EBPβ/AEP pathway. Although tremendous progress has been made, there are still several limitations to this study.

This study was limited by the absence of other commonly used T2DM animal models to represent the diversity seen in type 2 diabetes patients. Such animal models include $Lep^{ob/ob}$ mouse (mutation of the obese gene encoding leptin), $Lep^{db/db}$ (leptin receptors do not function), and Zucker fatty rats (mutated leptin receptor) (194). However, these mice develop hyperglycemia, obesity, and glucose intolerance around 4 weeks of age, thereby difficult to compare with naturally induced diabetes models reported in this study as the Thy1-C/EBPβ-HFD mice showed symptoms resembling diabetes at 6 months of age.

Due to practical constraints, this thesis did not use metabolic cages to quantitatively measure and monitor metabolic performance in these mice in an automated and synchronized manner. The system can yield data regarding oxygen consumption, carbon dioxide, production, energy expenditure, and respiratory exchange ratio (RER). The metabolic cages can also be used for the measurement of horizontal and vertical motions as an index of locomotor activity (mean spontaneous activity) and water/food intake over a certain period of time (195). Originally, a hyperglycemic clamp was also a part of this study. It is to assess insulin secretion and β-cell function in awake mice (196). However, our animal facility had the presence of mouse parvovirus (MPV), so we were not able to ship our mice out for the metabolic cages and hyperglycemic clamp experiments.

A limitation of this study is that very little background information on the role of AEP in metabolism and diabetes can be found. Our lab has previously observed that mice with AEP

knockout develop disorders resembling hemophagocytic syndrome (hemophagocytic lymphohistiocytosis, HLH), which is a rare but potentially fatal condition due to hyperinflammatory response. Symptoms include prolonged fever and cytopenia. In addition, AEP-knockout mice develop HLH classic syndromes with high body temperature and reduced natural killer cell activity (197). Thus, we did not include $AEP^{-/-}$ mice for the major experiments in chapters 3 and 4 as the mice have confounding phenotypes that might disrupt the main aim of this study. Other research studies have shown that metabolic diseases can contribute to HLH onset, suggesting that AEP plays an important role in altering pathways involved in the metabolism (198, 199). Hence, future studies illustrating AEP's role in metabolism will help provide insights into the diagnosis and causes of diabetes and provide the theoretical foundations for the research question of this study.

Notwithstanding these limitations, this study offers valuable insights into the critical role that C/EBPβ/AEP pathway plays in linking AD and diabetes. Several questions remain to be answered. The precise mechanism of AEP in skeletal muscles under diabetic states remains to be elucidated. A further study could assess the long-term effects of AEP on cholesterol levels. Further research could also be conducted to determine the therapeutic efficiency of aspirin in treating AD and diabetes, and a greater focus on AEP could produce interesting findings that explain its role in metabolism and diabetes.

REFERENCES

1. Soria Lopez JA, Gonzalez HM, Leger GC. Alzheimer's disease. Handb Clin Neurol. 2019;167:231-55.
2. Dos Santos Picanco LC, Ozela PF, de Fatima de Brito Brito M, Pinheiro AA, Padilha EC, Braga FS, et al. Alzheimer's Disease: A Review from the Pathophysiology to Diagnosis, New Perspectives for Pharmacological Treatment. Curr Med Chem. 2018;25(26):3141-59.
3. 2021 Alzheimer's disease facts and figures. Alzheimers Dement. 2021;17(3):327-406.
4. Zhang XX, Tian Y, Wang ZT, Ma YH, Tan L, Yu JT. The Epidemiology of Alzheimer's Disease Modifiable Risk Factors and Prevention. J Prev Alzheimers Dis. 2021;8(3):313-21.
5. Tamaoka A. [Alzheimer's disease: definition and National Institute of Neurological and Communicative Disorders and Stroke and the Alzheimer's Disease and Related Disorders Association (NINCDS-ADRDA)]. Nihon Rinsho. 2011;69 Suppl 10 Pt 2:240-5.
6. Breijyeh Z, Karaman R. Comprehensive Review on Alzheimer's Disease: Causes and Treatment. Molecules. 2020;25(24).
7. Nelson PT, Alafuzoff I, Bigio EH, Bouras C, Braak H, Cairns NJ, et al. Correlation of Alzheimer disease neuropathologic changes with cognitive status: a review of the literature. J Neuropathol Exp Neurol. 2012;71(5):362-81.
8. Salmon DP, Thal LJ, Butters N, Heindel WC. Longitudinal evaluation of dementia of the Alzheimer type: a comparison of 3 standardized mental status examinations. Neurology. 1990;40(8):1225-30.
9. Blasko I, Stampfer-Kountchev M, Robatscher P, Veerhuis R, Eikelenboom P, Grubeck-Loebenstein B. How chronic inflammation can affect the brain and support the development of Alzheimer's disease in old age: the role of microglia and astrocytes. Aging Cell. 2004;3(4):169-76.
10. Bouter C, Henniges P, Franke TN, Irwin C, Sahlmann CO, Sichler ME, et al. (18)F-FDG-PET Detects Drastic Changes in Brain Metabolism in the Tg4-42 Model of Alzheimer's Disease. Front Aging Neurosci. 2018;10:425.
11. Reitz C, Mayeux R. Alzheimer disease: epidemiology, diagnostic criteria, risk factors and biomarkers. Biochem Pharmacol. 2014;88(4):640-51.
12. Albert MS, DeKosky ST, Dickson D, Dubois B, Feldman HH, Fox NC, et al. The diagnosis of mild cognitive impairment due to Alzheimer's disease: recommendations from the National Institute on Aging-Alzheimer's Association workgroups on diagnostic guidelines for Alzheimer's disease. Alzheimers Dement. 2011;7(3):270-9.
13. Hansson O, Lehmann S, Otto M, Zetterberg H, Lewczuk P. Advantages and disadvantages of the use of the CSF Amyloid beta (Abeta) 42/40 ratio in the diagnosis of Alzheimer's Disease. Alzheimers Res Ther. 2019;11(1):34.
14. Hansson O, Zetterberg H, Buchhave P, Londos E, Blennow K, Minthon L. Association between CSF biomarkers and incipient Alzheimer's disease in patients with mild cognitive impairment: a follow-up study. Lancet Neurol. 2006;5(3):228-34.
15. Rosenmann H. CSF biomarkers for amyloid and tau pathology in Alzheimer's disease. J Mol Neurosci. 2012;47(1):1-14.
16. Shoji M. Cerebrospinal Fluid and Plasma Tau as a Biomarker for Brain Tauopathy. Adv Exp Med Biol. 2019;1184:393-405.
17. Bohnen NI, Djang DS, Herholz K, Anzai Y, Minoshima S. Effectiveness and safety of 18F-FDG PET in the evaluation of dementia: a review of the recent literature. J Nucl Med. 2012;53(1):59-71.

18. Ashton NJ, Pascoal TA, Karikari TK, Benedet AL, Lantero-Rodriguez J, Brinkmalm G, et al. Plasma p-tau231: a new biomarker for incipient Alzheimer's disease pathology. Acta Neuropathol. 2021;141(5):709-24.
19. Gonzalez MC, Ashton NJ, Gomes BF, Tovar-Rios DA, Blanc F, Karikari TK, et al. Association of Plasma p-tau181 and p-tau231 Concentrations With Cognitive Decline in Patients With Probable Dementia With Lewy Bodies. JAMA Neurol. 2022;79(1):32-7.
20. Meyer PF, Ashton NJ, Karikari TK, Strikwerda-Brown C, Kobe T, Gonneaud J, et al. Plasma p-tau231, p-tau181, PET biomarkers and cognitive change in older adults. Ann Neurol. 2022.
21. Langan RC, Goodbred AJ. Vitamin B12 Deficiency: Recognition and Management. Am Fam Physician. 2017;96(6):384-9.
22. Akiyama H, Barger S, Barnum S, Bradt B, Bauer J, Cole GM, et al. Inflammation and Alzheimer's disease. Neurobiol Aging. 2000;21(3):383-421.
23. Newcombe EA, Camats-Perna J, Silva ML, Valmas N, Huat TJ, Medeiros R. Inflammation: the link between comorbidities, genetics, and Alzheimer's disease. J Neuroinflammation. 2018;15(1):276.
24. Hsia AY, Masliah E, McConlogue L, Yu GQ, Tatsuno G, Hu K, et al. Plaque-independent disruption of neural circuits in Alzheimer's disease mouse models. Proc Natl Acad Sci U S A. 1999;96(6):3228-33.
25. O'Brien RJ, Wong PC. Amyloid precursor protein processing and Alzheimer's disease. Annu Rev Neurosci. 2011;34:185-204.
26. Arnold SE, Hyman BT, Flory J, Damasio AR, Van Hoesen GW. The topographical and neuroanatomical distribution of neurofibrillary tangles and neuritic plaques in the cerebral cortex of patients with Alzheimer's disease. Cereb Cortex. 1991;1(1):103-16.
27. Schmechel DE, Saunders AM, Strittmatter WJ, Crain BJ, Hulette CM, Joo SH, et al. Increased amyloid beta-peptide deposition in cerebral cortex as a consequence of apolipoprotein E genotype in late-onset Alzheimer disease. Proc Natl Acad Sci U S A. 1993;90(20):9649-53.
28. Pierrot N, Tyteca D, D'Auria L, Dewachter I, Gailly P, Hendrickx A, et al. Amyloid precursor protein controls cholesterol turnover needed for neuronal activity. EMBO Mol Med. 2013;5(4):608-25.
29. Cole SL, Vassar R. The Alzheimer's disease beta-secretase enzyme, BACE1. Mol Neurodegener. 2007;2:22.
30. De Strooper B, Iwatsubo T, Wolfe MS. Presenilins and gamma-secretase: structure, function, and role in Alzheimer Disease. Cold Spring Harb Perspect Med. 2012;2(1):a006304.
31. Haass C, Kaether C, Thinakaran G, Sisodia S. Trafficking and proteolytic processing of APP. Cold Spring Harb Perspect Med. 2012;2(5):a006270.
32. Weggen S, Beher D. Molecular consequences of amyloid precursor protein and presenilin mutations causing autosomal-dominant Alzheimer's disease. Alzheimers Res Ther. 2012;4(2):9.
33. Yoon SS, Jo SA. Mechanisms of Amyloid-beta Peptide Clearance: Potential Therapeutic Targets for Alzheimer's Disease. Biomol Ther (Seoul). 2012;20(3):245-55.
34. Deane R, Bell RD, Sagare A, Zlokovic BV. Clearance of amyloid-beta peptide across the blood-brain barrier: implication for therapies in Alzheimer's disease. CNS Neurol Disord Drug Targets. 2009;8(1):16-30.
35. Brion JP, Anderton BH, Authelet M, Dayanandan R, Leroy K, Lovestone S, et al. Neurofibrillary tangles and tau phosphorylation. Biochem Soc Symp. 2001(67):81-8.

36. Takeuchi H, Iba M, Inoue H, Higuchi M, Takao K, Tsukita K, et al. P301S mutant human tau transgenic mice manifest early symptoms of human tauopathies with dementia and altered sensorimotor gating. PLoS One. 2011;6(6):e21050.
37. Colom-Cadena M, Spires-Jones T, Zetterberg H, Blennow K, Caggiano A, DeKosky ST, et al. The clinical promise of biomarkers of synapse damage or loss in Alzheimer's disease. Alzheimers Res Ther. 2020;12(1):21.
38. Kashyap G, Bapat D, Das D, Gowaikar R, Amritkar RE, Rangarajan G, et al. Synapse loss and progress of Alzheimer's disease -A network model. Sci Rep. 2019;9(1):6555.
39. Chapman PF, White GL, Jones MW, Cooper-Blacketer D, Marshall VJ, Irizarry M, et al. Impaired synaptic plasticity and learning in aged amyloid precursor protein transgenic mice. Nat Neurosci. 1999;2(3):271-6.
40. Bastrikova N, Gardner GA, Reece JM, Jeromin A, Dudek SM. Synapse elimination accompanies functional plasticity in hippocampal neurons. Proc Natl Acad Sci U S A. 2008;105(8):3123-7.
41. Saito T, Matsuba Y, Mihira N, Takano J, Nilsson P, Itohara S, et al. Single App knock-in mouse models of Alzheimer's disease. Nat Neurosci. 2014;17(5):661-3.
42. Rosenberg PB. Clinical aspects of inflammation in Alzheimer's disease. Int Rev Psychiatry. 2005;17(6):503-14.
43. Choi SH, Bosetti F. Cyclooxygenase-1 null mice show reduced neuroinflammation in response to beta-amyloid. Aging (Albany NY). 2009;1(2):234-44.
44. Tuppo EE, Arias HR. The role of inflammation in Alzheimer's disease. Int J Biochem Cell Biol. 2005;37(2):289-305.
45. Griffin WS, Sheng JG, Roberts GW, Mrak RE. Interleukin-1 expression in different plaque types in Alzheimer's disease: significance in plaque evolution. J Neuropathol Exp Neurol. 1995;54(2):276-81.
46. Gomez-Nicola D, Boche D. Post-mortem analysis of neuroinflammatory changes in human Alzheimer's disease. Alzheimers Res Ther. 2015;7(1):42.
47. Cribbs DH, Berchtold NC, Perreau V, Coleman PD, Rogers J, Tenner AJ, et al. Extensive innate immune gene activation accompanies brain aging, increasing vulnerability to cognitive decline and neurodegeneration: a microarray study. J Neuroinflammation. 2012;9:179.
48. Sudduth TL, Schmitt FA, Nelson PT, Wilcock DM. Neuroinflammatory phenotype in early Alzheimer's disease. Neurobiol Aging. 2013;34(4):1051-9.
49. Cloutier A, Guindi C, Larivee P, Dubois CM, Amrani A, McDonald PP. Inflammatory cytokine production by human neutrophils involves C/EBP transcription factors. J Immunol. 2009;182(1):563-71.
50. Li Q, Barres BA. Microglia and macrophages in brain homeostasis and disease. Nat Rev Immunol. 2018;18(4):225-42.
51. Bachiller S, Jimenez-Ferrer I, Paulus A, Yang Y, Swanberg M, Deierborg T, et al. Microglia in Neurological Diseases: A Road Map to Brain-Disease Dependent-Inflammatory Response. Front Cell Neurosci. 2018;12:488.
52. Mrak RE, Sheng JG, Griffin WS. Glial cytokines in Alzheimer's disease: review and pathogenic implications. Hum Pathol. 1995;26(8):816-23.
53. Akama KT, Van Eldik LJ. Beta-amyloid stimulation of inducible nitric-oxide synthase in astrocytes is interleukin-1beta- and tumor necrosis factor-alpha (TNFalpha)-dependent, and involves a TNFalpha receptor-associated factor- and NFkappaB-inducing kinase-dependent signaling mechanism. J Biol Chem. 2000;275(11):7918-24.

54. Belarbi K, Jopson T, Tweedie D, Arellano C, Luo W, Greig NH, et al. TNF-alpha protein synthesis inhibitor restores neuronal function and reverses cognitive deficits induced by chronic neuroinflammation. J Neuroinflammation. 2012;9:23.
55. Lee JW, Lee YK, Yuk DY, Choi DY, Ban SB, Oh KW, et al. Neuro-inflammation induced by lipopolysaccharide causes cognitive impairment through enhancement of beta-amyloid generation. J Neuroinflammation. 2008;5:37.
56. Silva MVF, Loures CMG, Alves LCV, de Souza LC, Borges KBG, Carvalho MDG. Alzheimer's disease: risk factors and potentially protective measures. J Biomed Sci. 2019;26(1):33.
57. Husain MA, Laurent B, Plourde M. APOE and Alzheimer's Disease: From Lipid Transport to Physiopathology and Therapeutics. Front Neurosci. 2021;15:630502.
58. Skoog I, Lernfelt B, Landahl S, Palmertz B, Andreasson LA, Nilsson L, et al. 15-year longitudinal study of blood pressure and dementia. Lancet. 1996;347(9009):1141-5.
59. Kling MA, Trojanowski JQ, Wolk DA, Lee VM, Arnold SE. Vascular disease and dementias: paradigm shifts to drive research in new directions. Alzheimers Dement. 2013;9(1):76-92.
60. Awad N, Gagnon M, Messier C. The relationship between impaired glucose tolerance, type 2 diabetes, and cognitive function. J Clin Exp Neuropsychol. 2004;26(8):1044-80.
61. Korczyn AD. Why have we failed to cure Alzheimer's disease? J Alzheimers Dis. 2012;29(2):275-82.
62. Wu Y, Fu R, Lei C, Deng Y, Lou W, Wang L, et al. Estimates of Type 2 Diabetes Mellitus Burden Attributable to Particulate Matter Pollution and Its 30-Year Change Patterns: A Systematic Analysis of Data From the Global Burden of Disease Study 2019. Front Endocrinol (Lausanne). 2021;12:689079.
63. Hotamisligil GS, Shargill NS, Spiegelman BM. Adipose expression of tumor necrosis factor-alpha: direct role in obesity-linked insulin resistance. Science. 1993;259(5091):87-91.
64. Schuster DP, Duvuuri V. Diabetes mellitus. Clin Podiatr Med Surg. 2002;19(1):79-107.
65. Fletcher B, Gulanick M, Lamendola C. Risk factors for type 2 diabetes mellitus. J Cardiovasc Nurs. 2002;16(2):17-23.
66. Virkamaki A, Ueki K, Kahn CR. Protein-protein interaction in insulin signaling and the molecular mechanisms of insulin resistance. J Clin Invest. 1999;103(7):931-43.
67. King AJ. The use of animal models in diabetes research. Br J Pharmacol. 2012;166(3):877-94.
68. Luo ML, Liu XP, Wang F, Liu XX, Liu WF, Wu D, et al. Conditioned Medium from Human Umbilical Vein Endothelial Cells Promotes Proliferation, Migration, Invasion and Angiogenesis of Adipose Derived Stem Cells. Curr Med Sci. 2018;38(1):124-30.
69. Tucsek Z, Toth P, Sosnowska D, Gautam T, Mitschelen M, Koller A, et al. Obesity in aging exacerbates blood-brain barrier disruption, neuroinflammation, and oxidative stress in the mouse hippocampus: effects on expression of genes involved in beta-amyloid generation and Alzheimer's disease. J Gerontol A Biol Sci Med Sci. 2014;69(10):1212-26.
70. Zatterale F, Longo M, Naderi J, Raciti GA, Desiderio A, Miele C, et al. Chronic Adipose Tissue Inflammation Linking Obesity to Insulin Resistance and Type 2 Diabetes. Front Physiol. 2019;10:1607.
71. Pantanetti P, Garrapa GG, Mantero F, Boscaro M, Faloia E, Venarucci D. Adipose tissue as an endocrine organ? A review of recent data related to cardiovascular complications of endocrine dysfunctions. Clin Exp Hypertens. 2004;26(4):387-98.

72. Gallardo-Montejano VI, Yang C, Hahner L, McAfee JL, Johnson JA, Holland WL, et al. Perilipin 5 links mitochondrial uncoupled respiration in brown fat to healthy white fat remodeling and systemic glucose tolerance. Nat Commun. 2021;12(1):3320.
73. Rui L. Energy metabolism in the liver. Compr Physiol. 2014;4(1):177-97.
74. Akshintala D, Chugh R, Amer F, Cusi K. Nonalcoholic Fatty Liver Disease: The Overlooked Complication of Type 2 Diabetes. In: Feingold KR, Anawalt B, Boyce A, Chrousos G, de Herder WW, Dhatariya K, et al., editors. Endotext. South Dartmouth (MA)2000.
75. Richter EA, Hargreaves M. Exercise, GLUT4, and skeletal muscle glucose uptake. Physiol Rev. 2013;93(3):993-1017.
76. Meshkani R, Adeli K. Hepatic insulin resistance, metabolic syndrome and cardiovascular disease. Clin Biochem. 2009;42(13-14):1331-46.
77. Phielix E, Mensink M. Type 2 diabetes mellitus and skeletal muscle metabolic function. Physiol Behav. 2008;94(2):252-8.
78. Saini V. Molecular mechanisms of insulin resistance in type 2 diabetes mellitus. World J Diabetes. 2010;1(3):68-75.
79. Rivera EJ, Goldin A, Fulmer N, Tavares R, Wands JR, de la Monte SM. Insulin and insulin-like growth factor expression and function deteriorate with progression of Alzheimer's disease: link to brain reductions in acetylcholine. J Alzheimers Dis. 2005;8(3):247-68.
80. Profenno LA, Porsteinsson AP, Faraone SV. Meta-analysis of Alzheimer's disease risk with obesity, diabetes, and related disorders. Biol Psychiatry. 2010;67(6):505-12.
81. Kuehn BM. In Alzheimer Research, Glucose Metabolism Moves to Center Stage. JAMA. 2020;323(4):297-9.
82. Miklossy J, Qing H, Radenovic A, Kis A, Vileno B, Laszlo F, et al. Beta amyloid and hyperphosphorylated tau deposits in the pancreas in type 2 diabetes. Neurobiol Aging. 2010;31(9):1503-15.
83. Messier C, Awad N, Gagnon M. The relationships between atherosclerosis, heart disease, type 2 diabetes and dementia. Neurol Res. 2004;26(5):567-72.
84. Watson GS, Craft S. Modulation of memory by insulin and glucose: neuropsychological observations in Alzheimer's disease. Eur J Pharmacol. 2004;490(1-3):97-113.
85. Steen E, Terry BM, Rivera EJ, Cannon JL, Neely TR, Tavares R, et al. Impaired insulin and insulin-like growth factor expression and signaling mechanisms in Alzheimer's disease--is this type 3 diabetes? J Alzheimers Dis. 2005;7(1):63-80.
86. Freiherr J, Hallschmid M, Frey WH, 2nd, Brunner YF, Chapman CD, Holscher C, et al. Intranasal insulin as a treatment for Alzheimer's disease: a review of basic research and clinical evidence. CNS Drugs. 2013;27(7):505-14.
87. de la Monte SM. Brain insulin resistance and deficiency as therapeutic targets in Alzheimer's disease. Curr Alzheimer Res. 2012;9(1):35-66.
88. Holscher C, Li L. New roles for insulin-like hormones in neuronal signalling and protection: new hopes for novel treatments of Alzheimer's disease? Neurobiol Aging. 2010;31(9):1495-502.
89. Talbot K, Wang HY, Kazi H, Han LY, Bakshi KP, Stucky A, et al. Demonstrated brain insulin resistance in Alzheimer's disease patients is associated with IGF-1 resistance, IRS-1 dysregulation, and cognitive decline. J Clin Invest. 2012;122(4):1316-38.
90. Hong M, Lee VM. Insulin and insulin-like growth factor-1 regulate tau phosphorylation in cultured human neurons. J Biol Chem. 1997;272(31):19547-53.

91. de la Monte SM, Chen GJ, Rivera E, Wands JR. Neuronal thread protein regulation and interaction with microtubule-associated proteins in SH-Sy5y neuronal cells. Cell Mol Life Sci. 2003;60(12):2679-91.
92. Rankin CA, Sun Q, Gamblin TC. Tau phosphorylation by GSK-3beta promotes tangle-like filament morphology. Mol Neurodegener. 2007;2:12.
93. Festa A, Hanley AJ, Tracy RP, D'Agostino R, Jr., Haffner SM. Inflammation in the prediabetic state is related to increased insulin resistance rather than decreased insulin secretion. Circulation. 2003;108(15):1822-30.
94. Kacirova M, Zmeskalova A, Korinkova L, Zelezna B, Kunes J, Maletinska L. Inflammation: major denominator of obesity, Type 2 diabetes and Alzheimer's disease-like pathology? Clin Sci (Lond). 2020;134(5):547-70.
95. Bai Y, Sun Q. Macrophage recruitment in obese adipose tissue. Obes Rev. 2015;16(2):127-36.
96. Boden G. Effects of free fatty acids (FFA) on glucose metabolism: significance for insulin resistance and type 2 diabetes. Exp Clin Endocrinol Diabetes. 2003;111(3):121-4.
97. Jialal I, Kaur H, Devaraj S. Toll-like receptor status in obesity and metabolic syndrome: a translational perspective. J Clin Endocrinol Metab. 2014;99(1):39-48.
98. Shi H, Kokoeva MV, Inouye K, Tzameli I, Yin H, Flier JS. TLR4 links innate immunity and fatty acid-induced insulin resistance. J Clin Invest. 2006;116(11):3015-25.
99. Galimberti D, Scarpini E. Inflammation and oxidative damage in Alzheimer's disease: friend or foe? Front Biosci (Schol Ed). 2011;3:252-66.
100. Sears B, Perry M. The role of fatty acids in insulin resistance. Lipids Health Dis. 2015;14:121.
101. Banks WA, Kastin AJ, Broadwell RD. Passage of cytokines across the blood-brain barrier. Neuroimmunomodulation. 1995;2(4):241-8.
102. Tarkowski E, Blennow K, Wallin A, Tarkowski A. Intracerebral production of tumor necrosis factor-alpha, a local neuroprotective agent, in Alzheimer disease and vascular dementia. J Clin Immunol. 1999;19(4):223-30.
103. de la Monte SM, Neely TR, Cannon J, Wands JR. Ethanol impairs insulin-stimulated mitochondrial function in cerebellar granule neurons. Cell Mol Life Sci. 2001;58(12-13):1950-60.
104. Lester-Coll N, Rivera EJ, Soscia SJ, Doiron K, Wands JR, de la Monte SM. Intracerebral streptozotocin model of type 3 diabetes: relevance to sporadic Alzheimer's disease. J Alzheimers Dis. 2006;9(1):13-33.
105. McGeer PL, Schulzer M, McGeer EG. Arthritis and anti-inflammatory agents as possible protective factors for Alzheimer's disease: a review of 17 epidemiologic studies. Neurology. 1996;47(2):425-32.
106. Ramji DP, Foka P. CCAAT/enhancer-binding proteins: structure, function and regulation. Biochem J. 2002;365(Pt 3):561-75.
107. van der Krieken SE, Popeijus HE, Mensink RP, Plat J. CCAAT/enhancer binding protein beta in relation to ER stress, inflammation, and metabolic disturbances. Biomed Res Int. 2015;2015:324815.
108. Sato Y, Nishio Y, Sekine O, Kodama K, Nagai Y, Nakamura T, et al. Increased expression of CCAAT/enhancer binding protein-beta and -delta and monocyte chemoattractant protein-1 genes in aortas from hyperinsulinaemic rats. Diabetologia. 2007;50(2):481-9.

109. Cardinaux JR, Allaman I, Magistretti PJ. Pro-inflammatory cytokines induce the transcription factors C/EBPbeta and C/EBPdelta in astrocytes. Glia. 2000;29(1):91-7.
110. Ejarque-Ortiz A, Medina MG, Tusell JM, Perez-Gonzalez AP, Serratosa J, Saura J. Upregulation of CCAAT/enhancer binding protein beta in activated astrocytes and microglia. Glia. 2007;55(2):178-88.
111. Hungness ES, Luo GJ, Pritts TA, Sun X, Robb BW, Hershko D, et al. Transcription factors C/EBP-beta and -delta regulate IL-6 production in IL-1beta-stimulated human enterocytes. J Cell Physiol. 2002;192(1):64-70.
112. Tengku-Muhammad TS, Hughes TR, Ranki H, Cryer A, Ramji DP. Differential regulation of macrophage CCAAT-enhancer binding protein isoforms by lipopolysaccharide and cytokines. Cytokine. 2000;12(9):1430-6.
113. Cortes-Canteli M, Wagner M, Ansorge W, Perez-Castillo A. Microarray analysis supports a role for ccaat/enhancer-binding protein-beta in brain injury. J Biol Chem. 2004;279(14):14409-17.
114. Taubenfeld SM, Milekic MH, Monti B, Alberini CM. The consolidation of new but not reactivated memory requires hippocampal C/EBPbeta. Nat Neurosci. 2001;4(8):813-8.
115. Lukiw WJ. Gene expression profiling in fetal, aged, and Alzheimer hippocampus: a continuum of stress-related signaling. Neurochem Res. 2004;29(6):1287-97.
116. Li R, Strohmeyer R, Liang Z, Lue LF, Rogers J. CCAAT/enhancer binding protein delta (C/EBPdelta) expression and elevation in Alzheimer's disease. Neurobiol Aging. 2004;25(8):991-9.
117. Ramberg V, Tracy LM, Samuelsson M, Nilsson LN, Iverfeldt K. The CCAAT/enhancer binding protein (C/EBP) delta is differently regulated by fibrillar and oligomeric forms of the Alzheimer amyloid-beta peptide. J Neuroinflammation. 2011;8:34.
118. Kapadia R, Tureyen K, Bowen KK, Kalluri H, Johnson PF, Vemuganti R. Decreased brain damage and curtailed inflammation in transcription factor CCAAT/enhancer binding protein beta knockout mice following transient focal cerebral ischemia. J Neurochem. 2006;98(6):1718-31.
119. Cortes-Canteli M, Luna-Medina R, Sanz-Sancristobal M, Alvarez-Barrientos A, Santos A, Perez-Castillo A. CCAAT/enhancer binding protein beta deficiency provides cerebral protection following excitotoxic injury. J Cell Sci. 2008;121(Pt 8):1224-34.
120. Timchenko NA. Aging and liver regeneration. Trends Endocrinol Metab. 2009;20(4):171-6.
121. Wang ZH, Xiang J, Liu X, Yu SP, Manfredsson FP, Sandoval IM, et al. Deficiency in BDNF/TrkB Neurotrophic Activity Stimulates delta-Secretase by Upregulating C/EBPbeta in Alzheimer's Disease. Cell Rep. 2019;28(3):655-69 e5.
122. Wang ZH, Gong K, Liu X, Zhang Z, Sun X, Wei ZZ, et al. C/EBPbeta regulates delta-secretase expression and mediates pathogenesis in mouse models of Alzheimer's disease. Nat Commun. 2018;9(1):1784.
123. Xia Y, Wang ZH, Zhang J, Liu X, Yu SP, Ye KX, et al. C/EBPbeta is a key transcription factor for APOE and preferentially mediates ApoE4 expression in Alzheimer's disease. Mol Psychiatry. 2020.
124. Trautwein C, Caelles C, van der Geer P, Hunter T, Karin M, Chojkier M. Transactivation by NF-IL6/LAP is enhanced by phosphorylation of its activation domain. Nature. 1993;364(6437):544-7.

125. Croniger CM, Millward C, Yang J, Kawai Y, Arinze IJ, Liu S, et al. Mice with a deletion in the gene for CCAAT/enhancer-binding protein beta have an attenuated response to cAMP and impaired carbohydrate metabolism. J Biol Chem. 2001;276(1):629-38.
126. Liu S, Croniger C, Arizmendi C, Harada-Shiba M, Ren J, Poli V, et al. Hypoglycemia and impaired hepatic glucose production in mice with a deletion of the C/EBPbeta gene. J Clin Invest. 1999;103(2):207-13.
127. Tanaka T, Yoshida N, Kishimoto T, Akira S. Defective adipocyte differentiation in mice lacking the C/EBPbeta and/or C/EBPdelta gene. EMBO J. 1997;16(24):7432-43.
128. Chung SS, Lee JS, Kim M, Ahn BY, Jung HS, Lee HM, et al. Regulation of Wnt/beta-catenin signaling by CCAAT/enhancer binding protein beta during adipogenesis. Obesity (Silver Spring). 2012;20(3):482-7.
129. Lu M, Seufert J, Habener JF. Pancreatic beta-cell-specific repression of insulin gene transcription by CCAAT/enhancer-binding protein beta. Inhibitory interactions with basic helix-loop-helix transcription factor E47. J Biol Chem. 1997;272(45):28349-59.
130. Millward CA, Heaney JD, Sinasac DS, Chu EC, Bederman IR, Gilge DA, et al. Mice with a deletion in the gene for CCAAT/enhancer-binding protein beta are protected against diet-induced obesity. Diabetes. 2007;56(1):161-7.
131. Chen JM, Dando PM, Stevens RA, Fortunato M, Barrett AJ. Cloning and expression of mouse legumain, a lysosomal endopeptidase. Biochem J. 1998;335 (Pt 1):111-7.
132. Miller G, Matthews SP, Reinheckel T, Fleming S, Watts C. Asparagine endopeptidase is required for normal kidney physiology and homeostasis. FASEB J. 2011;25(5):1606-17.
133. Li DN, Matthews SP, Antoniou AN, Mazzeo D, Watts C. Multistep autoactivation of asparaginyl endopeptidase in vitro and in vivo. J Biol Chem. 2003;278(40):38980-90.
134. Stathopoulou C, Gangaplara A, Mallett G, Flomerfelt FA, Liniany LP, Knight D, et al. PD-1 Inhibitory Receptor Downregulates Asparaginyl Endopeptidase and Maintains Foxp3 Transcription Factor Stability in Induced Regulatory T Cells. Immunity. 2018;49(2):247-63 e7.
135. Liu C, Sun C, Huang H, Janda K, Edgington T. Overexpression of legumain in tumors is significant for invasion/metastasis and a candidate enzymatic target for prodrug therapy. Cancer Res. 2003;63(11):2957-64.
136. Liu Z, Jang SW, Liu X, Cheng D, Peng J, Yepes M, et al. Neuroprotective actions of PIKE-L by inhibition of SET proteolytic degradation by asparagine endopeptidase. Mol Cell. 2008;29(6):665-78.
137. Zhang Z, Obianyo O, Dall E, Du Y, Fu H, Liu X, et al. Inhibition of delta-secretase improves cognitive functions in mouse models of Alzheimer's disease. Nat Commun. 2017;8:14740.
138. Zhang Z, Song M, Liu X, Kang SS, Kwon IS, Duong DM, et al. Cleavage of tau by asparagine endopeptidase mediates the neurofibrillary pathology in Alzheimer's disease. Nat Med. 2014;20(11):1254-62.
139. Zhang Z, Song M, Liu X, Su Kang S, Duong DM, Seyfried NT, et al. Delta-secretase cleaves amyloid precursor protein and regulates the pathogenesis in Alzheimer's disease. Nat Commun. 2015;6:8762.
140. Ma L, Shen YQ, Khatri HP, Schachner M. The asparaginyl endopeptidase legumain is essential for functional recovery after spinal cord injury in adult zebrafish. PLoS One. 2014;9(4):e95098.
141. Zhang Z, Xie M, Ye K. Asparagine endopeptidase is an innovative therapeutic target for neurodegenerative diseases. Expert Opin Ther Targets. 2016;20(10):1237-45.

142. Choi JH, Lee MY, Kim Y, Shim JY, Han SM, Lee KA, et al. Isolation of genes involved in pancreas regeneration by subtractive hybridization. Biol Chem. 2010;391(9):1019-29.
143. Basurto-Islas G, Grundke-Iqbal I, Tung YC, Liu F, Iqbal K. Activation of asparaginyl endopeptidase leads to Tau hyperphosphorylation in Alzheimer disease. J Biol Chem. 2013;288(24):17495-507.
144. Clees AS, Stolp V, Haupl B, Fuhrmann DC, Wempe F, Seibert M, et al. Identification of the Cysteine Protease Legumain as a Potential Chronic Hypoxia-Specific Multiple Myeloma Target Gene. Cells. 2022;11(2).
145. Shrestha S, Singhal S, Sens DA, Somji S, Davis BA, Guyer R, et al. Elevated glucose represses lysosomal and mTOR-related genes in renal epithelial cells composed of progenitor CD133+ cells. PLoS One. 2021;16(3):e0248241.
146. Duan Y, Zeng L, Zheng C, Song B, Li F, Kong X, et al. Inflammatory Links Between High Fat Diets and Diseases. Front Immunol. 2018;9:2649.
147. Janson J, Laedtke T, Parisi JE, O'Brien P, Petersen RC, Butler PC. Increased risk of type 2 diabetes in Alzheimer disease. Diabetes. 2004;53(2):474-81.
148. Hagberg CE, Falkevall A, Wang X, Larsson E, Huusko J, Nilsson I, et al. Vascular endothelial growth factor B controls endothelial fatty acid uptake. Nature. 2010;464(7290):917-21.
149. Broadfield LA, Duarte JAG, Schmieder R, Broekaert D, Veys K, Planque M, et al. Fat Induces Glucose Metabolism in Nontransformed Liver Cells and Promotes Liver Tumorigenesis. Cancer Res. 2021;81(8):1988-2001.
150. Guillemot-Legris O, Masquelier J, Everard A, Cani PD, Alhouayek M, Muccioli GG. High-fat diet feeding differentially affects the development of inflammation in the central nervous system. J Neuroinflammation. 2016;13(1):206.
151. Sambon M, Wins P, Bettendorff L. Neuroprotective Effects of Thiamine and Precursors with Higher Bioavailability: Focus on Benfotiamine and Dibenzoylthiamine. Int J Mol Sci. 2021;22(11).
152. Zhang BB, Zhou G, Li C. AMPK: an emerging drug target for diabetes and the metabolic syndrome. Cell Metab. 2009;9(5):407-16.
153. Ko CY, Chang WC, Wang JM. Biological roles of CCAAT/Enhancer-binding protein delta during inflammation. J Biomed Sci. 2015;22:6.
154. Lage R, Dieguez C, Vidal-Puig A, Lopez M. AMPK: a metabolic gauge regulating whole-body energy homeostasis. Trends Mol Med. 2008;14(12):539-49.
155. Viollet B, Foretz M, Guigas B, Horman S, Dentin R, Bertrand L, et al. Activation of AMP-activated protein kinase in the liver: a new strategy for the management of metabolic hepatic disorders. J Physiol. 2006;574(Pt 1):41-53.
156. Mullur R, Liu YY, Brent GA. Thyroid hormone regulation of metabolism. Physiol Rev. 2014;94(2):355-82.
157. Yang CS, Lam CK, Chari M, Cheung GW, Kokorovic A, Gao S, et al. Hypothalamic AMP-activated protein kinase regulates glucose production. Diabetes. 2010;59(10):2435-43.
158. Takai T, Matsuda T, Matsuura Y, Inoue K, Suzuki E, Kanno A, et al. Casein kinase 2 phosphorylates and stabilizes C/EBPbeta in pancreatic beta cells. Biochem Biophys Res Commun. 2018;497(1):451-6.
159. Choudhury M, Qadri I, Rahman SM, Schroeder-Gloeckler J, Janssen RC, Friedman JE. C/EBPbeta is AMP kinase sensitive and up-regulates PEPCK in response to ER stress in hepatoma cells. Mol Cell Endocrinol. 2011;331(1):102-8.

160. Bosch F, Sabater J, Valera A. Insulin inhibits liver expression of the CCAAT/enhancer-binding protein beta. Diabetes. 1995;44(3):267-71.
161. MacDougald OA, Cornelius P, Liu R, Lane MD. Insulin regulates transcription of the CCAAT/enhancer binding protein (C/EBP) alpha, beta, and delta genes in fully-differentiated 3T3-L1 adipocytes. J Biol Chem. 1995;270(2):647-54.
162. Du K, Ding J. Insulin regulates TRB3 and other stress-responsive gene expression through induction of C/EBPbeta. Mol Endocrinol. 2009;23(4):475-85.
163. Foti MC, DiLabio GA, Ingold KU. Overlooked difference between hydrogen bonds of equal strength formed between catechol and an oxygen or nitrogen base. Experiments and DFT calculations. J Am Chem Soc. 2003;125(47):14642-7.
164. Tang Y, Xiong K, Shen M, Mu Y, Li K, Liu H. CCAAT-enhancer binding protein (C/EBP) beta regulates insulin-like growth factor (IGF) 1 expression in porcine liver during prenatal and postnatal development. Mol Cell Biochem. 2015;401(1-2):209-18.
165. Matsuda T, Kido Y, Asahara S, Kaisho T, Tanaka T, Hashimoto N, et al. Ablation of C/EBPbeta alleviates ER stress and pancreatic beta cell failure through the GRP78 chaperone in mice. J Clin Invest. 2010;120(1):115-26.
166. Rahman SM, Janssen RC, Choudhury M, Baquero KC, Aikens RM, de la Houssaye BA, et al. CCAAT/enhancer-binding protein beta (C/EBPbeta) expression regulates dietary-induced inflammation in macrophages and adipose tissue in mice. J Biol Chem. 2012;287(41):34349-60.
167. Ho L, Qin W, Pompl PN, Xiang Z, Wang J, Zhao Z, et al. Diet-induced insulin resistance promotes amyloidosis in a transgenic mouse model of Alzheimer's disease. FASEB J. 2004;18(7):902-4.
168. Kim B, Backus C, Oh S, Hayes JM, Feldman EL. Increased tau phosphorylation and cleavage in mouse models of type 1 and type 2 diabetes. Endocrinology. 2009;150(12):5294-301.
169. Gibson GE, Hirsch JA, Fonzetti P, Jordan BD, Cirio RT, Elder J. Vitamin B1 (thiamine) and dementia. Ann N Y Acad Sci. 2016;1367(1):21-30.
170. Gibson GE, Hirsch JA, Cirio RT, Jordan BD, Fonzetti P, Elder J. Abnormal thiamine-dependent processes in Alzheimer's Disease. Lessons from diabetes. Mol Cell Neurosci. 2013;55:17-25.
171. Cortes-Canteli M, Aguilar-Morante D, Sanz-Sancristobal M, Megias D, Santos A, Perez-Castillo A. Role of C/EBPbeta transcription factor in adult hippocampal neurogenesis. PLoS One. 2011;6(10):e24842.
172. Farooqui AA, Horrocks LA, Farooqui T. Modulation of inflammation in brain: a matter of fat. J Neurochem. 2007;101(3):577-99.
173. Sanchez-Mejia RO, Mucke L. Phospholipase A2 and arachidonic acid in Alzheimer's disease. Biochim Biophys Acta. 2010;1801(8):784-90.
174. Vane JR, Botting RM. The mechanism of action of aspirin. Thromb Res. 2003;110(5-6):255-8.
175. Kinoshita S, Akira S, Kishimoto T. A member of the C/EBP family, NF-IL6 beta, forms a heterodimer and transcriptionally synergizes with NF-IL6. Proc Natl Acad Sci U S A. 1992;89(4):1473-6.
176. Wang HY, Arden KC, Bermingham JR, Jr., Viars CS, Lin W, Boyer AD, et al. Localization of serine kinases, SRPK1 (SFRSK1) and SRPK2 (SFRSK2), specific for the SR family of splicing factors in mouse and human chromosomes. Genomics. 1999;57(2):310-5.

177. Wang HY, Lin W, Dyck JA, Yeakley JM, Songyang Z, Cantley LC, et al. SRPK2: a differentially expressed SR protein-specific kinase involved in mediating the interaction and localization of pre-mRNA splicing factors in mammalian cells. J Cell Biol. 1998;140(4):737-50.
178. Ngo JC, Chakrabarti S, Ding JH, Velazquez-Dones A, Nolen B, Aubol BE, et al. Interplay between SRPK and Clk/Sty kinases in phosphorylation of the splicing factor ASF/SF2 is regulated by a docking motif in ASF/SF2. Mol Cell. 2005;20(1):77-89.
179. Zhong XY, Ding JH, Adams JA, Ghosh G, Fu XD. Regulation of SR protein phosphorylation and alternative splicing by modulating kinetic interactions of SRPK1 with molecular chaperones. Genes Dev. 2009;23(4):482-95.
180. Zhou Z, Qiu J, Liu W, Zhou Y, Plocinik RM, Li H, et al. The Akt-SRPK-SR Axis Constitutes a Major Pathway in Transducing EGF Signaling to Regulate Alternative Splicing in the Nucleus. Mol Cell. 2018;71(5):872.
181. Ding JH, Zhong XY, Hagopian JC, Cruz MM, Ghosh G, Feramisco J, et al. Regulated cellular partitioning of SR protein-specific kinases in mammalian cells. Mol Biol Cell. 2006;17(2):876-85.
182. Jang SW, Liu X, Fu H, Rees H, Yepes M, Levey A, et al. Interaction of Akt-phosphorylated SRPK2 with 14-3-3 mediates cell cycle and cell death in neurons. J Biol Chem. 2009;284(36):24512-25.
183. Hong Y, Jang SW, Ye K. The N-terminal fragment from caspase-cleaved serine/arginine protein-specific kinase2 (SRPK2) translocates into the nucleus and promotes apoptosis. J Biol Chem. 2011;286(1):777-86.
184. Hong Y, Chan CB, Kwon IS, Li X, Song M, Lee HP, et al. SRPK2 phosphorylates tau and mediates the cognitive defects in Alzheimer's disease. J Neurosci. 2012;32(48):17262-72.
185. Jang SW, Yang SJ, Ehlen A, Dong S, Khoury H, Chen J, et al. Serine/arginine protein-specific kinase 2 promotes leukemia cell proliferation by phosphorylating acinus and regulating cyclin A1. Cancer Res. 2008;68(12):4559-70.
186. Wang ZH, Liu P, Liu X, Manfredsson FP, Sandoval IM, Yu SP, et al. Delta-Secretase Phosphorylation by SRPK2 Enhances Its Enzymatic Activity, Provoking Pathogenesis in Alzheimer's Disease. Mol Cell. 2017;67(5):812-25 e5.
187. Reichardt LF. Neurotrophin-regulated signalling pathways. Philos Trans R Soc Lond B Biol Sci. 2006;361(1473):1545-64.
188. Connor B, Young D, Yan Q, Faull RL, Synek B, Dragunow M. Brain-derived neurotrophic factor is reduced in Alzheimer's disease. Brain Res Mol Brain Res. 1997;49(1-2):71-81.
189. Ferrer I, Marin C, Rey MJ, Ribalta T, Goutan E, Blanco R, et al. BDNF and full-length and truncated TrkB expression in Alzheimer disease. Implications in therapeutic strategies. J Neuropathol Exp Neurol. 1999;58(7):729-39.
190. Phillips HS, Hains JM, Armanini M, Laramee GR, Johnson SA, Winslow JW. BDNF mRNA is decreased in the hippocampus of individuals with Alzheimer's disease. Neuron. 1991;7(5):695-702.
191. Rohe M, Synowitz M, Glass R, Paul SM, Nykjaer A, Willnow TE. Brain-derived neurotrophic factor reduces amyloidogenic processing through control of SORLA gene expression. J Neurosci. 2009;29(49):15472-8.
192. Ando S, Kobayashi S, Waki H, Kon K, Fukui F, Tadenuma T, et al. Animal model of dementia induced by entorhinal synaptic damage and partial restoration of cognitive deficits by BDNF and carnitine. J Neurosci Res. 2002;70(3):519-27.

193. Xia Y, Wang ZH, Liu P, Edgington-Mitchell L, Liu X, Wang XC, et al. TrkB receptor cleavage by delta-secretase abolishes its phosphorylation of APP, aggravating Alzheimer's disease pathologies. Mol Psychiatry. 2021;26(7):2943-63.
194. Daniels Gatward LF, Kennard MR, Smith LIF, King AJF. The use of mice in diabetes research: The impact of physiological characteristics, choice of model and husbandry practices. Diabet Med. 2021;38(12):e14711.
195. Speakman JR. Measuring energy metabolism in the mouse - theoretical, practical, and analytical considerations. Front Physiol. 2013;4:34.
196. DeFronzo RA, Tobin JD, Andres R. Glucose clamp technique: a method for quantifying insulin secretion and resistance. Am J Physiol. 1979;237(3):E214-23.
197. Chan CB, Abe M, Hashimoto N, Hao C, Williams IR, Liu X, et al. Mice lacking asparaginyl endopeptidase develop disorders resembling hemophagocytic syndrome. Proc Natl Acad Sci U S A. 2009;106(2):468-73.
198. Gokce M, Unal O, Hismi B, Gumruk F, Coskun T, Balta G, et al. Secondary hemophagocytosis in 3 patients with organic acidemia involving propionate metabolism. Pediatr Hematol Oncol. 2012;29(1):92-8.
199. Duval M, Fenneteau O, Doireau V, Faye A, Emilie D, Yotnda P, et al. Intermittent hemophagocytic lymphohistiocytosis is a regular feature of lysinuric protein intolerance. J Pediatr. 1999;134(2):236-9.